EXPERIMENTS ON SPIN-POLARIZED ATOMIC HYDROGEN AT HIGH DENSITY

ACADEMISCH PROEFSCHRIFT

ter verkrijging van de graad van
doctor in de Wiskunde
en Natuurwetenschappen
aan de Universiteit van Amsterdam,
op gezag van de Rector Magnificus,
Dr. D.W. Bresters,
hoogleraar in de Faculteit der Wiskunde en
Natuurwetenschappen,
in het openbaar te verdedigen in de Aula der Universiteit
(tijdelijk in het Wiskundegebouw, Roetersstraat 15, Amsterdam)
op dinsdag 1 juli 1986 te 13.30 uur.

door

Rudolf Sprik

geboren te Doetinchem

AMSTERDAM 1986

Promotor: Prof. Dr. I.F. Silvera

Co-promotor: Dr. J.T.M. Walraven

The work described in this thesis was carried out at the

Natuurkundig Laboratorium
der
Universiteit van Amsterdam
Valckenierstraat 65
1018 XE Amsterdam

and was financially supported by the 'Stichting voor Fundamenteel Onderzoek der Materie (FOM)'.

EXPERIMENTS ON SPIN-POLARIZED ATOMIC HYDROGEN AT HIGH DENSITY

R. Sprik

CONTENTS

Chapter 1 Introduction

1.1 Background

The idea to study a gas of atomic hydrogen at high density originates from many years ago[1] and was inspired by the prospect of the many-body quantum nature of such a gas. One expects a gas of hydrogen atoms, consisting of two tightly bound fermions (one electron, electron spin S=1/2 and one proton, nuclear spin I=1/2), to behave as a gas of (weakly) interacting Bose particles and to remain gaseous down to T=0K.[2] This allows a continuous variation of the density over a large dynamic range, so that H can be used to test the quantum statistical theories and related phenomena. In particular H should display a transition to the Bose Einstein condensed phase (e.g. for 100mK at $n=1.6\times10^{19}cm^{-3}$).[3] Comparison of the hydrogen gas with the properties of another Bose system, ^4He, - its neighbor in the periodic table -, illustrates the potential richness of such a system (superfluidity, Bose Einstein condensation etc.). The simple structure of H should enable a more profound theoretical description of its quantum character than is possible for helium.

Under the normal conditions of the earth's atmosphere, a gas of hydrogen atoms is unstable against recombination to the molecular form (H_2), preventing the study of a gas of freely moving hydrogen atoms of significant density. In the past few years new experimental techniques have been developed which increase the stability of the gas by many orders of magnitude. The essential ingredients of such experiments are the use of low temperatures, high magnetic fields and the particular lining of the experimental cell. The first major improvement was obtained by Silvera and Walraven[4] in 1979 by the use of a stabilization cell with a lining of superfluid ^4He film and in magnetic fields up to 10T at about 300mK. The high magnetic field and the low temperature force the atoms to become electron spin-polarized (H↓), which suppresses the recombination to the molecular bound state (see section 1.3). The lining is crucial in suppressing the recombination of the atoms at the wall (section 1.3). The obtained densities of H↓ ($n\leq2.\times10^{14}cm^{-3}$) were still far below the densities which are of interest to study the many-body quantum properties of the gas. Rapidly, new experiments were developed[5-7] in which the density was increased to 10^{16}-$10^{17}cm^{-3}$. These experiments gave quantitative information on the behavior of the decay as function of temperature and magnetic field. Measurements of the adsorption energy of atomic hydrogen on the helium film indicated that one could gain stability by the use of ^3He linings.[8,9]

This thesis describes two experiments which contributed to the increase of the experimentally accessible densities. The first experiment was performed in a cell where all magnetic impurities were carefully removed from the heart of the cell. Due to the peculiar behavior of the recombination, a gas with both electronic and nuclear-spin polarized (doubly polarized atomic hydrogen ,H↓↧) develops; this will be explained in section

1.4. The formation of H↓↑ was predicted by Statt and Berlinsky[10] and first observed by Cline et al.[11] In a previous attempt by van Yperen et al.[8] the double polarization was not observed, but it inspired the construction of the magnetically clean cell (see chapters 2 and 3; magnetic impurities destroy the double polarization in the gas). In this 'clean' cell we observed H↓↑. The stability of H↓↑ is dramatically increased up to densities $n \leq 2 \times 10^{17} cm^{-3}$, however still below the desired conditions for BEC.[12] In more recent experiments using magnetic resonance techniques the specific occupation of the various hyperfine states was measured directly and confirmed the build-up of H↓↑.[13-15]

The second experiment uses volume compression to increase the gas density. In our experiment the compression is performed in a quasi isobaric way, which will be explained in detail in chapters 4-6.[16,17] Such a scheme was also applied by the group in Finland.[18] Another compression scheme was developed by the M.I.T. group[19] at about the same time, based on volume compression and observation of the pressure decay. These compression techniques realize the highest densities currently available ($n < 4.5 \times 10^{18} cm^{-3}$).[18] Although at such densities the mean-free-path of an atom is considerably smaller than the geometrical dimensions of the cell, it is still not high enough to attain the region of quantum degeneracy.

Despite the fact that the densities are still below the BEC limit, the atomic hydrogen gas displays a number of interesting and unexpected phenomena at lower densities. They will not all be treated in the present thesis, but may turn out to be a topic worthy of study. Many interesting properties are also expected for spin-polarized deuterium (D↓, S=1/2, I=1; a fermion system) and many of the considerations for H↓ also hold for D↓. The deuterium system will not be treated in this thesis. A recent review of most of the work on atomic hydrogens can be found in a number of articles: Silvera,[20] Walraven,[21] Greytak and Kleppner,[22] Silvera and Walraven.[23]

This thesis will be restricted to the experiments mentioned above and some of the essentials needed to understand the physics of a gas of hydrogen atoms. Chapter 1 introduces some of these concepts. Sections 1.2-1.3 cover the single, pair and many atom properties of hydrogen atoms. Sections 1.4-1.5 describe the processes that limit the stability of the gas at the densities realized in the experiments. Chapters 2 and 3 describe the experiment performed in a cell without magnetic impurities on doubly polarized atomic hydrogen. Chapter 4,5 and 6 describe the compression experiment. Chapter 7 deals with the analysis of the thermal conditions of a gas at high density; this is of interest for future use of the compression techniques. The thesis is concluded with chapter 8 which will give some prospects concerning the possibility of obtaining BEC conditions.

Some of the chapters in this thesis are or will be published elsewhere. Chapter 2 is an article submitted to the Physical Review B. Chapters 3 and 6 are reprints of publications in the Physical Review Letters (ref. 12,16). Chapter 5 is a reprint of a publication in the Physical Review B (ref. 17).

1.2 Atomic hydrogen gas in a magnetic field

In the following sections interactions that play a role in the stabilization of atomic hydrogen in a high magnetic field and at low temperature are introduced. First the hyperfine states of a single hydrogen atom in a magnetic field, next the interatomic potentials between two hydrogen atoms, and finally the consequence of these interactions in a gas of atomic hydrogen are discussed.

1.2.1 Hyperfine levels

The energy levels and the eigenstates of atomic hydrogen in a static magnetic field are mainly determined by two contributions:

- The Zeeman energy of the electron spin (S=1/2) and the nuclear spin (I=1/2) in the static magnetic field B.
- The hyperfine coupling of the nuclear and the electronic moment (coupling constant $a/h=1420.405751773(1)$MHz[23]). The hyperfine interaction for atomic hydrogen originates from the Fermi contact term[24] of the electronic density at the place of the nucleus. Such a contact term occurs in any atomic state where the overlap of the electronic density with the nuclear volume is substantial (e.g. orbital momentum L=0), which is the case for atomic hydrogen in the ground state.

These two contributions result in a hamiltonian (H):

$$H = g_e\mu_B \vec{B} \cdot \vec{s} - g_n\mu_n \vec{B} \cdot \vec{I} + a \vec{I} \cdot \vec{s}. \qquad (1.2.1)$$

Here $g_e=2.0023193134(70)$ and $g_n=5.5856912(22)$ the electronic- and nuclear g-factors respectively, $\mu_B=9.274096(65)\times10^{-24}$J/T the Bohr magneton and $\mu_n=5.050951(50)\times10^{-27}$J/T the nuclear magneton ($g_n\mu_n\equiv2.821234(11)\times10^{-26}$J/T, $g_e\mu_B=18.569664(72)\times10^{-24}$J/T)(values from ref. 23).

The eigenstates in the order of their energy are:

$$\begin{aligned} |d\rangle &= |\uparrow\downarrow\rangle \\ |c\rangle &= \cos(\theta)|\uparrow\uparrow\rangle + \sin(\theta)|\downarrow\downarrow\rangle \\ |b\rangle &= |\downarrow\uparrow\rangle \\ |a\rangle &= \sin(\theta)|\uparrow\uparrow\rangle - \cos(\theta)|\downarrow\downarrow\rangle, \end{aligned} \qquad (1.2.2)$$

where θ is defined by:

$$\tan(2\theta) = a/[(g_e\mu_B + g_n\mu_n)B].$$

(Sometimes the approximation $\sin(\theta)=\epsilon$ and $\cos(\theta)=1$ is used at high fields; notice that strictly speaking the eigenstates are then not normalized.)

The energy eigenvalues are the familiar Breit-Rabi levels[25] (see fig.1.2.1); in particular the energy difference between the a-b ($\Delta I=1$, a nuclear spin transition) and the b-c levels ($\Delta S=1$, an electron spin transition) are given by:

(1.2.2)

$$E_{a-b} = + a/2 + a/2 \left[\left((\mu^+/a)B \right)^2 + 1 \right]^{1/2} - (\mu^-/2)\, B$$

$$E_{b-c} = - a/2 + a/2 \left[\left((\mu^+/a)B \right)^2 + 1 \right]^{1/2} + (\mu^-/2)\, B,$$

with $\mu^+ \equiv g_e\mu_B + g_n\mu_n$ and $\mu^- \equiv g_e\mu_B - g_n\mu_n$.

At low field the total spin $\vec{F} = \vec{I} + \vec{s}$ is a 'good' quantum number and the states are represented by the singlet ground state (F=0, m_F=0) and the triplet state (F=1, m_F=-1,0,+1) (see fig.1.2.1). At very high fields the eigenstates tend to pure Zeeman states. For the fields used in the experiments in this thesis, only the b- and d-states are pure Zeeman states. The state with the lowest energy (a-state) has a small fraction ϵ of the Zeeman state $|\uparrow\downarrow\rangle$. The fraction ϵ vanishes as 1/B and leads to peculiar recombination properties of the gas. This will be discussed extensively in section 1.3 and is the key feature of the experiments presented in chapter 2 and 3.

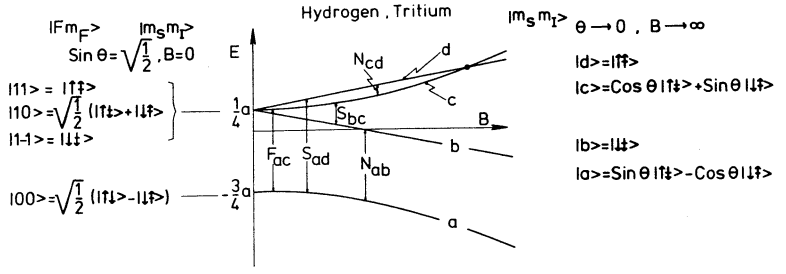

fig.1.2.1 Hyperfine spectrum of H in a magnetic field. Magnetic transitions are also indicated (S - electronic, N - nuclear, F - forbidden).

1.2.2 Interatomic potentials

The hamiltonian eq.1.2.1 only takes into account the single atom properties. If two atoms are considered, one has to include the interactions between the atoms as well. In a first approximation this leads to the electronic singlet potential (V^s, $X^1\Sigma_g^+$ state, total electron spin S=0 (for notation of the molecular states see e.g. Herzberg[26])) and the electronic triplet potential (V^t, $b^3\Sigma_u^+$ state, total electron spin S=1, m_S=-1,0,1). The singlet state is the lowest energy state of the hydrogen molecule (fig.1.2.2).

The singlet and triplet potentials are accurately known from first principle calculations. In the adiabatic approximation the protons are considered to be instantaneously fixed with respect to the electron motion and one accounts for Coulomb interaction, resulting in a hamiltonian:

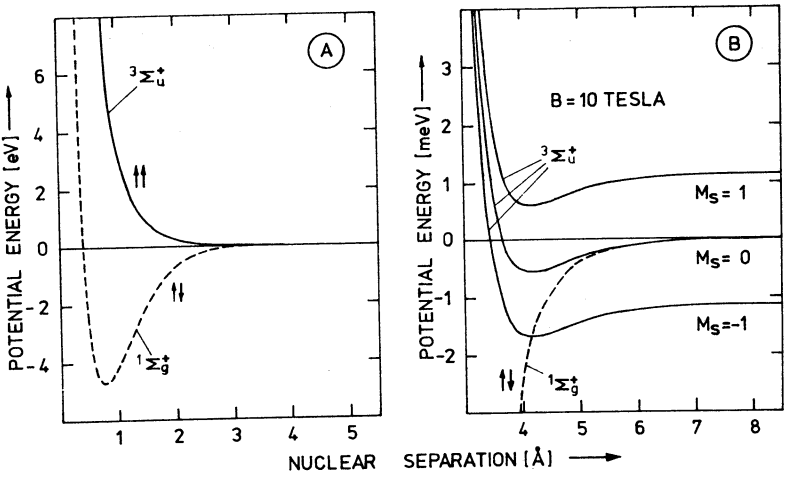

fig.1.2.2 Singlet ($^1\Sigma_g^+$) and triplet ($^3\Sigma_u^+$) interaction potential for two H atoms at B=0 (a) and B=10Tesla (b).

(1.2.3)

$$H = (1/(2m))(p_1^2 + p_2^2) - e^2 (r_{1A}^{-1} + r_{2A}^{-1} + r_{1B}^{-1} + r_{2B}^{-1} + r_{ab}^{-1} + r_{12}^{-1}),$$

where $p_1^2/2m$ is the kinetic energy of the electrons, index 1,2 refer to the nuclei and index A,B to the electrons. A simple Heitler-London wave function[26] leads in first approximation to the anti-symmetric singlet state (φ_-) and the symmetric triplet state (φ_+):

(1.2.4)

$$\varphi_\pm = (1/\sqrt{2}) [u_A(r_1) u_B(r_2) \pm u_A(r_2) u_B(r_1)],$$

where $u_{A,B}$ are the unperturbed single atom wavefunctions.

The symmetric function φ_+ is associated with the triplet potential, V^t and the anti-symmetric function φ_- with the singlet potential, V^s (see fig.1.2.2).

The coulomb interaction part of the hamiltonian eq.1.2.3 can be expressed as an effective hamiltonian:

(1.2.5a)

$$H_c = V_D(r_{12}) + J(r_{12}) \vec{s}_1 \cdot \vec{s}_2.$$

Here the direct interaction V_D and the 'exchange' interaction J are defined by:

(1.2.5b)

$$V_D(r) = (1/4) V^s(r) + (3/4) V^t(r), \quad J(r) = v^t(r) - V^s(r).$$

The total wave function is a product of the orbital-part and the spin-parts. In the center of mass coordinate system the orbital part has two sets of quantum numbers; the vibrational quantum number, v, and the rotational quantum number, L. Symmetry conditions for the molecule determine the allowed molecular states (see table 1.2.1).

Ab initio calculations of V^s and V^t have been an active field since the first days of quantum mechanics. The major improvements were obtained after the introduction of computers and numerical techniques to solve the Schrödinger equation.[27] Most calculations start from the adiabatic approximation, assuming the electrons to follow the movement of the nuclei instantaneously (E_{ad}, adiabatic approximation). The potentials within this approximation are calculated and tabulated by Kolos and Wolniewicz.[28] A further improvement of the potential curves is obtained within the adiabatic approximation by including corrections for the nuclear motion up to first order. The corrections obtained this way are usually called: adiabatic corrections (ΔE_{ad}).[27] Further improvement of the potential is realized by including relativistic correction terms in the hamiltonian (ΔE_{rel}). The combination of E_{ad} and ΔE_{ad}, ΔE_{rel} is sometimes called the 'best molecular potential'.[29] For the singlet ground state of H_2 this potential is tabulated by Bishop and Shih[30], combining the known potentials and corrections at that time. Later improvements by Wolniewicz[31] are not included. For the triplet potential only E_{ad} is tabulated[28], although one expects ΔE_{ad} to be small.[28] To test the accuracy of the potentials the experimentally observed rotation and vibration levels of molecular hydrogen have been compared with the calculated ones.[30] The ab initio values for the levels are obtained by combining the calculated potential and the centrifugal forces for angular momentum $L>0$ in an effective hamiltonian and solving the eigenvalue problem of the Schrödinger equation. Improvements are obtained by (semi empirical) modifications of the hamiltonian.[27] The various experimentally obtained rotation and vibration levels near the dissociation limit for the singlet ground state are given fig.1.2.3 (after data of Dabrowski[32]); they will be used in other sections.

From the accurate ab initio calculations of the H_2 potential it is well known that the triplet potential exhibits a shallow minimum at r_m=4.15Å (7.84 a.u.) with a well depth of E_0/k_B=6.46K (4.49cm^{-1}).[28] This minimum is caused by van der Waals forces between the atoms. A simple Heitler-London approach (eq.1.2.4) will not give this minimum. The van der Waals minimum is however not deep enough to allow a bound triplet state, even for the rotational and vibrational ground state. The importance of this van der Waals minimum with respect to the stabilization of atomic hydrogen will be discussed in the next section.

Molecule and spin of nucleon		I_{mol}	L	$\mp(I_{mol})\mp(L)$	Nuclear weight gI	Designation
Hydrogen	State	0	Even			para
Tritium	Symmetry	AS	S	AS	1	
$I_N=\frac{1}{2}$	State	1	Odd			ortho
	Symmetry	S	AS	AS	3	
Deuterium	State	1	Odd			para
$I_N=1$	Symmetry	AS	AS	S	3	
	State	0,2	Even			ortho
	Symmetry	S	S	S	6	

table 1.2.1 *The different nuclear spin-states and rotational states for the hydrogen, deuterium and tritium molecule. AS = Antisymmetric, S = Symmetric; I_{mol} is the total molecular nuclear spin and L the rotational quantum number (after ref. 23)*

Substance	m (amu)[a]	ϵ (K)[b]	σ (Å)	ϵ/σ^3 (atm)	$N_a\sigma^3$ (cm^3/mole)[c]	η[d]
H	1.008	6.46	3.69	17.5	30.2	0.547
D	2.014	6.46	3.69	17.5	30.2	0.274
^{3}He	3.016	10.22	2.556	83.39	10.06	0.2409
T	3.016	6.46	3.69	17.5	30.2	0.183
^{4}He	4.003	10.22	2.556	83.39	10.06	0.1815
H_2	2.016	37.0	2.92	202.5	15.0	0.0763
D_2	4.028	37.0	2.92	202.5	15.0	0.0382
Ne	20.18	35.6	2.74	235.8	12.4	0.0085
Ar	39.95	120.0	3.41	412.3	23.9	0.00088

a) 1 amu = 1.66024×10^{-27} kg.

b) $k = 1.38054 \times 10^{-16}$ JK^{-1}

c) $N_a = 6.02252 \times 10^{23}$ particles/mole

d) $\hbar = 1.05430 \times 10^{-34}$ Js

table 1.2.2 *Some (interaction) parameters for atomic hydrogen and other simple systems. η = quantum parameter, ϵ coupling constant, σ the 'core diameter', ϵ/σ^2 and $N_a\sigma^3$ (after Miller and Nosanow[41]).*

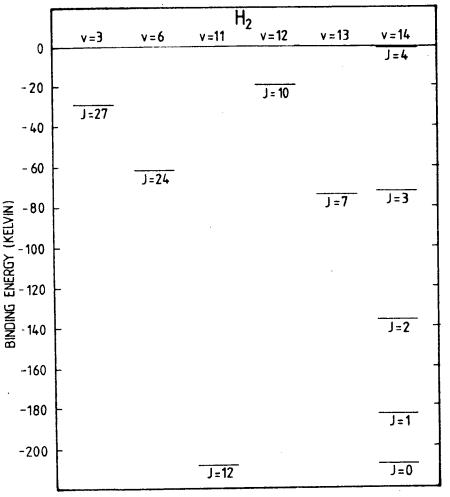

fig.1.2.3 Rotation-vibration levels of singlet potential near the dissociation limit (after Silvera and Walraven[23]).

In a magnetic field the hamiltonian eq.1.2.5 is extended with the Zeeman energy of the electrons. With respect to the total electrons spin $\vec{S}=\vec{s}_1+\vec{s}_2$ (capital letters indicate total spin, lower case letters indicate atomic spins) one finds that the degeneracy in the triplet manifold (S=1, m_s=-1,0,1) is removed, and depending on the field the lowest potential curve (m_s=-1) is shifted below the singlet potential (see fig.1.2.2b). The crossing of the singlet and triplet, m_s=-1 is given by the condition (r_c the inter atomic separation and E_c the energy at the crossing):

$$V^t(r_c)-2*g_e\mu_B B = V^s(r_c) \quad , \; E_c \equiv V^s(r_c). \tag{1.2.6}$$

For example at B=10T, $r_c \simeq 4.2$Å.

In first instance the influence of the nuclear spin of both the protons in the molecule is expressed in the restriction on the orbital part of the wave function as soon as the total nuclear spin is fixed (see tab.1.2.1). If the intra-atomic hyperfine interaction is included in the hamiltonian eq.1.2.5, the restrictions on the total molecular states are more complicated. In principle 16 different nuclear- and electronic spin states lead to 16 different hyperfine potentials.[33-35] At zero-field only 11 are distinct. In homo-nuclear molecules for B>0, there are 16 different potentials.

To illustrate the influence of the hyperfine interaction on the interatomic potential, let us consider the effective hamiltonian of two atoms in a magnetic field:

(1.2.7)

$$H = V_D(r_{12}) + J(r_{12})\ \vec{s}_1 \cdot \vec{s}_2$$
$$+ g_e\mu_B \vec{B} \cdot (\vec{s}_1 + \vec{s}_2) - g_n\mu_n \vec{B} \cdot (\vec{I}_1 + \vec{I}_2)$$
$$+ a\ \vec{I}_1 \cdot \vec{s}_1 + a\ \vec{I}_2 \cdot \vec{s}_2.$$

The first part describes the interatomic potential obtained by ab initio calculations; the second part is the Zeeman energy of the electrons and protons in an external field B and the third part the intra-atomic hyperfine interaction (when the atoms are very close together one has to account for hyperfine coupling between electrons and nuclei on different atoms as well; these interactions will be neglected here).

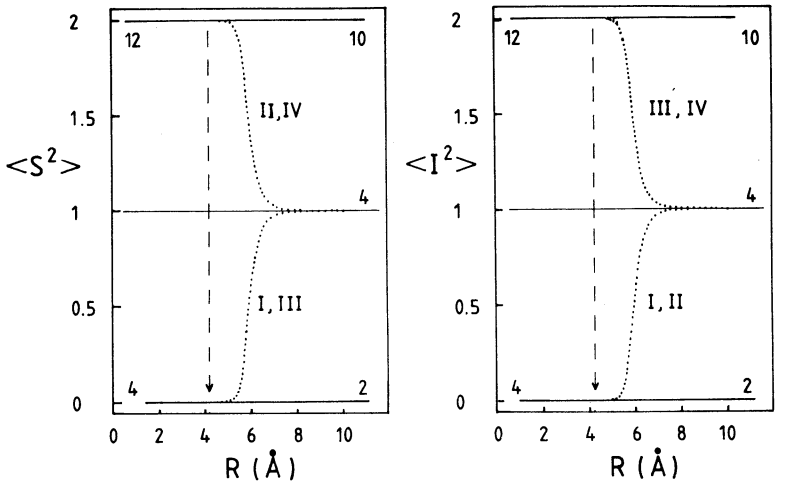

fig.1.2.4 Expectation values $\langle S^2 \rangle$ and $\langle I^2 \rangle$ for the 16 hyperfine molecular spinstates (see eq.1.2.7) at a field of B=10T (numbers indicate multiplicity). The four levels that change character as function of the distance are indicated and are represented at small distance by ($|S,M_S\ I,M_I\rangle$):
I - $|0,0\ 0,0\rangle$, II - $|1,0\ 0,0\rangle$, III - $|0,0\ 1,0\rangle$, IV - $|1,0\ 1,0\rangle$.
The dashed line indicates the position of the singlet-triplet potential crossing (see fig.1.2.5).

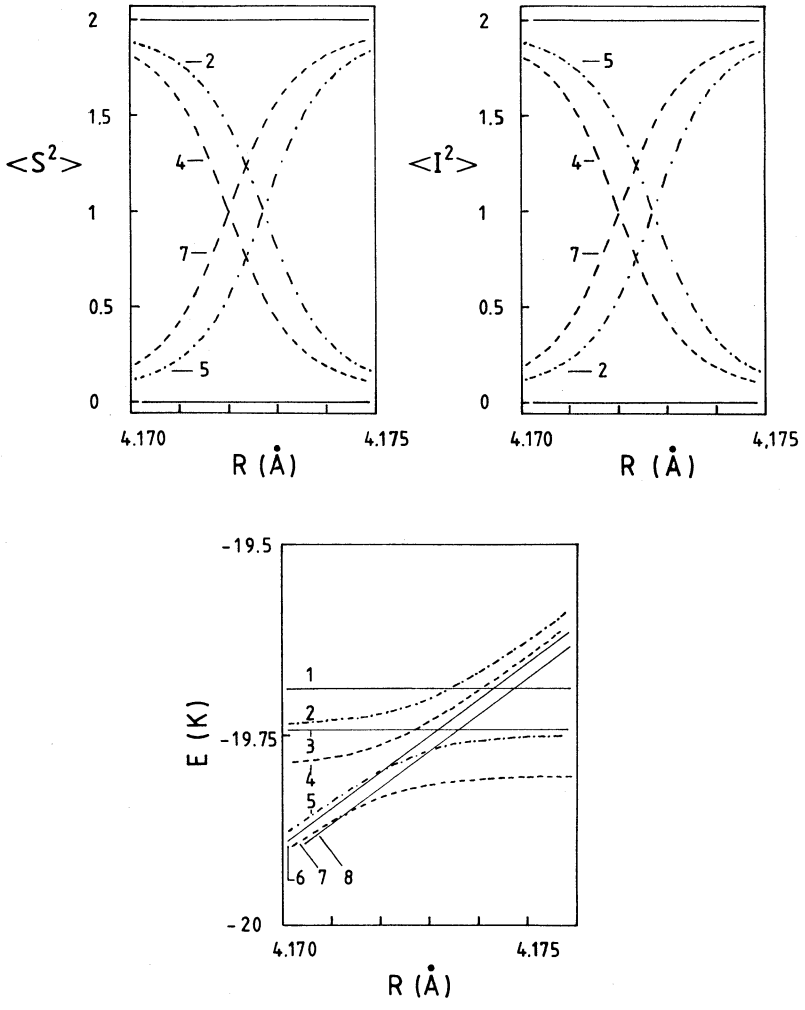

fig.1.2.5 Molecular hyperfine states near the singlet-triplet crossing at B=10T. The two pairs (2,5) (M_F=1) and (4,7) (M_F=0) display an avoided crossing.
At small distances the states are represented by (S,M_S I,M_I):
1 - (1,1 1,1) 2 - (1,1 0,0) 3 - (1,1 1,0) 4 - (1,1 1,-1)
5 - (0,0 1,1) 6 - (0,0 1,0) 7 - (0,0 0,0) 8 - (0,0 1,-1)

The hamiltonian eq.1.2.7 has two well defined limit regions. For small separations, the interatomic potential is dominant, and we expect the spin states to conform to the situation in the previous sections. At large separation, the potential part can be neglected with respect to the intra-

atomic hyperfine interaction. Thus the spin states are described as a pair of atoms in specific hyperfine states. In the intermediate regime neither the total spin variables $\vec{S}$ and $\vec{I}$ or the total atomic spins $\vec{f}_1$, $\vec{f}_2$ provide proper quantum numbers. This aspect is illustrated in fig.1.2.4, where the total electron spin ($<\vec{S}^2>=S(S+1)$) and nuclear spin ($<\vec{I}^2>=I(I+1)$) is plotted as function of the separation. It follows that the transition region between the mentioned limits is roughly between r_0=10 - 14 a.u. (5.2-7.3Å). The total momentum of the system, including orbital momentum, is conserved. For a particular choice of the orbital momentum this implies conservation of the total spin projection: $M=m_S+m_I$ for any separation. The influence on the potential curves in the neighborhood of the triplet minimum is rather limited. It displaces the potentials by amounts typically of the order of the hyperfine coupling constant (a/k≈68mK) and each level in fig.1.2.2b is split into 4 levels.

The crossing point of the triplet and singlet potentials (eq.1.2.6) is also of interest. The hyperfine interactions introduce a mixing of the various states. This is illustrated in fig.1.2.5 for a field of B=10T. The states with the same M value lead to an 'avoided' crossing and a change of the character of those states.

The hyperfine potentials derived above are obtained in the limit of very slow relative motion of the atoms. In problems where the transition rates between the various molecular states are calculated due to a perturbation (e.g. magnetic relaxation due to dipolar coupling between the spins) one has to take into account the relative motion due to the thermal conditions of the gas. If the relative velocity is large, the interaction between the atoms can be treated in the 'sudden approximation',[36] i.e. the (spin) states of the incoming atoms are determined by the hyperfine states of the incoming pair. As a result the relative potential between the atoms can be approximated by projecting the incoming hyperfine states on a singlet and triplet part. For very slow relative motion the incoming pair state adiabatically follows the changing separation and the relative potential is determined by one of the hyperfine potential curves described above. The transition between the two regimes can be estimated by using a simple criterium for the regime where the sudden approximation holds (see e.g. Messiah[36]):

$$\tau \ll \hbar / \Delta\mathcal{H}, \tag{1.2.8}$$

where τ the interaction time and $\Delta\mathcal{H}$ the variance of the time dependent interaction:

$\Delta\mathcal{H} \equiv (<0|\mathcal{H}|0>^2 - <0|\mathcal{H}^2|0>)^{1/2}$.

With

$$\mathcal{H} = (1/\tau) \int (H_0 + H(t)) \, dt$$

the 'average' hamiltonian during the interaction. Using the exchange interaction $J(r)\vec{s}_1.\vec{s}_2$ as the time dependent part of the hamiltonian one finds: $\Delta H^2 \simeq (1/4)\ J^2$ with $J = (1/(r_1-r_2)) \int J(r)\ dr \simeq 45mK$ for r_1=5.2Å and r_2=7.3Å. Simply using the average thermal velocity $\bar{v} = (8kT/(\pi m))^{1/2}$ to estimate τ: $\tau \simeq (r_2-r_1)/\bar{v}$, eq.1.2.8 results in a relative velocity of 0.65m/s and T<20μK. Although one has to do a better calculation than the simple estimate above, it illustrates that the sudden approximation remains valid to very low temperatures. At low temperatures the influence of the form of the potential on the motion of the atoms becomes important and has to be accounted for.

Apart from the interatomic potentials described above, also dipolar interactions between the spins of the two atoms are important. They can induce transitions between the various hyperfine levels. The dipolar coupling between two magnetic moments $\vec{\mu}=\gamma\hbar\vec{s}=g_i\mu_i\vec{s}$ where $\vec{s}$ can be an electron or a proton of any of the two atoms, is given by:[37]

$$V_{\mu_1\mu_2}(\vec{r}_{12}) = -\ (\mu_0/(4\pi r_{12}^3))\ [\ \vec{\mu}_1.\vec{\mu}_2 - 3(\vec{\mu}_1.\vec{r}_{12})(\vec{\mu}_1.\vec{r}_{12})]. \qquad (1.2.9)$$

The dipolar coupling between spins will be treated in more detail in relation with the dipolar relaxation mechanism in chapter 2,3.

1.2.3 Quantum degeneracy; Bose Einstein Condensation

A gas of atomic hydrogen from a statistical physics point of view should behave as an (interacting) Bose gas,[38] since it consists of two tightly bound fermions. Let us for the time being assume that indeed the interactions are so weak that the gas can be treated as an ideal Bose gas. Such an ideal Bose gas has been the topic of quantum statistical physics[39] and shows a peculiar transition for the occupation of the zero-momentum state (Bose Einstein Condensation, BEC). Fig.1.2.6 gives some thermodynamical properties for a three dimensional ideal Bose gas near this transition. The transition occurs for an ideal Bose gas with atomic hydrogen mass (m) at:

$$T_c = (\ (2\pi\hbar^2)/(mk))\ [\ n/g_{3/2}(1)\ ]^{2/3},\ n_c = g_{3/2}(1)\Lambda^{-3} \qquad (1.2.10)$$

and for the pressure:

$$p_c = nkT\ (\ g_{3/2}(1)/g_{5/2}(1)),$$

where $g_{3/2}(1)\simeq 2.612$ and $g_{5/2}(1)\simeq 1.342$ are constants and $\Lambda=[(2\pi\hbar^2)/(mkT)]^{1/2}$ the thermal wavelength. In general the constants are defined by $g_\sigma(z)=\Sigma_{l=1,\infty} z^l/l^\sigma$ (σ=3/2, 5/2). It is assumed that only one of the two lower hyperfine states is occupied and thus that the states are not degenerate. Roughly speaking, the transition is achieved when the thermal wavelength equals the

interatomic distance.

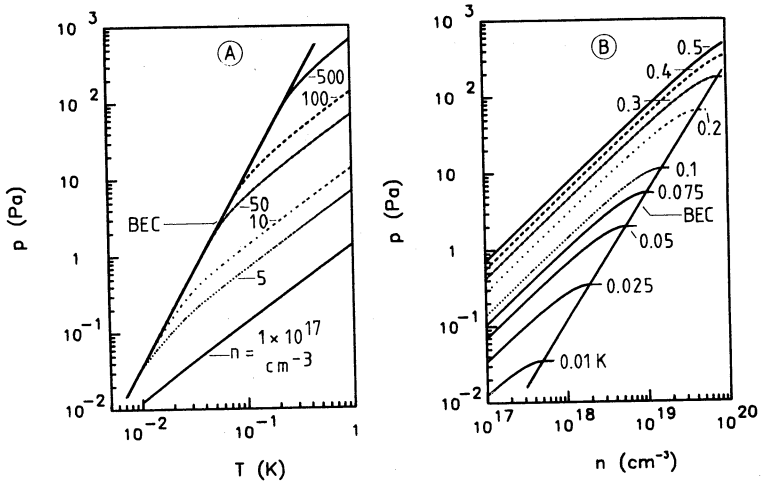

fig.1.2.6 Some thermodynamic properties of the ideal H↓↕ Bose-gas. a) Isochores b) Isotherms.

Let us now examine the influence of the interactions between the hydrogen atoms. As discussed in the previous section, the $^3\Sigma_u^+$ potential between two hydrogen atoms has a very shallow van der Waals minimum and furthermore, atomic hydrogen is a very light atom. In fig.1.2.7 the $^3\Sigma_u^+$ potential is compared with the attractive potential between two helium atoms and in tab.1.2.2 the various parameters of atomic hydrogens and some well known (rare) gases are given. With the use of the quantum corresponding states theory (de Boer et al.[40]) one can compare the various gases and their thermodynamic properties. The inter atomic potentials are expressed in such a way (e.g. Lennard Jones form: $V(r) = 4\epsilon[(\sigma/r)^{12} - (\sigma/r)^6]$, see table 1.2.2) that the free energy (F) can be written in reduced variables T^* and V^*: $F^*(T^*,V^*)$. Nosanow and co-workers[41] extended this theory by including the parameter η: $\eta = \hbar^2/(m_H\epsilon\sigma^2)$ as an additional variable to F^*. η correlates the kinetic energy of the particles and the well depth of the potential. Analysis of the generalized phase diagrams lead to the conclusion that H↓ should remain gaseous down to T=0K under equilibrium pressure and only at a pressure of p=54bar[41] will it display a phase transition directly to the solid state. The precise influence of the potential has to be calculated in more detail. This has been done in hard sphere approximation for the potential (see tab.1.2.2).[42] This treatment is only applicable when the interactions are weak. One can then calculate the various thermodynamic and transport properties. Ref. 22 gives a comprehensive overview of these

properties. Also Monte Carlo calculations of the equation of state for H confirm the weak interaction nature of the H system at high field.[43]

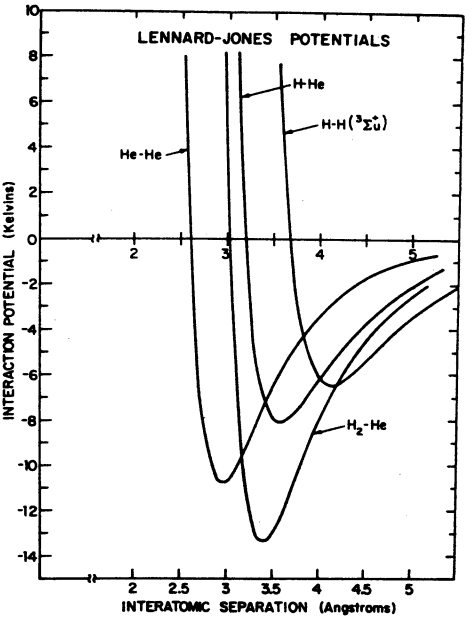

fig.1.2.7 Comparison of the H-H triplet interaction and some other Lennard-Jones potentials.

The transport properties of the H-gas have been studied theoretically by a number of authors.[44,45] Especially the spin-waves in (doubly) spin-polarized hydrogen attracted attention[46,45] and will probably be studied more extensively in the coming years. To treat all the different contributions would reach outside the scope of this thesis. The mentioned review articles[20-23] will give further references.

One of the difficulties with systems other than H↓ in tab.1.2.2 is that those systems do not interact weakly; the hard sphere approximation is limited. Furthermore, due to the gaseous nature of H↓, the density can be varied over a wide range (compare e.g. with ^{4}He, which is a liquid under BEC conditions). The atomic hydrogens form a tempting exception.

1.3 Destabilization processes in H↓

The stability of atomic hydrogen is determined by a number of processes. The various channels by which it can recombine to the molecular state will be treated briefly in this section.

1.3.1 Recombination in H↓

The stability of a gas of hydrogen atoms is limited; the characteristic time to recombine to the molecular state depends strongly on the temperature, the field and the density and on the geometry of the experimental cell. Jones et al.[1] showed that two H atoms have a very small possibility to recombine by emission of electromagnetic radiation, hence two atoms can only recombine to a (highly excited) molecular bound states (H_2^*) if the conservation of energy and momentum in the system is fulfilled by the presence of a third body (X): $H + H + X \rightarrow H_2^* + X$.

At sufficiently high temperature (e.g. at room temperature) the formation of long-lived meta-stable states (H_2') is the most important channel.[47] Further transition of the H_2' state to the H_2^* state occurs when H_2' interacts with X before decomposing into two atoms again. The position of the H_2' levels is well above the dissociation level and these levels are not occupied at low temperatures (T<1K).

At low temperatures the third-body has to be present at the time the two (potentially) recombining atoms meet. This third body can in principle be any body present in the cell. When X is another hydrogen atom, one obtains from simple kinetic gas arguments that the reaction rate of a gas of atoms is proportional to the cube of the density:

$$dN_v/dt = - K_3 n_v^2 N_v. \qquad (1.3.1)$$

With N_v the total number of atoms in the volume, K_3 the reaction rate and n_v the H-gas density.

Helium is usually present in the low temperature stabilization cells. This may form the third-body in the bulk if there is a He vapor pressure present (density n_{He}; e.g. the saturated vapor pressure for ^4He becomes appreciable for T≥0.9K). The recombination rate is in this case proportional to the square of the H density:

$$dN_v/dt = - K_{He} n_{He} n_v N_v. \qquad (1.3.2)$$

The essential role of the helium film in the cell is to prevent the accumulation of hydrogen atoms on the wall. Nevertheless a helium surface has a (small) adsorption energy for H atoms (see next section), and a certain surface density n_s of H atoms builds up on the walls. For these atoms the wall plays the role of a third body:

$$dN_s/dt = - K^s n_s N_s. \qquad (1.3.3)$$

To first order the relation between the bulk- and surface densities is determined by an isotherm (see section 1.3.2 for more details):

$$n_s = n_v \Lambda e^{E_a/kT}. \qquad (1.3.4)$$

The decay of the total number of particles $N=N_v+N_s$ is expressed in terms of the various contributions in a rate equation:

$$(1/V)\ dN/dt = -\ K_{He}^{eff}\ n^2 - K_3^{eff}\ n^3. \qquad (1.3.5)$$

With

$$K_{He}^{eff} = K_{He}\ n_{He} + (A/V)\ K^s\ [\ \Lambda\ e^{E_a/kT}\ ]^2$$

and

$$K_3^{eff} = K_3 \qquad + (A/V)\ K_3^s\ [\ \Lambda\ e^{E_a/kT}\ ]^3,$$

where A/V is the surface to volume ratio. The effective rates K^{eff} are defined by making use of eq.1.3.4 and are useful to express the influence of the surface processes on the bulk densities, since in most experiments the bulk properties (e.g. pressure) are measured.

Up to now the influence of the magnetic field on the recombination rates has not been included. Its influence can be appreciated by looking at fig.1.2.1 and fig.1.2.2. In a strong magnetic field and at low temperature only the two lowest hyperfine states |a> and |b> with electron spins 'down' are occupied (e.g. at B=10T and T=0.5K $n_c/n_b=\exp[-(g_e\mu_B B)/(kT)]\simeq 2\times10^{-12}$). Such a gas of a and b state atoms is usually denoted by H↓; electron spin polarized atomic hydrogen. The interactions between atoms with parallel electron spins proceeds via the triplet potential V^t with $m_s=-1$ (see fig.1.2.3). The transition probability from this triplet state to the singlet state of the bound molecule is suppressed, because the overlap of the incoming states and the resulting molecular state is limited. In fact the transition has to be mediated by a perturbation (e.g. dipolar coupling between the spins) or by mixing of the states (e.g. intra-atomic hyperfine interaction).

In an open cell geometry another possible destabilization process is the thermal escape from the cell. As is treated in detail by Walraven and Silvera[48], the gradient in the magnetic field will work to compress the hydrogen atoms in the two lowest hyperfine states to the highest field regions, resulting in a density profile as a function of magnetic field and cell temperature:

$$n = n(0)\ e^{-(B_0-B)\mu/kT} \qquad (1.3.6)$$

$$\equiv n(0)\ C_M(z)^{-1},$$

where $C_M(z)$ is the magnetic compression factor.

The thermal escape from this magnetic bottle is a first-order process

with a typical decay time:

$$\tau = 4C_M V_{eff} / (K\bar{v}A), \qquad (1.3.7)$$

where C_M is the magnetic compression factor, V_{eff} the effective volume of the cell, A the area of the cross-sectional area of the filling tube, K the Clausing factor and $\bar{v} = (8kT/(\pi m))^{1/2}$ the average thermal velocity. For a typical cell with V_{eff}=1cm^3, A=0.125cm^2 (Φ=6mm), K≈0.1 and B_0-B≈2T at T=300mK this gives a characteristic time: τ=330s. The time τ is usually longer because the fluxing vapors of helium result in an additional compression.[48] For closed geometries as applied e.g. in the compression experiments the thermal escape is suppressed.

1.3.2 Surface and volume

Hydrogen atoms have a single bound state on a (saturated) helium surface with adsorption energies of ≈1K for pure ^{4}He surfaces and ≈0.4K for ^{3}He surfaces or ^{3}He/^{4}He mixtures.[49] The behavior of the adsorbed hydrogen atoms and the bound states has been the topic of a number of papers.[50] One of the theoretical difficulties is the calculation of an accurate value for the binding energy and the bound state wave function. Calculations of the chemical potential of an H atom inside bulk ^{4}He show a positive value of 40.0K,[51] indicating that the H atoms will be kept outside the bulk liquid at low temperature.

A simple approximation of the H atom liquid helium interaction is obtained by assuming a stepwise interface and taking the liquid helium to be continuous. Integration of the H-He Lennard-Jones potential (σ=3.19Å, ϵ=6.57K, see section 1.1) over a half-sphere results in a potential: $V_{H-\ell He}(r)=C_9/r^9 - C_3/r^3$ with $C_9=n_{He}(4\pi\epsilon\sigma^{12})/45$ and $C_3=n_{He}(4\pi\epsilon\sigma^6)/6$.[52] This potential gives an adsorption energy of E_a=0.36K on ^{4}He (for liquid helium $n_{He} \simeq 2.18\times10^{22}cm^{-3}$), clearly in discrepancy with the observed value of E_b≈1.K. Mantz and Edwards[50] calculated the states and binding energy taking into account a density profile for the interface. They obtain E_a=0.63K, a value close to the observed one. The state itself has its maximum probability density at ≈6.0Å and extends beyond 15Å from the interface.

The equilibrium between the gas system and the system adsorbed on the surface is determined by posing the equilibrium condition for the chemical potential of the gas (μ_g) and that of the surface system (μ_s). For the gas phase one may use the ideal Bose gas approximation for μ_g as long as the density is low ($\Lambda^3 \ll n_c^{-1}$). The adsorbed atoms are in first approximation described as a two-dimensional gas, resulting in the following surface coverage and volume density in terms of the chemical potentials μ_v and μ_s in the bulk and on the wall respectively:[53]

(1.3.8)

$$n_v\Lambda^3 = g_{3/2}\{\exp(\mu_v/kT)\}$$

$$n_s\Lambda^2 = \ln\{1 - \exp((\mu_s + E_a)/(kT))\} = g_1\{\exp((\mu_s + E_a)/(kT))\}.$$

In thermodynamic equilibrium $\mu_v=\mu_s=\mu$ and the adsorption isotherm is than derived by eliminating μ from eqs.1.3.8. For conditions where the classical Boltzmann limit is valid ($\Lambda^3 \ll n_c^{-1}$), the functions g_1 and $g_{3/2}$ can be approximated by the first term of their expansion in (μ/kT) and one obtains eq.1.3.4. Due to the Bose nature of the atoms, eq.1.3.6 leads to a surface coverage that is higher than the classical expression eq.1.3.4. (the opposite is true for fermions).

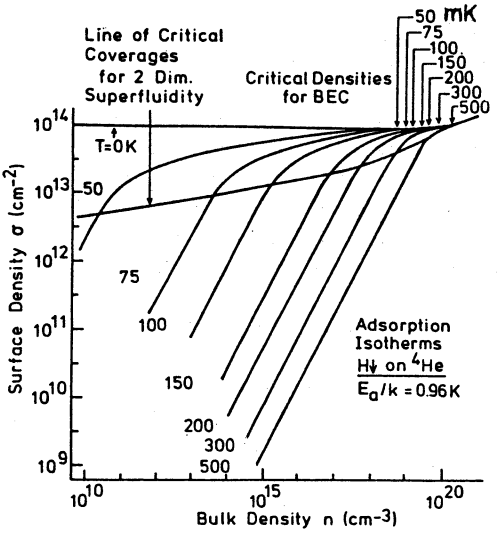

fig.1.3.1 Adsorption isotherms of H on a ^{4}Helium surface (after Silvera and Walraven[23]).

If the interaction between the hydrogen atoms is included,[53] the isotherms show a saturation of the surface coverage (fig.1.3.1). This saturation is essential when one aims at BEC. As can be seen from fig.1.3.1 the BEC conditions in the gas phase (indicated by an arrow) are attained under conditions where the surface is saturated. Presently the estimated saturation coverages are: $\sigma_{sat}=1\times10^{14}cm^{-2}$ on a ^{4}He surface and $\sigma_{sat}=3.5\times10^{15}cm^{-2}$ on a ^{3}He surface.[23]

The film thickness (d) of a saturated helium film depends on the height (h) of the film position above the free surface of helium: $d=k.h^{(-1/n)}$ (with $k\simeq3\times10^{-6}$ and $n\simeq2.3$-2.6, depending on the substrate (see e.g. Wilks[54])). In a

typical hydrogen stabilization cell d is well above 200Å. For unsaturated films the situation is different. Recently the binding energy of hydrogen has been studied as a function of film thicknes,[55] showing that a substantial increase of E_a is measured for films thinner than 10Å. Qualitatively, one expects influences on the binding energy as soon as the interaction between H and substrate become noticeable, or indirectly if the properties of the interface (helium density, profile etc.) are influenced.

1.3.3 State dependent recombination

The drastic reduction of the recombination in a magnetic field (see section 1.3.1.) was associated with the limited overlap of two atoms in the triplet m_s=-1 with the molecular singlet state. Due to the hyperfine mixing (section 1.2.1) the electron spin polarization in the lowest hyperfine state |a> is not complete, but proportional to the mixing parameter ϵ. As a result the recombination probability for a,a and a,b pairs is larger than for a pure b,b pair. When the initial a- and b-state populations are equal, the a-state population is more rapidly depleted than the b-state and a gas builds up of predominantly b-state atoms. Since both the electron- and nuclear-spin are polarized in the b-state, one calls this doubly polarized hydrogen (H↓↑). The decay is analyzed by introducing the recombination rates K_{ab}^{eff} and K_{aa}^{eff} for the a,b and the a,a process respectively:

(1.3.9)

$$(1/V)\ dA/dt = -2\,K_{aa}^{eff}\,a^2 - K_{ab}^{eff}\,ab + G_{ab}^{eff}\,(a+b)(b-a) + G_{imp}(b-a)$$

$$(1/V)\ dB/dt = -K_{ab}^{eff}\,ab - G_{ab}^{eff}\,(a+b)(b-a) - G_{imp}(b-a).$$

If indeed only the recombination terms in eq.1.3.9 determined the decay of the gas, the system would ultimately only consist of b-state atoms and the gas would be perfectly stable. However, a number of magnetic relaxation processes may induce transitions between the b-state and the other hyperfine states (see fig.1.1.1). Especially the transition between b,a acts to maintain the equilibrium polarization between the a- and b-state. This relaxation process is also included in eq.1.3.7, with relaxation rate G_{ab} due to dipolar coupling between H atoms and G_{imp} due to (ferro) magnetic impurities in or on the wall of the cell. The dipolar coupling between the atoms occurs between atoms in the bulk and also between adsorbed particles, leading to an effective rate G_{ba}^{eff}, analogously to the effective recombination rates.

For B≤10T the energy difference between the a and b level is in the order of ≃60mK and thus at T>≃100mK the a- and b-state are equally populated in thermal equilibrium. The competition between the state-dependent

recombination and the relaxation determines the final degree of double polarization that is obtained. In the case that the relaxation is much faster than the recombination, e.g. by relaxation of the spins due to interactions with magnetic impurities on the wall (G_{imp}), the recombination rate in H↓ is expressed by ($n_a=n_b=n/2$):

$$K^{eff} = (K_{aa}^{eff} + K_{ab}^{eff})/2. \qquad (1.3.10)$$

In a doubly polarized system the stability is determined by the intrinsic relaxation rate from the b- to a-state ($G_{imp}=0.$). In that case eq.1.3.9 reduces to:

$$(1/V)\ dB/dt = -2\ G_{ba}^{eff}\ b^2 \quad , \text{where} \quad b \approx n. \qquad (1.3.11)$$

At low temperature the surface contribution will dominate G_{ab}^{eff}, and in the first experiments with H↓↑ this was directly used to obtain G_{ab}^{s} at low temperature (see chapter 2,3). Despite extensive theoretical calculations on the various processes that could contribute to G_{ab}^{s},[56] the observed and calculated values differed more than a factor of 50. In the next section this discrepancy will be removed by considering third-order surface recombination, as was first suggested by Hess et al.[19] The detailed analysis of the decay of H↓↑ will be treated in relation with the magnetic clean cell in chapter 2. Giving information on the G_{ab} and the ratio $\gamma=K_{aa}/K_{ab}$.

Also b→c electronic relaxation is possible (rate constant $G_{bc}^{\uparrow}$). The energy difference between the c- and b-level at high field (e.g. 13.4K at 10T) is much higher than the ambient temperature and the relaxation requires thermal activation. In thermal equilibrium the population of the c and d levels is determined by the Boltzmann factor: $\exp(-g_e\mu_B B/kT)$. Only at high temperature and/or low magnetic fields this relaxation process becomes important, and due to its exponential increase as function of temperature can lead to instabilities in the gas (see chapter 4-6). The reverse process, c→b relaxation (rate constant $G_{bc}^{\downarrow}$), is not suppressed by the Boltzmann factor and leads to fast relaxation from the c to b level. A more detailed analysis will be postponed until chapter 6.

1.3.4 Three-body recombination

In the picture described in the previous section only second-order (and first-order if we include impurity relaxation and thermal escape) processes were taken into account. For temperatures below ≈800mK this means that the recombination processes only occur between adsorbed particles and that the relaxation processes occur in the bulk or for adsorbed particles, depending on the temperature and the resulting surface coverage.

At sufficiently high gas densities however, a new destabilization process becomes important; recombination in the bulk with another H-atom as

third body to conserve energy and momentum (eq.1.3.1). These third-order processes were observed for the first time in the compression experiments (see chapter 4-6), indicating that at BEC conditions they will determine the stability of the sample. A number of considerations that were made in section 1.3.2 for second-order recombination also hold for third-order. Kagan et al.[57] calculated the various possible third-order recombination processes.

In H↓ third-order recombination occurs between triples where some of the atoms are in mixed hyperfine states (i.e. a or c). The driving mechanism is, analogous to the K_{aa} and K_{ab} second-order recombination, the so called 'exchange recombination'. Examples are K_{abb},K_{aab} etc. As soon as the c and d-state become occupied (low magnetic field and/or high temperature) also third-order 'exchange recombination' with one of the atoms in the c (d) state becomes important (e.g. K_{bbc}). In principle there are 20 different triples, see chapter 4-6. The exchange recombination processes K_{abb}, K_{aab} and K_{aaa} processes are suppressed as the field increases.

A third-order recombination term exists between three H-atoms in the b-state (K^v_{bbb}). Kagan et al. suggest that it is driven by the dipolar coupling between the three different H-atoms. Clearly, this destabilization process is very important for the limitations to obtain BEC. Measurements (see chapters 4-6) indicate that $K^v_{bbb} \simeq 1.2 \times 10^{-39} cm^6 s^{-1}$ at B=10T is only weakly temperature dependent and decreases as function of magnetic field. The predicted magnetic field dependence shows an increase of a factor of two between 5 to 10T, and a maximum near 20T,[58] there is a factor of nearly 2 difference between the theoretical value and the observed one.

An additional complication in the analysis of these third-order terms is the fate of the third H-atom that is not recombining. As follows e.g. from the calculation of K_{bbb} the third atom predominantly is left in the c-state ('double spin flip', occurring with a fraction of θ=0.93;a fraction 1-θ leaves in the b-state),[57,58] the Zeeman energy needed for this double spin flip is provided by the energy difference between the incoming states and the outgoing (bound) molecule + third atom. Subsequently this c-state atom can recombine, or change to an other hyperfine state by relaxation. Which will be the most important, depends on field, temperature and geometry of the cell. In principle all the other third-order processes may be associated with different hyperfine states of the outgoing third atom. This is discussed in more detail in chapter 6.

The third-order b-state recombination also occurs between the adsorbed atoms (rate $K^s_{bbb}=4 \times 10^{-25} cm^4 s^{-1}$, see chapter 2) and will determine the stability of the H↓↑ gas at low temperature and high density. Another aspect of K^s_{bbb} is its influence on the low (bulk) density decays. In section 1.3.2 it was discussed that by measuring the decay rate of a doubly polarized gas at low temperature the surface relaxation rate G^s_{ab} was obtained. However, the three-body K^s_{bbb} will also be present. The extrapolation of the surface three-body rate K^s_{bbb} as measured in high density to the density regime

where most of the experiments were performed which determined G^s_{ab} indicates that K^s_{bbb} is still the dominant stability determining process even at these lower densities. This misinterpretation of the low temperature decays was first noted by the M.I.T. group.[19] Reanalyzing the old data in this light gives reasonable agreement with theory for G^s (see chapter 2). Thus a long standing discrepancy between theory and experiment of the surface relaxation rates seems to be settled. Recent direct measurements of the decay of the surface coverages by ESR techniques at very low temperatures, confirms the picture described above.[14] In chapter 2 some of the re-analysis of our own measurements will be presented, including a more detailed analysis of the field dependence.

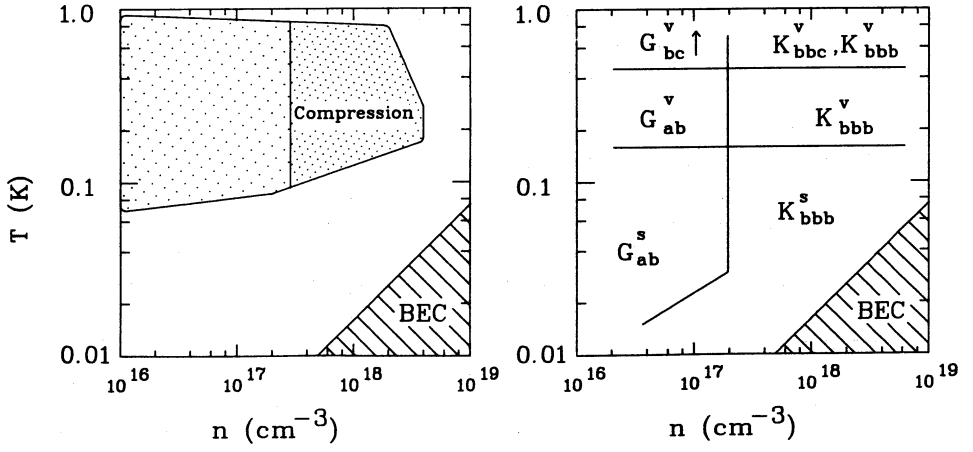

fig.1.4.1 a) Shaded area indicates the experimentally accessed region. Double shaded area indicates the region accessed using compression techniques.

b) Dominant decay processes in doubly polarized atomic hydrogen (H↓↑) in a magnetic field (B≈8T).

1.4 Limitations on high density

Before embarking on a detailed description of the experiments and their analysis, let us summarize the known destabilization processes, focussing on the limitations to obtain high density. The highest stability of the gas is obtained for a doubly polarized system (H↓↑). In H↓↑ the destabilization processes are restricted to (see fig.1.4.1):

- relaxation processes from the b-state to the other hyperfine states (b→a,b→c). The electronic transition (b→c) can be suppressed by working at low temperature and/or high field.
- recombination processes with three b-state atoms (rate constant $L_3=7\times10^{-39}cm^6s^{-1}$ at B=10T).

At low enough temperatures, where the surface coverage is substantial, the surface third-order recombination (rate constant $L_3^s\simeq4\times10^{-25}cm^4s^{-1}$) is dominant and will determine the stability of the gas. Using the saturated surface coverage $\sigma_{sat}=1\times10^{14}cm^{-2}$ for ^4He surface leads to a typical half-lifetime of 72ms in a bubble compression technique as developed in chapters 4-6 at BEC conditions with T=100mK ($n_c=1.6\times10^{19}cm^{-3}$) and B=10T. Although these are short life times, it is in principle not impossible to observe some of the fascinating quantum properties during such a decay. Another important problem is the released recombination energy for such a decay rate (56μW in a $1mm^3$ bubble), which has to be removed from the gas. Any heating of the gas will finally end in the occupation of the c,d states and the exponentially growing contribution of the destabilization processes associated with them. The thermal problems will be the subject of chapter 7.

Although these prospects are not very promising, a number of new ideas are being developed to beat the problems to obtain the BEC conditions. They will be discussed in the final chapter of this thesis.

References

1 C.E. Hecht, Physica 25, 1159 (1959).
J.T. Jones Jr., M.H. Johnson, H.L. Meyer, S. Katz and R.S. Wright, Aeronutronic Systems Inc. Publ.u-216 (a subsidiary of Ford Motor Company), 1 (1958).
M.W. Windsor, 'Formation and Trapping of Free Radicals', editors A.M. Bass, H.P. Broida, Academic Press, New York (1960).

2 R.L. Danilowicz, J.V. Dugan and R.D. Etters, J.Chem.Phys. 65, 498 (1976).

3 T.D. Lee, K. Huang and C.N. Yang, Phys.Rev. 106, 1135 (1957).

4 I.F. Silvera and J.T.M. Walraven, Phys.Rev.Lett. 44, 164 (1980).

5 R.W. Cline, D.A. Smith, T.J. Greytak and D. Kleppner, Phys.Rev.Lett. 45, 2117 (1980).

6 W.N. Hardy, M. Morrow, R. Jochemsen, B.W. Statt, P.R. Kubik, R.M. Marsolais, A.J. Berlinsky and A. Landesman, Phys.Rev.Lett. 45, 453 (1980).
M. Morrow, R. Jochemsen, A.J. Berlinsky and W.N. Hardy, Phys.Rev.Lett. 46, 195 (1981) ; Erratum 47 (1981) 455.

7 J.T.M. Walraven, I.F. Silvera and A.P.M. Matthey, Phys.Rev.Lett. 45, 449 (1980).
A.P.M. Matthey, J.T.M. Walraven and I.F. Silvera, Phys.Rev.Lett. 46, 668 (1981).

8 G.H. van Yperen, A.P.M. Matthey, J.T.M. Walraven and I.F. Silvera, Phys.Rev.Lett. 47, 800 (1981).

9 R. Jochemsen, M. Morrow, A.J. Berlinsky and W.N. Hardy, Phys.Rev.Lett. 47, 852 (1981).

10 B.W. Statt and A.J. Berlinsky, Phys.Rev.Lett. 45, 2105 (1980).

11 R.W. Cline, T.J. Greytak and D. Kleppner, Phys.Rev.Lett. 47, 1195 (1981).

12 R. Sprik, J.T.M. Walraven, G.H. van Yperen and I.F. Silvera, Phys.Rev.Lett. 49, 153 (1982).

13 G.H. van Yperen, I.F. Silvera, J.T.M. Walraven, J. Berkhout and J.G. Brisson, Phys.Rev.Lett. 50, 53 (1983).
G.H. van Yperen, J.T.M. Walraven and I.F. Silvera, Phys.Rev.B 30, 2386 (1984).

14 B.W. Statt, W.N. Hardy, A.J. Berlinsky and E. Klein, J.Low Temp.Phys. 61, 471 (1985).
M.W. Reynolds, I. Shinkoda, W.N. Hardy, A.J. Berlinsky, F. Bridges and B.W. Statt, Phys.Rev.B 31, 7503 (1985).

15 B. Yurke, J.S. Denker, B.R. Johnson, N. Bigelow, L.P. Levy, D.M. Lee and J.H. Freed, Phys.Rev.Lett. 50, 1137 (1983).

16 R. Sprik, J.T.M. Walraven and I.F. Silvera, Phys.Rev.Lett. 51, 479 (1983) ;Erratum 51, 942 (1983).

17 R. Sprik, J.T.M. Walraven and I.F. Silvera, Phys.Rev.B 32, 5668 (1985).

18 T. Tommila, S. Jaakkola, M. Krusius, I. Krylov, E. Tjukanov, Phys. Rev. Lett. 56, 941 (1986).
T. Tommila, S. Jaakkola, M. Krusius, K. Salonen and E. Tjukanov, Proceedings LT-17 (Karlsruhe) Elsevier Science Publishers, 453 (1984).

19 H.F. Hess, D.A. Bell, G.P. Kochanski, R.W. Cline, D. Kleppner and T.J. Greytak, Phys.Rev.Lett. 51, 483 (1983).
H.F. Hess, D.A. Bell, G.P. Kochanski, D. Kleppner and T.J. Greytak, Phys.Rev.Lett. 52, 1520 (1984).
D.A. Bell, G.P. Kochanski, L. Pollack, H.F. Hess, D. Kleppner and T.J. Greytak, Physica (LT-17), 449 (1984).
D.A. Bell, H.F. Hess, G.P. Kochanski, S. Buchman, L. Pollack, Y.M. Xiao, D. Kleppner and T.J. Greytak, preprint (1985).

20 I.F. Silvera, Physica 109 & 110B, 1499 (1982) (LT-16).

21 J.T.M. Walraven, Physica 126B, 176 (1984) (LT-17).

22 T.J. Greytak and D. Kleppner, 'New trends in atomic physics', Vol.II G.Grynberg and R.Stora (Ed.), Elsevier Sci.Publ., Les Houches , 1125 (1984).

23 I.F. Silvera, J.T.M. Walraven, Progress in Low Temperature Physics, preprint (1986).

24 see e.g. L.D. Landau, E.M. Lifshitz, 'Quantum Mechanics (Non-relativistic Theory)',Pergamon Press (1977).

25 G. Breit and I.I. Rabi, Phys.Rev. 38, 2082 (1931).

26 G. Herzberg, 'Spectra of Diatomic Molecules', D. van Nostrand Company, (1950).
27 D.M. Bishop, L.M. Cheung Adv.Quan.Chem. 12, 1 (1980).
28 W. Kolos and L. Wolniewicz, J.Chem.Phys. 43, 2429 (1965).
W. Kolos and L. Wolniewicz, J.Chem.Phys. 49, 404 (1968).
W. Kolos and L. Wolniewicz, Chem.Phys.Lett. 24, 457 (1974).
W. Kolos and L. Wolniewicz, J.Mol.Spectr. 54, 303 (1975).
29 W. Kolos, L. Wolniewicz, J.Chem.Phys. 41, 3663 (1964).
30 D.M. Bishop and S. Shih, J.Chem.Phys. 64, 162 (1976).
31 L. Wolniewicz, J.Chem.Phys. 78, 6173 (1983).
32 I. Dabrowski, Can.J.Phys. 62, 1639 (1984).
33 J.E. Harriman, M. Twerdochlib, M.B. Milleur and J.O. Hirschfelder, Proc.Nat.Acad.Sci.USA 57, 1558 (1967).
34 M.B. Milleur, L.A. Curtiss, M. Twerdochlib and J.O. Hirschfelder, J.Chem.Phys. 48, 4261 (1968).
35 Y.H. Uang, R.F. Ferrante and W.C. Stwalley, J.Chem.Phys. 74, 6256 (1981).
36 A. Messiah, 'Quantum Mechanics', North-Holland Publ.Comp., Amsterdam (1970).
37 A. Abragam, 'Principles of Nuclear Magnetism', Oxford University Press (1961).
38 The Bose nature of composite particles like atomic hydrogen (electron & proton) has been the topic of a number of papers see e.g. J.H. Freed, J.Chem.Phys. 72, 1414 (1980) and references in there. Experimentally the Bose nature follows from the magnetic relaxation of the H-gas in the bulk: A. Lagendijk, G.H. van Yperen, J.T.M. Walraven, J.Physique Lett. 45, L-929 (1984).
39 K. Huang, 'Statistical Mechanics', John Wiley & Sons, New York (1963).
40 J. de Boer, Physica 14, 139 (1948).
J. de Boer and R.B. Bird, MOLECULAR THEORY OF GASES AND LIQUIDS J.O.Hirschfelder, C.F.Curtiss and R.B.Bird(Ed.),John Wiley, New York, 424 (1954).
41 M.D. Miller, L.H. Nosanow and L.J. Parish, Phys.Rev.Lett. 35, 581 (1975).
M.D. Miller and L.H. Nosanow, Phys.Rev.B. 15, 4376 (1977).
M.D. Miller, L.H. Nosanow and L.J. Parish, Phys.Rev.B 15, 214 (1977).
L.H. Nosanow, J.de Phys. 41 C7, 1 (1980) (Aussois).
42 M.D. Miller, Phys.Rev.B 18, 4730 (1978).
M.D. Miller, Ann.Phys. 127, 367 (1980).
E. Krotscheck, R.A. Smith, J.W. Clark and R.M. Panoff, Phys.Rev.B 24, 6383 (1981).
M.L. Ristig, S. Fantoni and K.E. Kürten, Z.Phys.B-Cond.Matter 51, 1 (1983).
43 J.V. Dugan, R.D. Etters, J.Chem.Phys. 59 6171 (1973).
R.D. Etters, J.V. Dugan and R.W. Palmer, J.Chem.Phys. 62, 313 (1975).

R.D. Etters, R.L. Danilowicz and R.W. Palmer, J.Low Temp.Phys. 33, 305 (1978).
P. Entel and J. Anlauf, Z.Phys.B-Condensed Matter 42, 191 (1981).
44 W.J. Mullin, Phys.Rev.Lett. 44, 1420 (1980).
D.J. Friend and R.D. Etters, J.Low Temp.Phys. 39, 409 (1980).
V. Lefèvre-Seguin, P.J. Nacher, C. Lhuillier and F. Laloë , J.de Phys. 43, 1199 (1982).
E.V.L. Mello, J.J. Rehr and O.E. Vilches, Phys.Rev.B. 28, 3759 (1983).
T.K. Lim, J.Chem.Phys. 77, 6197 (1982).
T.K. Lim and S.Y. Larsen, J.Chem.Phys. 75, 955 (1981).
T.K. Lim and P.A. Maurone, J.Chem.Phys. 79, 1452 (1983).
45 C. Lhuillier and F. Laloë, J.de Phys. 43, 225 (1982).
C. Lhuillier and F. Laloë, J.de Phys. 43, 197 (1982).
C. Lhuillier, J.de phys. 44, 1 (1983).
J.M.V.A. Koelman, H.J.M.F. Noteborn, L.P.H. de Goeij, B.J. Verhaar, J.T.M. Walraven, Phys.Rev.B 32 7195 (1985).
46 B.R. Johnson, J.S. Denker, N. Bigelow, L.P. Levy, J.H. Freed and D.M. Lee, Phys.Rev.Lett. 52, 1508 (1984).
L.P. Levy and A.E. Ruckenstein, Phys.Rev.Lett. 52, 1512 (1984).
47 R.E. Roberts, R.B. Bernstein and C.F. Curtiss, J.Chem.Phys. 50, 5163 (1969).
R.J. Le Roy and R.B. Bernstein, J.Chem.Phys. 54, 5114 (1971).
48 J.T.M. Walraven and I.F. Silvera, Phys.Rev.Lett. 44, 168 (1980).
49 see ref. 8,9 for ^{3}He, ^{3}He/^{4}He-mixtures.
For ^{4}He the observed binding energy is ≈0.95K, see e.g. ref. 55.
50 I.B. Mantz and D.O. Edwards, Phys.Rev.B 20, 4518 (1979).
C. De Simone and B. Maraviglia, Chem.Phys.Lett. 60, 289 (1979).
W.C. Stwalley, Chem.Phys.Lett. 88, 404 (1982).
51 K.E. Kurten and M.L. Ristig, Phys.Rev.B 31, 1346 (1985).
and M.D. Miller, Phys.Rev.B 18, 4730 (1978).
52 J.G. Dash, 'Films on Solid Surfaces', Academic Press (1975).
53 I.F. Silvera and V.V. Goldman, Phys.Rev.Lett. 45, 915 (1980).
54 J. Wilks, 'The Properties of Liquid and Solid Helium', Clarendon Press, Oxford (1967).
55 H.P. Godfried, E.R. Eliel, J.G. Brisson, J.D. Gillaspy, C. Mallardeau, J.C. Mester and I.F. Silvera, Phys.Rev.Lett. 55, 1311 (1985).
56 A. Lagendijk, Phys.Rev.B 25, 2054 (1982).
A.E. Ruckenstein, E.D. Siggia, Phys.Rev.B 25, 6031 (1982).
B.W. Statt, Phys.Rev.B 25, 6035 (1982).
R.M.C. Ahn, J.P.H.W. van den Eijnde, C.J. Reuver, B.J. Verhaar, I.F. Silvera, Phys.Rev.B 26, 452 (1982). R.M.C. Ahn, J.P.H.W. van den Eijnde, B.J. Verhaar, Phys.Rev.B 27, 5424 (1983). J.P.H.W. van den Eijnde, C.J. Reuver, B.J. Verhaar, Phys.Rev.B 28, 6309 (1983).
A. Lagendijk, I.F. Silvera, B.J. Verhaar, Phys.Rev.B 33, 626 (1986).

57 Yu. Kagan, I.A. Vartanyantz, G.V. Shlyapnikov, Sov.Phys. JETP 54, 590 (1982).

58 L.P.H. de Goeij, J.P.J. Driessen, B.J. Verhaar and J.T.M. Walraven, Phys.Rev.Lett. 53, 1919 (1984).

Chapter 2

Experiments with 'doubly' spin-polarized atomic hydrogen

R. Sprik, J.T.M. Walraven, G.H. van Yperen[+],
Natuurkundig Laboratorium, Universiteit van Amsterdam,
Valckenierstraat 65, 1018 XE Amsterdam, The Netherlands.

and

Isaac F. Silvera
Lyman Laboratory of Physics, Harvard University,
Cambridge, MA 02138, USA.

Abstract

We analyze and reinterpret experiments with electron and nuclear spin ('doubly') polarized hydrogen (H↓↑) in a cell with a very low concentration of magnetic impurities. The destabilizing magnetic relaxation due to remaining impurities (G_1^s) is found to be suppressed by increasing the thickness of the helium film covering the walls of the cell. Using recent information on surface three-body recombination, we obtain good quantitative agreement with more recent experiments if we assume thermal gradients, up to $\Delta T/T \approx 0.1$. We extract both the value and field dependence for the three-body surface recombination ($L_3^s = 1.5(2) \times 10^{-24} cm^4 s^{-1}$ at B=8T). We also extract the magnetic field dependence of the impurity relaxation.

+ Present address: Philips Medical Systems, Best, The Netherlands.

[Submitted to Physical Review B, 1 april 1986]

I Introduction

The gaseous state of atomic hydrogen (H) has been studied extensively at low temperatures (T = 60mK-1K) in liquid helium covered sample cells.[1-4] By polarizing the electronic spins (H↓) in a high magnetic field (B=10T) densities in the range $n=10^{16}$-$10^{17}cm^{-3}$ were achieved. Still higher densities up to $4.5x10^{18}$ cm^{-3} were reported for samples in which both the electronic and nuclear spins were polarized (H↓↓). Nevertheless these densities are not sufficiently high to observe the transition to the Bose-Einstein condensed phase, predicted at $n_c=(mk_BT_c/3.31\hbar^2)^{2/3} \simeq 1.6x10^{19}$ cm^{-3} for T_c=100mK. In this paper we discuss experiments with a cell void of magnetic impurities in which we studied H↓↓ and address some of the limitations to reach high densities. The results were published earlier as a short report[5] (further referred to as (I)).

The barrier to achieving high densities of atomic hydrogen is recombination to H_2 which must take place by three-body collisions involving two or three H atoms. Although electron-spin polarization strongly reduces the recombination probability, H↓ has been found to recombine at a rate proportional to n^2 (with He surface atoms participating as 'third bodies') and density limits are encountered for $n\simeq10^{16}$-$10^{17}cm^{-3}$ when the recombination rate is of the order of the filling rate of a cell. The main recombination processes between atoms in the two lower hyperfine states (H↓) are driven by the admixture of electron spin ↑. These hyperfine states are the mixed state $|a\rangle=|\downarrow\uparrow\rangle - \epsilon|\uparrow\downarrow\rangle$ and the pure state $|b\rangle=|\downarrow\downarrow\rangle$, where $\epsilon=a/(4\mu_BB)$. Here a is the hyperfine mixing constant and μ_B the Bohr magneton; ↑ indicates electron spin projection of 1/2 and ↓, nuclear spin projection of 1/2 (the hyperfine states are labelled a,b,c and d with increasing energy[1-4]). As described by Statt and Berlinsky[6] the absence of the admixture in the b-state favors recombination of a-a and a-b pairs and leads to a rapid depletion of the a-state, thus leaving a residual gas of only b-state atoms: the doubly polarized state H↓↓. Since b-state atoms are in pure electron-spin-polarized states, they do not recombine by the second order process (n_b^2) with He third-bodies, as a consequence the stability of H↓↓ depends on the magnetic relaxation from the b-state to the mixed hyperfine states $|a\rangle$ or $|c\rangle$. Alternatively, as pointed out by Kagan et al.[7,8] recombination may proceed directly, without the relaxational step, through a process involving three b-state hydrogen atoms and thus scaling as n_b^3.

The first successful observation of the double-polarization mechanism and the enhanced stability of the gas was made by Cline et al.[9]. The recombination times were found to be orders of magnitude longer than those found for H↓ and densities of $3x10^{17}cm^{-3}$ were achieved. Earlier experiments by van Yperen et al.[10] did not show a build-up of H↓↓ and high rates of recombination consistent with previous measurements[11-13] were observed. The fast recombination found by van Yperen et al. was attributed to rapid magnetic b→a relaxation induced by magnetic impurities in the wall of the

sample cell. Once we recognized the role of magnetic impurities as an important source of relaxation we decided to construct a new cell, carefully avoiding all conspicuous magnetic materials.

The interpretation of the measurements by Cline et al., (I) and similar experiments by others[14,15] was based on the model in which, at low temperature, surface relaxation followed by rapid recombination was assumed to be the dominant density decay mechanism. This interpretation led to a discrepancy of order 50 between experimental[5,9,14,15] and theoretical[16-19] values for the b→a surface relaxation rate constant G^s_{ab}.

With the development of techniques to compress a sample of H↓↑ to high density ($n>10^{18}cm^{-3}$)[20-24], measurements demonstrated the existence of the third-order recombination channels both in the bulk[20-24] and on the surface.[21-24] Hess et al.[22] realized that three-body surface recombination also had been important in previous experiments at much lower bulk densities. This reinterpretation of the destabilization processes on the surface in terms of recombination instead of relaxation was recently confirmed by Reynolds et al.[25] using E.S.R. techniques. At present theory and experiment for G^s_{ab} agree well.[25] Discrepancies can be attributed to the unknown surface roughness of the cell walls.

In this paper we reexamine the results of (I), extracting a value for the third-order surface recombination rate. A similar reanalysis of M.I.T. data has been given by Bell et al.[26]. We also discuss how impurity relaxation may be suppressed by using thick ^{4}He films and extract the field dependence of both the three-body rate and the impurity relaxation. We find that no satisfactory theory is available to describe our results for third-order recombination. Bulk magnetic relaxation is found to be in agreement with other measurements[5,9,14,15] and theory.[6,16-19,27] In addition some technical details on the construction of the cell and the analysis of the decays are discussed.

II Experimental cell without magnetic impurities

The experimental cell is schematically shown in Fig.1. The H is fed in from the bottom and observed with a pressure gauge, which is integrated into the body of the cell and placed in the center of an 11 Tesla superconducting magnet. During operation all surfaces are covered with a film of liquid helium. The main sample volume has the pancake shape of the pressure gauge. The design combines a small volume, $V\approx 5\times10^{-3}cm^3$, with a large surface to volume ratio, $A/V\approx 40\text{-}140cm^{-1}$. The pancake shape implies that most surfaces in the cell are perpendicular to the direction of the main magnetic field. This may have consequences as surface relaxation is predicted to be anisotropic as will be discussed in section VI.

Before the actual design was made, all construction materials employed in the cell of van Yperen et al.[10] were carefully examined with respect to their magnetic properties. Chemical analysis of the OFHC copper (oxygen free high conductivity) to be used for the body of the cell showed that the

contents of magnetic impurities in the bulk of our OFHC copper is low (<10ppm).[28] Furthermore, to be effective as relaxation centers magnetic impurities have to be clustered since only magnetic fields due to sizable (ferro) magnetic grains (>50Å) range far enough to induce relaxation in the H↓ moving on top or near the helium film. The magnetic impurities observed in the chemical analysis may be diluted in the copper and are then harmless. A much more serious problem is the contamination of the copper surface caused by the machining of the copper. Chemical analyses of the first 0.5μm of a machined piece of copper showed that the iron concentration in the top layer was 100 times larger than the bulk concentration. This indicated that one should etch off a layer of material after machining the copper with a magnetic tool bit, a procedure that was not performed in the construction of the cell of van Yperen et al. Some other materials used in the construction of that cell were investigated in a pendulum magnetometer between 1.6-300K. Stycast 2850GT (catalyst 11) appeared to be ferromagnetic whereas Stycast 1266 was found to be diamagnetic to low temperatures (see also a recent publication[29]) and was used instead. Scotch #56 tape, a yellow mylar based tape used in the interior part of the cell of van Yperen et al., was found to be slightly diamagnetic but was avoided in the new cell employing better attachment methods. Finally all copper electrical wires were stripped of their original possibly magnetic insulating varnishes and were reinsulated with Stycast 1266.

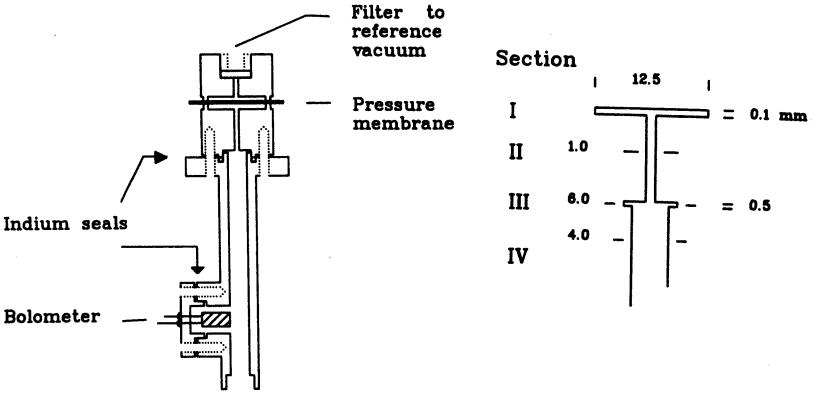

fig.1 Schematic overview of hydrogen stabilization cell. Including the dimensions used to estimate the effective volumes and surfaces used in the analysis.

The construction of the membrane pressure gauge was done with great care to avoid contamination of the surfaces of the gauge. The evaporation of the gold layer on the Kapton membrane was done in a clean and simple evaporation apparatus, specially constructed for this purpose (see Fig.2), using high purity gold (99.999% pure). All copper parts in the heart of the

cell were electro chemically etched in a solution of H_3PO_4/H_2O (60%) using properly shaped Pt-anodes. This etch technique allows a well controlled removal of the contaminated top layer of the copper. (In later cells purely chemical etching in HNO_3/H_2O acid was also used). Instead of a carbon 'trigger' bolometer with possible magnetic impurities a small solenoid of 10μm tungsten wire on a Stycast 1266 rod was used (no magnetic impurities) and placed ~3cm below the center of the magnet.

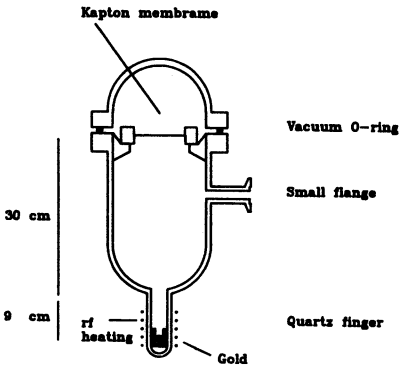

fig.2 Simple clean gold evaporation vacuum chamber

In contrast to one of our earlier cells, this one was void of sinter. As will be discussed later, this restricts the thermal contact between the helium and the copper cell body. The cell was connected to the same filling section as used by Van Yperen et al.[10] and installed in an Oxford Instruments dilution refrigerator with bottom access. This part of the experimental setup is described in detail elsewhere.[15,30]

III The measurements

The recombination kinetics of the H gas was studied by measuring the pressure decay as a function of time. As an example we show in Fig.3a a decay curve typical for 300mK and 8T. In the first part of the decay double polarization is building up, displaying itself as a rapid initial decay due to a-a and a-b recombination, followed by a much slower relaxation bottlenecked decay due to b→a relaxation in the gas phase. The rate constants characterizing the recombination (K_{aa} and K_{ab}) and relaxation (G_{ab} or G^i_{ab}) will be discussed in section IV.

The final polarization depends on the relative efficiency of the relaxation processes by which the b-state is depleted and the recombination processes that preferentially eliminate the a-state atoms.[6] This opens the possibility to prepare a sample in a condition were a/b is smaller than the equilibrium value at a given temperature. This is illustrated in Fig.3b. After filling the cell, a sample is first cooled to low temperature thus

building up a high degree of polarization and subsequently rapidly warmed up again to the original temperature. The initial decay of the pressure is slowed down by this procedure until relaxation restores the equilibrium situation at that temperature. This qualitative proof of bottlenecking by a (bulk) **relaxation** process (in contrast to bottlenecking by a third order recombination process) may be supported by a quantitative analysis. In section V we discuss in more detail the regime where bulk relaxation is the dominant decay process.

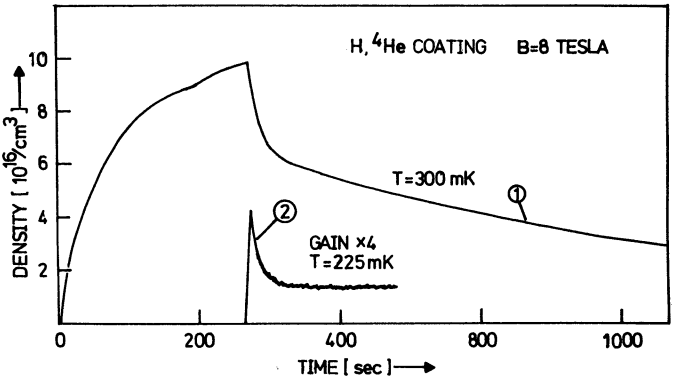

fig.3 *a) Building up of double polarization. 1 - T=300mK, high starting density, 2 - T=225mK, low starting density.*

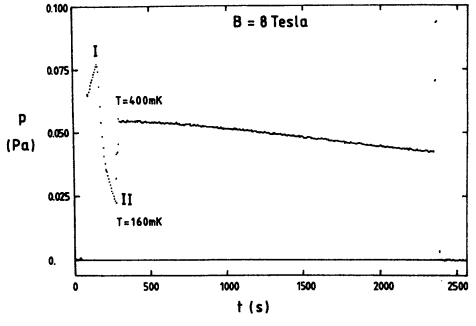

fig.3 *b) Decreased decay as a result of extra enhancement of the double polarization. At I the temperature is lowered rapidly from 400mK to 160mK and returns to 400mK at II.*

To describe the density decays in the doubly polarized region the data was fit to a simple polynomial expansion in terms of the density: $\dot{n} = C_1 n + C_2 n^2 + C_3 n^3$, and integrating $\dot{n}$ to obtain the model n(t) and optimize the coefficients C_1, C_2 and C_3 using a non-linear χ^2-fit of the model n(t) to

the observed n(t). Subsequently the coefficients were related to the various decay processes by making use of effective volumes and surfaces. The experimental density n was obtained from the pressure by assuming the gas to be ideal, i.e. $n=p/k_BT$.

Initially we introduced a small amount of helium in the cell, not sufficient to form a saturated helium film. Under this condition we observed the decay to be bottlenecked by a first order process (C_1). Subsequently the first order rate was suppressed by adding ^{4}He to the system and the decay became bottlenecked by a 'higher order' mechanism. After adding 56μmole the suppression effect was saturated and all quantitative experiments were done with a coating of at least that amount. We did not observe an influence of the building up of an H_2 coating in the cell as reported by Reynolds et al.[25] A more quantitative discussion of the results on the first-order relaxation will be postponed until section VI.

Most of the remarks made until now also hold for a system with a ^{3}He/^{4}He coating. Nevertheless we observed a remarkable difference between the pure ^{4}He case and the mixtures. This will also be discussed in section VI, after a more detailed discussion of our method of analysis.

IV The density decay kinetics

The major contributions to the decay process are described by the following rate equations:

$$\dot{a} = \varphi_a/V - a/\tau_T - G_{ab}^{ieff}(a-b) - G_{ab}^{eff}(a-b)(a+b) - 2K_{aa}^{eff}aa - K_{ab}^{eff}ab \qquad (IV.1)$$

$$\dot{b} = \varphi_b/V - b/\tau_T + G_{ab}^{ieff}(a-b) + G_{ab}^{eff}(a-b)(a+b) - K_{ab}^{eff}ab - 2L_3^{eff}b^3.$$

Here a and b represent the a- and b-state densities, respectively, V is the sample volume; the symbol A will be used for the surface area.

The first terms describe the filling flux of the cell for the two different hyperfine levels (φ_a and φ_b). We assumed $\varphi_a=\varphi_b$ although in principle these fluxes may be different if the polarization already develops in the filling tube before the atoms reach the actual cell. The second term represents the thermal escape from the cell with τ_T the characteristic time (see ref.31 for a further treatment). For our experimental conditions the B/T ratio of the magnetic field to the temperature is sufficiently large for this term to be negligible. The third term describes the relaxation between the hyperfine levels due to impurity relaxation. It depends on the hydrogen surface coverage σ and is expressed as an effective bulk rate constant

(IV.2)

$$G_{ab}^{ieff} = (A/V)\, G_{ab}^{is}\, (\sigma/n) \text{ with } (\sigma/n) = \Lambda \exp(E_a/k_BT).$$

Here $n \equiv a+b$, $\Lambda = (2\pi\hbar^2/mk_BT)^{1/2}$ is the thermal wavelength and E_a is the adsorption energy. The fourth terms of eq.(IV.1) account for magnetic relaxation between a and b hyperfine levels due to dipolar couplings between the H atoms.[16-19] Relaxation processes of this type occur both in the bulk and on the surface. The total effective rate constant is given by:

(IV.3)

$$G_{ab}^{eff} = (A/V)\, G_{ab}^{s} (\sigma/n)^2 \quad + \quad G_{ab}^{v}$$

Recombination appears through the next three terms of eq.(IV.1). The second order terms involve processes between surface adsorbed atoms in the hyperfine states $|a\rangle$ and $|b\rangle$. The presence of the surface enables the conservation of energy and momentum in the reaction. The a-b and a-a processes are represented by effective bulk rate constants

(IV.4)

$$K_{ab}^{eff} = (A/V)\, K_{ab}^{s}\, (\sigma/n)^2 \text{ and } K_{aa}^{eff} = (A/V)\, K_{aa}^{s}\, (\sigma/n)^2.$$

Recombination between two b-state atoms is assumed to be negligible ($K_{bb}^{s} \simeq 0$).[19] The last term of eq.IV.1 is related to the third order recombination rate constant (K_{bbb}^{eff}): $L_3^{eff} \equiv 2\theta\, K_{bbb}^{eff}$. The proportionality constant θ expresses the total number of b-state atoms that are lost in a K_{bbb} event. The constant θ depends on the fate of the third outgoing atom and ranges typically between 1.8 to 1.9.[20,23] The effective rate K_{bbb}^{eff} is defined by:

(IV.5)

$$K_{bbb}^{eff} = K_{bbb}^{v} \quad + \quad (A/V)\, K_{bbb}^{s}\, (\sigma/n)^3.$$

All terms except the last one were taken into consideration in the first analysis of the experiments in (I). In retrospect this is in part justified as the gas densities were sufficiently low ($n \leq 3\times10^{17}\,cm^{-3}$) to neglect the bulk contribution due to K_{bbb}^{v}. However, the surface contribution competes with the relaxation term G_{ab}^{s}. This point, first realized by Hess et al.[22] in relation with M.I.T. data, will be discussed in section V.

A complication in the analysis of the decays is the strong inhomogeneity of the magnetic field in the cell region. The density profile of the hydrogen gas in this inhomogeneous field changes as a function of temperature and field. It is determined by the balance of the magnetic field gradient forces and the thermal energy:[31]

(IV.6)

$$n(\vec{r}) = n_0 \exp(-\mu_B\, (B(0) - B(\vec{r})) / kT) \equiv n_0\, C(B,T),$$

where $\vec{r}$ is the position in the magnetic field with respect to the center of the magnet, n_0 the density in the center and μ_B is the Bohr magneton. It is

convenient to express this density profile in terms of a dimensionless compression factor C(B,T).

The magnet employed in the experiments has a parabolic field profile described by the radial component B_ρ and the axial component B_z:

$$B_z(z,\rho) = B_0 \left(1 - (z/z_m)^2 + 1/2\ (\rho/z_m)^2\right) \qquad \text{(IV.7)}$$

$$B_\rho(z,\rho) = z\rho/z_m^2,$$

with ρ the radial distance and z the axial distance from the center, B_0 the field strength in the center and z_m=51mm for this particular magnet. In the further analysis the small radial components of the field will be ignored.

For the actual cell, effective volumes (V^{eff}) and surfaces (A^{eff}) are calculated by dividing the cell into four cylindrical sections (see fig.1), where each section is treated using the method described in appendix A. For very low temperatures and/or high magnetic fields the density profile is concentrated near the field center. In the geometry sketched in fig.1 this means that only the 'pancake' shaped part (I) contributes to A^{eff} and V^{eff}. For high temperatures and/or low fields the profile extends into the fill tube of the cell as well. The various effective volumes and surfaces used in the analysis of our data are plotted in Fig.4.

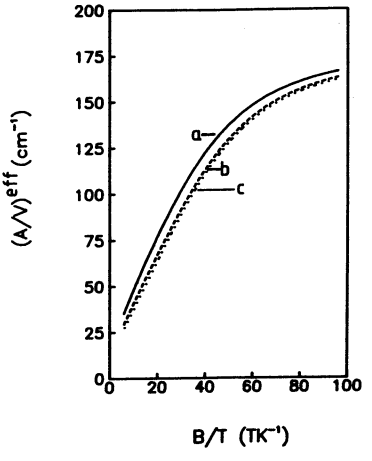

fig.4 Effective A/V ratio in the cell of fig.1 (see appendix A for definitions of effective surfaces and volumes).
a - A_1^{eff} / V_1^{eff},
b - A_2^{eff} / V_1^{eff},
c - A_3^{eff} / V_1^{eff}.

V Reanalysis of the data; Three-body surface recombination

After the observation of three-body surface recombination[21-23], we decided to reanalyze our data and obtain the three-body surface recombination rate (K^s_{bbb}). A similar reanalysis has been carried out by

Bell et al.[26] for the MIT data. First we will discuss the result of the reanalysis for the data of (I) for the temperature region where the surface processes are dominant. Then we discuss the results at higher temperature where the decay is dominated by bulk processes and the analysis of (I) remains unchanged.

The importance of K^s_{bbb} relative to surface relaxation (G^s_{ab}) may be estimated by comparing the measured three-body rate ($L_3^{eff} = 2\times10^{-24}cm^4s^{-1}$ [21-23,25]) with the calculated relaxation rate ($G^s_{ab}=3\times10^{-14}cm^2s^{-1}$ [19]). The three-body rate is found to become dominant over the two-body relaxation processes for a surface coverage $\sigma > G^s_{ab}/L^s_3 \simeq 3\times10^{10}cm^{-2}$. The typical surface coverage in the decay experiments of (I) varied from a starting coverage of $\sigma\simeq3\times10^{12}cm^{-2}$ to $\sigma\simeq5\times10^{10}cm^{-2}$ at the end of the recorded decay for temperature range (T<250mK) where the surface processes are dominant. This indicates that three-body recombination must have been the dominant surface decay processes.

The density-decay analysis in (I) did not provide evidence for a significant third order coefficient, C_3. As a consequence, in the present analysis we have investigated systematic effects. We found that the data are consistent with a third order process if we assume a temperature difference $(T-T_0)$ to develop between the H gas at temperature T and the copper walls of the sample cell at temperature T_0. This may result from the combined effect of recombination heating and thermal boundary resistance (R_k). To extract an estimate for $(T-T_0)$ from our data we use a procedure illustrated in Fig.5. The decays are well described by a second order fit ($p=\hat{C}_1p + \hat{C}_2p^2$) over their whole dynamic range, also in the high density regions where a temperature gradient is suspected. Note the good quality of the fit. Hence for the present purpose $\hat{C}_1$ and $\hat{C}_2$ may be used as fitting parameters to describe the decay. The values of $\hat{C}_1$ and $\hat{C}_2$ are readily deduced from the results of (I).

A proper description for the decay would be $\dot{n} = C_1(T)n + C_3(T)n^3$, where C_1 corresponds to first-order surface relaxation and C_3 to the third order surface recombination process:

(V.1)

$$C_1(T) = 2\, G^{ab}_{is}\, (A/V)^{eff}\, \Lambda\, \exp(E_a/kT)$$

$$C_3(T) = 2\theta\, K^s_{bbb}\, (A/V)^{eff}\, \Lambda^3\, \exp(3E_a/kT).$$

We now use the low density part of the decay ($\sigma<1\times10^{12}cm^{-2}$) where $T\simeq T_0$, to determine $C_1(T_0)$ and $C_3(T_0)$. Then from the difference of the observed rate (characterized by $\hat{C}_1$ and $\hat{C}_2$) and an extrapolated rate based on $C_1(T_0)$ and $C_3(T_0)$ (dashed line fig.5) we can estimate the temperature (T) in the gas. Typically the initial $(T-T_0)$ is in the order of only 10%, but the change of T during the decay turns out to be sufficient to mimic a second order behavior.

The importance of $T-T_0$ is determined by the heat production due to

recombination in the cell and the dominating thermal boundary (Kapitza) resistance (R_k)[13,32,33] between the helium and the copper wall:

$$T-T_0 \equiv R_k\, Q = R_k\, D\, \dot{n}\, V^{eff}, \qquad (V.2)$$

where Q is the produced heat, $D=3.6\times10^{-19}$J is the recombination energy per atom, and V^{eff} is the effective volume where the recombination is taking place. The estimated R_k on the basis of eq.V.2 is a factor 4 lower than literature values for the Kapitza resistance[33] between the helium film and the copper surface (the Kapton surface of the pressure gauge is not contributing to A). The Kapitza resistance between the hydrogen gas and the helium surface is apparently even lower than the helium-copper resistance.

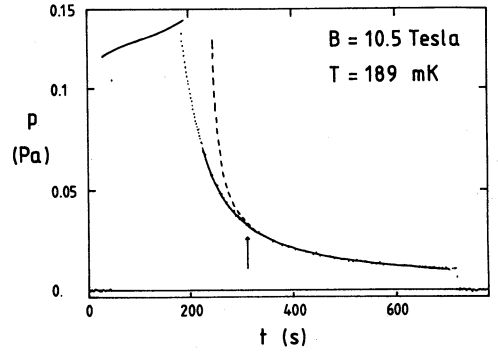

fig.5 *Estimation of the temperature difference $T-T_0$ in the sample. The solid line is a second order fit to the data over the whole range of the decay with fitting constants $\hat{C}_1$ and $\hat{C}_2$. The dashed line describes the extrapolated decay curve at the temperature T_0 based on first and third order decay processes as obtained from the part of the decay where $\sigma<1\times10^{12}cm^{-2}$ (indicated by the arrow). From the difference of the extrapolated curve and the observed decay ΔT can be estimated.*

Thus the picture emerges that the hydrogen gas and the helium film are at a temperature T, significantly higher than that of the copper cell wall for which the cell temperature is measured. Since the surface coverage σ depends exponentially on the temperature of the helium surface, and since this temperature depends on a power n (the source of the heating), the experimentally observed decay rates for fixed T_0 can acquire a different dependence on n, as $T\rightarrow T_0$ as n decays to zero. This problem has also been

recently observed and corrected for in the study of the adsorption energy by Godfried et al.[34]

Once aware of the thermal problems for the decays with T<250mK, we reanalyzed the decays always using the same surface coverage at the starting point of the fit independent of the temperature ($\sigma^{beg} = 1x10^{12}cm^2$). The typical decay rate $\dot{n}<1.2x10^{14}$ $cm^{-3}s^{-1}$ implies a released recombination heat D<1.7μW and the estimated thermal gradient is less than 1.3mK, much less than the temperature gradients in the analysis of (I). We stress the point that although this procedure is well justified in retrospect, the absence of gas temperature data prevents an ab initio preference for the present analysis over the analysis in (I).

For high temperature (i.e. when $2G^v_{ab} > L_3^{eff} n$; for $n=1x10^{17}cm^{-3}$ this is typically fulfilled when T>250mK) the three-body surface recombination can be neglected. It is sufficient in that case to analyze the decay using $\dot{n} = C_1 n + C_2 n^2$ for modelling the decay, as was done in (I). The first order coefficient provides information on the thermal escape and on the remaining first-order surface (impurity) relaxation. The second order coefficient describes the nuclear relaxation in the gas phase:

(V.3)

$$C_1 = 2\, G^{ab}_{si}\, (A/V)^{eff}\, (\sigma/n)$$

$$C_2 = 2\, G^v_{ab}.$$

VI Results

Figures 6 and 7 show our results for the first order coefficients. In Fig.6 the extracted effective first order relaxation rate ($G^{ieff}_{ab}/(A/V)$) is plotted as function of 1/T at 8T for different amounts of helium in the cell. This shows qualitatively the suppression of the surface relaxation as a function of the film thickness. It is difficult to make a quantitative estimate of the film thickness based on the amount of helium used. The geometric area of the cell is $\simeq 25cm^2$, but the different parts are at different temperatures.

Statt et al.[25] calculated the surface impurity relaxation induced by a distribution of Fe clusters in the copper of the cell wall. The resulting expression for the G^i depends exponentially on the film thickness d and the surface coverage σ. The dashed line in fig.6. is the calculated G^i on the basis of the model of Statt et al.[25] using a film thickness d=300Å, E_a=1.0K and a distribution for the iron particles corresponding to 66Å Fe spheres in copper with 10ppm Fe impurities (the same cluster size as found by Statt et al.: 75Å, for 0.1at%Fe in their OFHC copper). The much lower level of iron contamination in our OFHC copper may explain why we did not observe an influence of a H_2 coating under the helium film as was observed by Statt et al.[25]

Fig.7 shows the field dependence of the first order relaxation term at

T=189mK. The dashed line is again based on the model of Statt et al.[25] using the same film thickness and Fe distribution as in fig.8. The strong suppression of G^i with increasing magnetic field is caused by the field dependence of the magnetic transition frequency.[35] The model shows good qualitative agreement with the data both in fig.6. and fig.7. The model does not allow an accurate fit for the clustersize and film thickness independently.

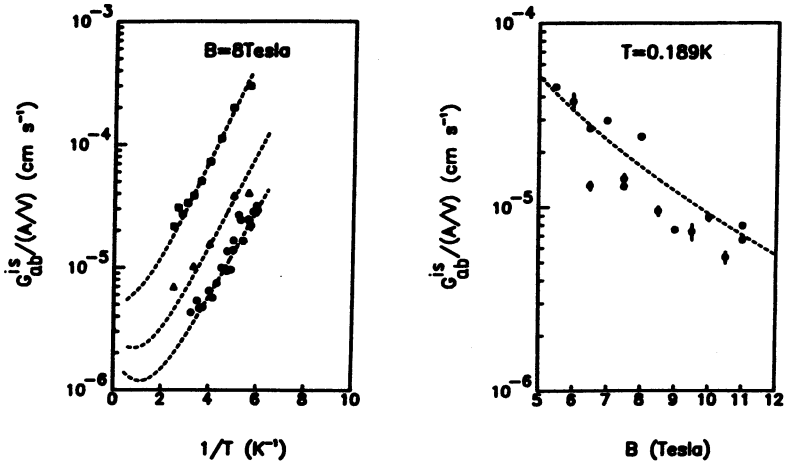

fig.6 (left) *Temperature dependence of first-order relaxation G^{is}_{ab} for several ^{4}He film thicknesses in the cell. The dashed lines are based on the model of Statt et al.[25] with a distribution of 66Å Fe spheres and 10ppm Fe impurities and film thicknesses: d=300Å, 250Å and 175Å for 56.1 (●), 39.3 (▲) and 16.8 (■) μmole ^{4}He in the cell respectively.*

fig.7 (right) *Field dependence of first-order term at T=0.189K with 56.1μmole ^{4}He in the cell. The dashed line is based on the same model as in fig.6 using the same distribution of Fe impurities and d=300Å. All decay curves are analyzed starting with a surface coverage $\sigma=10^{12}cm^2$.*

Recently Godfried et al.[34] observed an increasing adsorption energy E_a for films thinner than 10Å. The surface thicknesses used in experiments of fig.6. are likely to be much thicker. For the highest coverage (56μmole ^{4}He in the cell) the surface relaxation is sufficiently suppressed to allow double polarization to build up in the gas.

For data taken at higher temperatures, where surface three-body recombination can be ignored, the analysis of (I) remains valid. Furthermore, the difference $T-T_0$ is less important under these conditions. The observed second order rate can be attributed to bulk relaxation G^v_{ab}

(see fig.8). For G^v_{ab} the calculated values obtained with different calculation methods agree well with the observed experimental values of all the performed experiments.[5,9,14,15,25] Calculations within the excluded volume approximation and the distorted wave Born approximation (DWBA)[6,16-19,27] give results that agree very well with each other (see fig.8). The theoretical temperature and field dependence is well described by the fitting formula obtained by van den Eijnde et al.[36]:

(VI.1)

$$G^v_{ab} = (0.633T^{1/2} + 0.757\ \Delta E_{ab}\ T^{-1/2})\ 10^{-27}\ (1 + \delta/B)^2\ m^3s^{-1}$$

with

$$\delta/B = ((g_e\mu_B)\ /\ (g_n\mu_n))\ \epsilon \simeq (a\ /\ (\ 2g_n\mu_n))\ 1/B \simeq 16.68/B$$

and

ΔE_{ab} is the energy difference between hyperfine states a and b.

In (I) also decay rates on $^3He/^4He$ mixtures (helium added in a ratio $^3He:^4He$ of 4:2) were reported. The adsorption energy of ^3He is much lower than on ^4He (for ^3He $E_a \simeq 0.3\text{-}0.42K$[10,13]). Consequently the region where surface processes dominate the decay start at a much lower temperature than for ^4He surfaces (T<150mK). Nevertheless, the observed rates in (I) are lower than the estimated value on the basis of the surface coverage σ and the observed surface rates on ^4He. This was explained by noting the dependence of G^s_{ab} on the angle Ω between the magnetic field and the surface normal as pointed out by Lagendijk:[16]

(VI.2)

$$G^s_{ab} = G_{s,0}(T)\ \sin^2 2\Omega + G_{s,2}(T)\ \sin^2\Omega\ (1+\cos^2\Omega).$$

This dependence originates from the anisotropy of the dipole-dipole coupling between the spin moments. For $\Omega=0^0$ the rate constant is fully suppressed. However, as argued by Ahn et al.[19] the surface is <u>not</u> atomically flat and G^s_{ab} should be averaged over the surface roughness. As a result the effective G^s_{ab} is considerably suppressed for surfaces oriented perpendicular to the magnetic field. Recently Reynolds et al.[25] studied the influence of this anisotropy on the NMR transition-frequency of the adsorbed atoms and found evidence for the angle dependence of this interaction. In retrospect the suppression of the surface rates as quoted in (I) can be explained by assuming a temperature difference $T-T_0$. Using the same Kapitza resistance as observed in section on ^4He surfaces in our system, the temperature difference becomes: $T-T_0 \simeq 15mK$ for $T_0=80mK$. Therefore we excluded the measurements on ^3He for T<150mK from fig.8.

The results for the third order term are presented in figs. 9-10. In Fig.9 the effective third-order rate is plotted as function of 1/T. The slope is consistent with $E_a=1.0K$ and the intercept gives: $L^s_3=1.5(2)\times10^{-24}cm^4s^{-1}$. This is in good agreement with the observed value of the M.I.T. group[21-23] when taking into account $\theta=1.9$. The results for the field dependence of the three-body surface recombination are shown in Fig.10. A fit to these data, for comparison, using the same fit function as

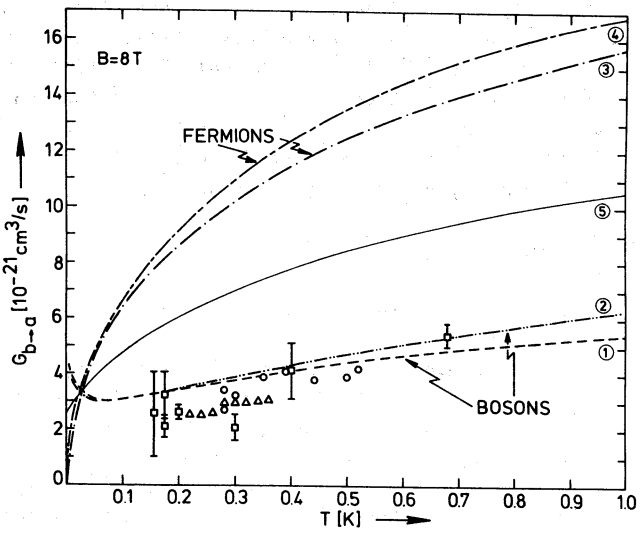

fig.8 *Nuclear relaxation G^{v}_{ab} in the bulk as function of T (from ref. 27, data points on ^{3}He films from (I) are left out).*

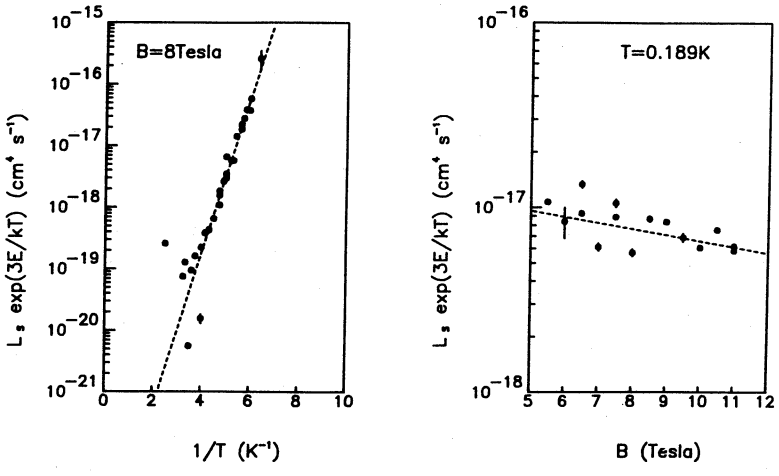

fig.9 (left) *Temperature dependence of surface three-body recombination at B=8T. The dashed line is a fit to the data for 1/T>4. with E=1.0K and L_3^s=1.5(2)x10^{-24}cm^{4}s^{-1}.*

fig.10 (right) *Field dependence of surface three-body recombination at T=189mK. The dashed line is the fit to the data (see eq.VI.3).*

Bell et al.[23], gives:

$$L_3^s(B) = L_3^s \, e^{\eta(B-8.0)} \text{ with } \eta=-0.07(2). \qquad \text{(VI.3)}$$

This is in good agreement with the values obtained at M.I.T.[21-23] (η=-0.06(2)) and U.B.C.[25] Although the decrease of the third order rate with growing field agrees with other experimental data[22,23], a disagreement exists with the calculations of de Goeij et al.[37] These calculations are based on the three-body dipolar recombination mechanism as proposed by Kagan et al.[7,8], the same process thought to be responsible for three-body recombination in the bulk at much higher densities. The calculated K^s_{bbb} ($6.5\times10^{-26}cm^4s^{-1}$) is smaller than the observed one ($K^s_{bbb}=L^s_3/2\theta$ = $5.3\times10^{-25}cm^4s^{-1}$ with θ=1.9) and has the opposite field dependence. In principle K^s_{bbb} is also anisotropic, but this effect is much weaker than that of the dipolar relaxation discussed earlier. Comparing theory with experiment, it appears that no theory is available that describes the available experimental three-body rate to a satisfactory level.

Analyzing the first part of the decay, when the gas is building up doubly polarization, one can extract the absolute values of K_{aa} and K_{ab}. However, since the average of these rates has already been measured in H↓, it is sufficient to measure the ratio: $\gamma=K_{aa}/K_{ab}$. This ratio γ can be obtained by a very simple method. When the system is at very low density ($n=10^{16}cm^{-3}$) the relaxation (G^{eff}_{ab}) in H↓↑ is slow and also three-body recombination on the surface (L^{eff}_3) can be ignored. The initial build-up of H↓↑ can than be studied without having to take into account the relaxation. (see Fig.3). The ratio of the initial density and the final density in the double polarized state is completely determined by the ratio γ. This is easily verified by integrating the rate equations:

$$\dot{a} = -2K^{eff}_{aa} a^2 - K^{eff}_{ab} ab \qquad \text{(VI.4)}$$

$$\dot{b} = - K^{eff}_{ab} ab.$$

One obtains the ratio of the final densities in terms of the initial densities and γ:

$$(n(t=\infty)/n(t=0)) = [\, 1 + (\, 2\gamma-1)\, (\, a(t=0)/b(t=0)\,)\,]^{(-1/(2\gamma-1))}. \qquad \text{(VI.5)}$$

An intrinsic uncertainty of this method is the assumption for the initial polarization. Since the experiments are done at low density, it is likely that the build-up of H↓↑ during the filling stage is negligible and that a(t=0)=b(t=0). The experimentally observed ratio was γ=2.23(0.25) for temperatures of T=225, 250, 300mK.

Experiments by Yurke et al.[14] made use of an RF field to saturate the initial polarization and to obtain a well defined initial condition. Also

E.S.R. techniques were used[25] to study this ratio. The results of these measurements are compiled in Fig.11. The value of γ ranges between 2.2-3.8. The temperature dependence of γ expresses the difference in temperature dependence of K_{aa} and K_{ab}. From the currently available data the detailed temperature dependence of γ is not clear.

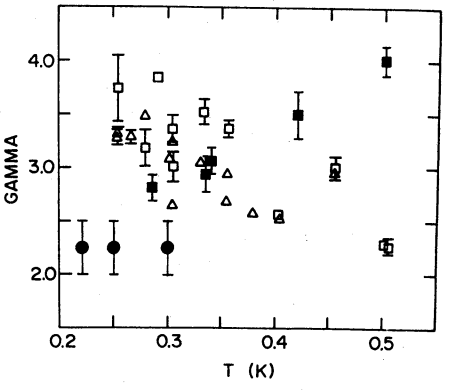

fig.11 Compilation of measurements of the ratio $\gamma=K_{aa}/K_{ab}$. (after Silvera and Walraven[4]).
(●) Sprik et al.[5]
(■) Yurke et al.[14]
(△□) Statt et al.[25]

Finally we estimate the polarization in our samples. Since at the time of the measurements we did not have a method at our disposal to directly measure the degree of polarization we can only estimate the final polarization in the sample using the model equations and using the measured decay constants. In subsequent experiments ESR techniques were introduced for this purpose by van Yperen et al.[15] and in much detail by Reynolds et al.[25] while Yurke et al.[14] used NMR. In (I) the influence of L_3^s was not included in the estimate of the polarization. It can be shown that the equilibrium degree of polarization in a sample where three-body terms are important, approaches a density dependent equilibrium value:[20]

$$a/b = G_{ab}^{eff} / (K_{ab}^{eff} - G_{ab}^{eff} - L_3^{eff}\, b) \qquad \text{(VI.6)}$$

$$\simeq G_{ab}^{s} / (K_{ab}^{s} - G_{ab}^{s} - L_3^{s}\,(\sigma/n)\, b).$$

Using $L_3^s=2\times10^{-24}cm^4s^{-1}$ this results in a maximum polarization of $a/b=99.9\%$ at B=8T, T=225mK and $n=5\times10^{15}cm^{-3}$. The presence of a three body term decreases the polarization, since it forms an extra mechanism to deplete the b-state relative to the a-state. If the polarization is small ($a/b\simeq1$), one has to include other decay mechanisms as well (see e.g. refs. 20,23).

VII Conclusion

The suppression of first order relaxation is an important step to obtain H↓↑. Careful elimination of (magnetic) surface impurities from the walls of the cell and application of thick helium films seem to be sufficient to suppress the impurity relaxation. The temperature and field dependence of the remaining first order surface relaxation is described by the model of Statt et al.[6]

Analysis of the decay curves at low temperatures, where surface processes are dominant, on the basis of first order relaxation (G^s_{ab}) and three-body recombination (L^s_3) gives rates that are consistent with more recent measurements.[21–23,25] Also the suppression of L^s_3 with increasing magnetic field is consistent with measurements of Bell et al.[22,23]

The apparent second order behavior used in the previous analysis (I) was caused by (small) temperature gradients in the gas that change during the decay. These temperature difference also account for the apparent suppression of the surface recombination as reported in (I) at very low temperature on ^{3}He films.

Acknowledgements

We thank A. Lagendijk, B.J. Verhaar for a number of stimulating discussions, O. Höpfner for technical support and J. van Zwol for assistance with the reinterpretation of the data. The financial support of the Stichting voor Fundamenteel Onderzoek der Materie and Department of Energy, grant number DE-FG02-85ER45190 is gratefully acknowledged.

Appendix A Field and temperature dependence of the volume to surface ratio

To illustrate the effect of a density profile on the decay rates, we examine a cylinder with radius R in the parabolic field described by eq.IV.7. In a small volume element with height dz, surface area dA and volume dV (see fig.12) a decay process (L) of order k with a volume contribution $L^V(B,T)$ and a surface contribution $L^S(B,T)$ can be described by the rate equation:

(A.1)

$$\dot{dN} = - dA\, L^S(B,T)\, (\sigma/n)^k\, n^k(z) - dV\, L^V(B,T)\, n^k(z).$$

In a portion of the cylinder between z_1 and z_2 this results in a rate of the total number of particles given by:

(A.2)

$$\dot{N} = \int_{z_1}^{z_2} \dot{dN} = - 2\pi R \int_{z_1}^{z_2} L^S(B,T)\, (\sigma/n)^k\, n^k\, dz - \pi R^2 \int_{z_1}^{z_2} L^V(B,T)\, n^k\, dz.$$

With the use of eq.IV.6 for the density profile, the total rate becomes:

$$\dot{N} = -2\pi R\int_{z_1}^{z_2} L^s(B,T)\, C^k(B,T)\, dz\ \ (\sigma/n)^k\, n_0{}^k - \pi R^2\int_{z_1}^{z_2} L^v(B,T)\, C^k(B,T)\, dz\ \ n_0{}^k \qquad (A.3)$$

and the total number of particles in this section of the cylinder is given by:

$$N \simeq \pi R^2\int_{z_1}^{z_2} n(z)\, dz = n_0\, \pi R^2\int_{z_1}^{z_2} C(B,T)\, dz. \qquad (A.4)$$

Combining equations IV.6, A.3 and A.4 results in an effective rate equation for the density in the center of the magnet. Since the pressure gauge measures the pressure in the center of the magnet, this equation is needed to model the observed pressure decay. It is also convenient to express the intrinsic field dependence of L^v and L^s in dimensionless constants l^v and l^s with respect to the situation in the field center:

$$L^v(B,T) \equiv l^v(B) L^v(B_0,T) \qquad (A.5)$$

$$L^s(B,T) \equiv l^s(B) L^s(B_0,T).$$

Using eqs. IV.6 and A.3-5 the rate equation for n_0, under uniform thermal conditions in the gas, can be written:

$$\dot{n}_0\, V_l^{eff} = -A_{Ls}^{eff}\, L^s(B_0,T)\, (\sigma/n)^k\, n_0{}^k - V_{Lv}^{eff}\, L^v(B_0,T)\, n_0{}^k, \qquad (A.6)$$

where the effective volumes and surfaces are defined by:

$$V_l^{eff} = V_{geo}\, \{\int_{z_1}^{z_2} C\, dz / \Delta z\}$$

$$A_{Ls}^{eff} = A_{geo}\, \{\int_{z_1}^{z_2} l^s\, C^k\, dz / \Delta z\} \qquad (A.7)$$

$$V_{Lv}^{eff} = V_{geo}\, \{\int_{z_1}^{z_2} l^v\, C^k\, dz / \Delta z\},$$

with $V_{geo}=\pi R^2\, \Delta z$, $A_{geo}=2\pi R\, \Delta z$ the geometric volume and surface and $\Delta z \equiv z_2 - z_1$ the length of the cylinder. For convenience we have used an abbreviated notation for $l^s(B)$, $l^v(B)$, $C(B,T)$.

Equation A.6 can be interpreted as an effective rate equation for a field B_0 and a density n_0 in the center. Instead of the geometric volumes and surfaces, one uses effective volumes and surfaces. These effective volumes and surfaces depend on the order of the process (k) and on the intrinsic field dependence of the specific decay process ($l^s(B)$ and $l^v(B)$).

In particular for dipolar relaxation and exchange recombination the intrinsic field dependences are:

(A.8)

$$l^{s}_{rel} = l^{v}_{rel} = ((1 + 16.68/B)/(1 + 16.68/B_0))^2$$

$$l^{s}_{rec} = 1 / (B/B_0)^2.$$

The corrections due to these intrinsic field dependences is small (<2%). This was verified by numerical evaluation of the effective surfaces in eq.A.7; the exponential character of the compression factor C dominates the (weaker) intrinsic field dependences. Thus it is sufficient to use only the compression factor to calculate the effective volumes and areas for a particular decay process of order k:

(A.9)

$$V^{eff}_{k} = V_{geo} \{ \int_{z_1}^{z_2} C^k \, dz / \Delta z \}$$

$$A^{eff}_{k} = A_{geo} \{ \int_{z_1}^{z_2} C^k \, dz / \Delta z \}.$$

Fig.13 shows the compression factors in a cylinder for decay processes of order k.

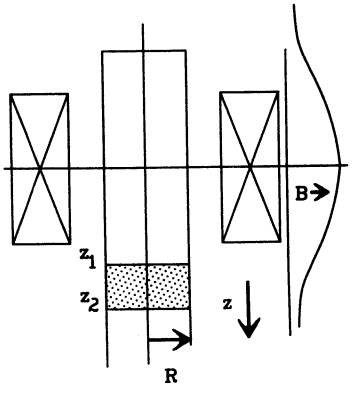

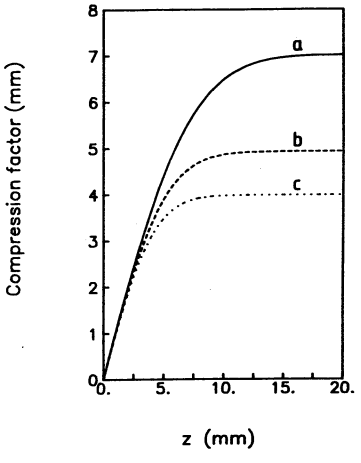

fig.12 (left) *Part of a cylinder with radius R between z_1 and z_2 with a volume element dV and a surface element dA.*

fig.13 (right) *Compression coefficients for a cylindrical cell in a parabolic field profile. See Appendix A for definitions of compression coefficients.*

$$a - \int_0^z C \, dz, \; b - \int_0^z C^2 \, dz, \; c - \int_0^z C^3 \, dz$$

References

1 I.F. Silvera, Physica 109 & 110B, 1499 (1982).

2 J.T.M. Walraven, Physica 126B, 176 (1984).

3 T.J. Greytak and D. Kleppner, 'New trends in atomic physics', Vol.II G.Grynberg and R.Stora (Ed.), Elsevier Sci.Publ., Les Houches, 1125 (1984).

4 I.F. Silvera and J.T.M. Walraven, to be published, Progress in Low Temperature Physics.

5 R. Sprik, J.T.M. Walraven, G.H. van Yperen and I.F. Silvera, Phys.Rev.Lett. 49, 153 (1982).

6 B.W. Statt and A.J. Berlinsky, Phys.Rev.Lett. 45, 2105 (1980).

7 Yu. Kagan, I.A. Vartanyantz and G.V. Shlyapnikov, Sov.Phys.JETP 54, 590 (1981).

8 Yu. Kagan, G.V. Shlyapnikov, Phys.Lett. 88A 356 (1982).

9 R.W. Cline, T.J. Greytak and D. Kleppner, Phys.Rev.Lett. 47, 1195 (1981).

10 G.H. van Yperen, A.P.M. Matthey, J.T.M. Walraven and I.F. Silvera, Phys.Rev.Lett. 47, 800 (1981).

11 A.P.M. Matthey, J.T.M. Walraven and I.F. Silvera, Phys.Rev.Lett. 46, 668 (1981). I.F. Silvera and J.T.M. Walraven, Phys.Rev.Lett. 44, 164 (1980). J.T.M. Walraven, I.F. Silvera and A.P.M. Matthey, Phys.Rev.Lett. 45, 449 (1980).

12 R.W. Cline, D.A. Smith, T.J. Greytak and D. Kleppner, Phys.Rev.Lett. 45, 2117 (1980).

13 M. Morrow, R. Jochemsen, A.J. Berlinsky and W.N. Hardy, Phys.Rev.Lett. 46, 195 (1981); Erratum 47, 455 (1981).
R. Jochemsen, M. Morrow, A.J. Berlinsky and W.N. Hardy, Phys.Rev.Lett. 47, 852 (1981).

14 B.R. Johnson, J.S. Denker, N. Bigelow, L.P. Lévy, J.H. Freed and D.M. Lee, Phys.Rev.Lett. 52, 1508 (1984).
B. Yurke, J.S. Denker, B.R. Johnson, N. Bigelow, L.P. Levy, D.M. Lee and J.H. Freed, Phys.Rev.Lett. 50, 1137 (1983).

15 G.H. van Yperen, I.F. Silvera, J.T.M. Walraven, J. Berkhout and J.G. Brisson, Phys.Rev.Lett. 50, 53 (1983).
G.H. van Yperen, J.T.M. Walraven and I.F. Silvera, Phys.Rev.B 30, 2386 (1984).

16 A. Lagendijk, Phys.Rev.B. 25, 2054 (1982).

17 A.E. Ruckenstein and E.D. Siggia, Phys.Rev.B 25, 6031 (1982).

18 B.W. Statt, Phys.Rev.B 25, 6035 (1982).

19 R.M.C. Ahn, J.P.H.W. van den Eijnde, C.J. Reuver, B.J. Verhaar and I.F. Silvera, Phys.Rev.B 26, 452 (1982). R.M.C. Ahn, J.P.H.W. van den Eijnde and B.J. Verhaar, Phys.Rev.B 27, 5424 (1983). J.P.H.W van den Eijnde, C.J. Reuver and B.J. Verhaar, Phys.Rev.B 28, 6309 (1983).

20 R. Sprik, J.T.M. Walraven and I.F. Silvera, Phys.Rev.Lett. 51, 479 (1983); Erratum 51, 942 (1983). R. Sprik, J.T.M. Walraven and I.F. Silvera, Phys.Rev.B 32, 5668 (1985).

21 H.F. Hess, D.A. Bell, G.P. Kochanski, R.W. Cline, D. Kleppner and T.J. Greytak, Phys.Rev.Lett. 51, 483 (1983).

22 H.F. Hess, D.A. Bell, G.P. Kochanski, D. Kleppner and T.J. Greytak, Phys.Rev.Lett. 52, 1520 (1984).

23 D.A. Bell, G.P. Kochanski, L. Pollack, H.F. Hess, D. Kleppner and T.J. Greytak, Physica (LT-17), 449 (1984).
D.A. Bell, H.F. Hess, G.P. Kochanski, S. Buchman, L. Pollack, Y.M. Xiao, D. Kleppner and T.J. Greytak, preprint (1985)

24 T. Tommila, S. Jaakkola, M. Krusius, K. Salonen and E. Tjukanov, Proceedings LT-17 (Karlsruhe) Elsevier Science Publishers, 453 (1984) and T. Tommila, S. Jaakkola, M. Krusius, I. Krylov, E. Tjukanov, Phys.Rev.Lett. 56, 941 (1986).

25 M.W. Reynolds, I. Shinkoda, W.N. Hardy, A.J. Berlinsky, F. Bridges and B.W. Statt, Phys.Rev.B 31, 7503 (1985).
B.W. Statt, W.N. Hardy, A.J. Berlinsky and E. Klein, J.L.T.P. 61, 471 (1985).
B.W. Statt, A.J. Berlinsky and W.N. Hardy, Phys.Rev.B 31, (1985) 3169.

26 D.A. Bell, G.P. Kochanski, D. Kleppner and T.J. Greytak, Physica (LT-17) 541 (1984).

27 A. Lagendijk, G.H. van Yperen and J.T.M. Walraven, J.de Phys.Lett. 45, L929 (1984).

28 Obtained by chemical analysis of our OFHC copper.

29 L.J. Azevedo, Rev.Sci.Instrum. 54, 1793 (1983).

30 J.T.M. Walraven and I.F. Silvera, Rev.Sci.Instr. 53, 1167 (1982).

31 J.T.M. Walraven and I.F. Silvera, Phys.Rev.Lett. 44, 168 (1980).

32 K.T. Salonen, I.F. Silvera, J.T.M. Walraven and G.H. van Yperen, Phys.Rev.B 25, 6002 (1982).
K. Salonen, S. Jaakkola, M. Karhunen, E. Tjukanov and T. Tommila, Proceedings LT-17, Elsevier Sci.Publ., 543 (1984).

33 O.V. Lounasmaa, 'Experimental Principles and Methods Below 1K', Academic Press, 1974.

34 H.P. Godfried, E.R. Eliel, J.G. Brisson, J.D. Gillaspy, C. Mallardeau, J.C. Mester and I.F. Silvera, Phys.Rev.Lett. 55, 1311 (1985).

35 W.N. Hardy, private communication.

36 J.P.H.W van den Eijnde, thesis 1984, University of Eindhoven.

37 L.P.H. de Goey, J.P.J. Driessen, B.J. Verhaar and J.T.M. Walraven, Phys.Rev.Lett. 53, 1919 (1984).

Chapter 3

State-Dependent Recombination and Suppressed Nuclear Relaxation in Atomic Hydrogen

R. Sprik, J.T.M. Walraven, G.H. van Yperen, and Isaac F. Silvera

Natuurkundig Laboratorium, Universiteit van Amsterdam,
Valckenierstraat 65, 1018 XE Amsterdam, The Netherlands.

Abstract

A gas of 99.8% electron- and proton-spin-polarized hydrogen has been prepared. The surface and volume nuclear relaxation rates have been measured and the magnetic field dependence $(1+16.68/B)^2$ has been confirmed. The ratio of the surface recombination rate constants for collisions between atoms in hyperfine states, a-a and a-b, is measured to be 2.23(25). Nuclear relaxation on the surface has been suppressed by using ^{3}He to make an atomically flat surface.

[Physical Review Letters, 49 153-157 (1982)]

State-Dependent Recombination and Suppressed Nuclear Relaxation in Atomic Hydrogen

R. Sprik, J. T. M. Walraven, G. H. van Yperen, and Isaac F. Silvera
Natuurkundig Laboratorium der Universiteit van Amsterdam, 1018-XE Amsterdam, The Netherlands
(Received 24 February 1982)

A gas of 99.8% electron- and nuclear-spin-polarized hydrogen has been prepared. The surface and volume nuclear relaxation rates have been measured and the magnetic field dependence $(1+16.68/B)^2$ has been confirmed. The ratio of the surface recombination rate constants for collisions between atoms in hyperfine states, a-a and a-b, is measured to be 2.23(25). Nuclear relaxation on the surface has been suppressed by using ^{3}He to make an atomically flat surface.

PACS numbers: 67.40.-w, 67.70.+n

Since a gas of spin-polarized atomic hydrogen ($H\downarrow$) was first stabilized a few years ago[1] experimental efforts have been devoted to achieving sufficiently high densities or low temperatures to observe Bose-Einstein condensation (BEC). Densities, n, of just under $10^{17}/cm^3$ were soon obtained.[2,3] These were limited by recombination of $H\downarrow$ to H_2 on the ^{4}He surfaces of the sample cell[4-6]: Because of the nonnegligible adsorption energy of $H\downarrow$ on He, $H\downarrow$ surface coverages (n_s) increase with decreasing temperature and the recombination (which increases with n_s^2) limits the density.

Higher densities can be achieved by producing a state-selected gas of hydrogen. $H\downarrow$ has two hyperfine states $|a\rangle = |\downarrow\uparrow\rangle - \epsilon|\uparrow\downarrow\rangle$ and $|b\rangle = |\downarrow\downarrow\rangle$ ($\downarrow$, electron spin; $\downarrow$, nuclear spin), where $\epsilon \simeq a/4\mu B$, with a the hyperfine constant, μ the Bohr magneton, and B the magnetic field. Statt and Berlinsky[7] have pointed out that a nuclear-spin-polarized gas of pure b state ($H\downarrow\downarrow$) would have a much lower recombination rate as these atoms do not have admixtures of the electron "up" state. They suggested that this state might be achieved by prefer-

ential recombination of a-state atoms. The idea is that a-a collisions and a-b collisions can lead to recombination whereas b-b cannot. If the a $\rightleftarrows$ b nuclear relaxation time T_1 is much longer than the characteristic recombination time, the a state will be depleted leaving $H\downarrow\downarrow$. Cline, Greytak, and Kleppner[8] succeeded in producing a gas of $H\downarrow\downarrow$ and measuring both the surface and the volume nuclear-spin-relaxation times T_1^s and T_1^v, respectively. The observed value $T_1^v \simeq 13$ h was in agreement with theory.[7,9] Van Yperen *et al.*[10] attempted this experiment earlier but found very rapid relaxation, $T_1 \lesssim 10$ sec.

In this Letter we report on recent experiments in which we have created and studied $H\downarrow\downarrow$ of purity up to 99.8%. A cell has been constructed with special care to eliminate surface magnetic impurities in the form of macroscopic grains (dimensions $\simeq 0.1$ μm), believed to be the cause of the short T_1's measured earlier. This cell, shown in Fig. 1, has a large area-volume ratio which enables the study of surface relaxation phenomena over a broad range of temperature. We describe how we have been able to strongly suppress surface relaxation with our special geometry which takes advantage of the predicted[11-13] anisotropy in the relaxation rate. This is vital for BEC as surface relaxation will be the limiting mechanism for achieving high densities. We also study the magnetic field dependence of T_1. In addition, we have determined the important ratio of the recombination rate constants, K_{aa} for a-a collision and K_{ab} for a-b collisions,[7] which, for simplicity, had earlier been assumed to be 1.

Both surface and volume nuclear-spin relaxation are of importance. The intrinsic surface relaxation rate $G_s \equiv (2T_1^s n_s)^{-1}$ is orders of magnitude faster than the volume rate G_v. Although both rates essentially arise from the magnetic dipolar interactions between atoms, the interaction can be averaged out by the motions. This motional averaging is less effective on the surface because the motions in two dimensions are slower than in three dimensions.[11] However, only very few atoms reside on the surface as can be seen from the adsorption isotherm for a mobile two-dimensional gas with a single bound state (such as $H\downarrow$ on He), $n_s = n\lambda \exp(\epsilon_a/kT)$, where $\lambda = (2\pi\hbar^2/mkT)^{1/2}$. The probability of finding an atom on the surface is $n_s A/nV = (A/V)\lambda \exp(\epsilon_a/kT)$, where A/V is the surface-to-volume ratio. Since atoms are rapidly exchanging between the surface and gas phases, to determine the effect of surface relaxation on gas-phase atoms we must multiply G_s by this factor which can be of the order 10^{-3}, rapidly increasing with decreasing temperature.

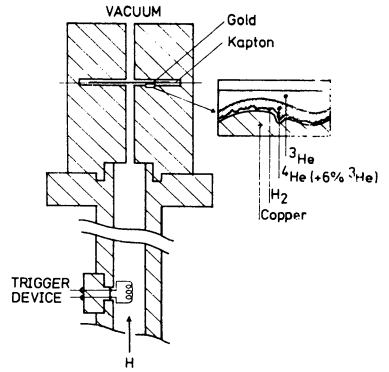

FIG. 1. Cross section of the hydrogen stabilization cell. The gold-plated Kapton is one plate of the capacitance pressure gauge. The inset shows what we believe to be a microscopic surface profile.

The rate equations for the decay of the density of a gas of $H\downarrow$ in states $|a\rangle$ and $|b\rangle$ are[7,8] (valid for $kT \gg E_b - E_a$, the hyperfine splitting)

$$\frac{dn_a}{dt} = \frac{\varphi_a}{V} - \frac{n_a}{\tau_T} - G_s^{ie}(n_a - n_b) - (G_v + G_s^e)(n_a - n_b)(n_a + n_b) - 2K_{aa}^e n_a n_a - K_{ab}^e n_a n_b, \tag{1a}$$

$$\frac{dn_b}{dt} = \frac{\varphi_b}{V} - \frac{n_b}{\tau_T} + G_s^{ie}(n_a - n_b) + (G_v + G_s^e)(n_a - n_b)(n_a + n_b) - K_{ab}^e n_a n_b. \tag{1b}$$

Here $n_a + n_b = n$ is the total volume density; all coefficients superscripted with an e refer to surface phenomena and have been converted to effective volume terms. In Eq. (1a) the first term is the flux of a atoms filling volume V; the second is the thermal leakage[14] out of the cell which can be suppressed by making $B/T \gg 1$. The third term arises from magnetic impurities on the surface of the cell with $G_s^{ie} = G_s^i (A/V)\lambda \exp(\epsilon_a/kT)$, where G_s^i is the surface impurity nuclear-spin relaxation rate. Since ^{3}He atoms bear nuclear magnetic moments, relaxation due to a ^{3}He impurity or a pure ^{3}He surface would also be described by such a term. The fourth term describes relaxation due to binary collisions in the gas, G_v, or on the surface, $G_s^e = G_s (A/V)\lambda^2 \exp(2\epsilon_a/kT)$. As first described by Lagendijk,[11-13] the sur-

face relaxation rate is anisotropic with

$$G_s(B,T)=[G_{s,0}(\infty,T)\sin^2 2\theta+G_{s,2}(\infty,T)\sin^2\theta(1+\cos^2\theta)](1+16.68/B)^2. \quad (2)$$

Here θ is the angle between the surface normal and the applied magnetic field; numerical evaluation shows that $G_{s,0}\gg G_{s,2}$. Note that for $\theta=0$, $G_s=0$. The fifth and sixth terms in Eqs. (1) describe surface recombination with $K_{aa}^{\,e}=K_{aa}(A/V)\lambda^2\exp(2\epsilon_a/kT)$, where K_{aa} is the intrinsic surface rate; a similar definition exists for K_{ab}. In Eqs. (1) we ignore volume recombination.

For an accurate description of our experiments a detailed characterization of the geometry and surface conditions is necessary. The microscopic area A of the (rough) surface can be somewhat larger than the macroscopic or projected area A_p; thus we define $A=\alpha A_p$. As a result of the magnetic field gradient and low temperature the gas has an inhomogeneous density distribution with an axial profile that depends exponentially on B/T.[14] In our system, for small values of B/T the gas is spread over the cell, whereas for large values it is confined to the pancake-shaped region of the pressure gauge. For this reason we use effective volumes[14] V^e and areas A^e in our analyses. $(A/V)^e$ varied between 40 and 140 cm^{-1} in our experiments. The gauge is designed to minimize the perpendicular area, $A_\perp$, corresponding to $\theta=90^\circ$ in Eq. (2). The area here is $A_p=A_\parallel+A_\perp=(2.50+0.039)\ \mathrm{cm}^2$. The upper surface is uncoated Kapton, and the lower is machined and etched copper. In the analyses in Fig. 2 we have used $A^e=A_p^{\,e}$. The rest of the system is similar to that shown in Fig. 1 of Ref. 9. A fine tungsten resistance wire is used to trigger[1] recombination of the $H^\downarrow$.

We first measured decay curves (n vs t) for $H^\downarrow$ as a function of ^{4}He film thickness. For thin (undersaturated) films we observed a large first-order decay term. We assume that this arises principally from isolated O_2 or Fe impurities on or in the copper surface giving rise to a $G_s^{\,i}$ term. A thick (~saturated) film of ^{4}He completely suppressed this.

The important ratio $\gamma=K_{aa}/K_{ab}$ can be determined if the relaxation can be ignored with respect to the recombination rates in Eqs. (1). Assuming $\varphi=0$, $\tau_T=\infty$, and $n_{a0}/n_{b0}=1$, one finds $n_\infty/n_0=(2\gamma)^{(1-2\gamma)^{-1}}/2$, where the zero ($\infty$) subscript refers to density at $t=0$ (∞). The following interesting limits exist: $n_\infty/n_0=0.5$, 0.25, and 0 in the cases $K_{ab}=0$, $K_{ab}=K_{aa}$, and $K_{aa}=0$, respectively.

In Fig. 2(a) we show typical decay curves for $H^\downarrow$ with a thick ^{4}He coverage, demonstrating the decay to an $H^{\downarrow\downarrow}$ state. For curve 2 we rapidly fill the cell for several seconds so that $n_{a0}=n_{b0}$ and then allow the gas density to decay to its long-time value. We find $n_\infty/n_0=0.32$ after correcting for a small temperature rise of the cell during filling. This leads to a temperature-independent value of $\gamma=K_{aa}/K_{ab}=2.23\pm0.25$ as measured for $T=225$, 250, and 300 mK. In the limit of rapid relaxation, the recombination rate constant is the average of K_{aa} and K_{ab}. Using the results of Matthey, Walraven, and Silvera[5] we find $K_{ab}B^2T^{-1/2}=1.6(5)\times10^{-7}\ \mathrm{cm}^2\ \mathrm{T}^2/\mathrm{K}^{1/2}$ sec.

In Fig. 2(b) we plot our data for nuclear relaxation along with that of Cline, Greytak, and Kleppner (CGK).[8] Each point represents a fit to a density decay curve, such as shown in Fig. 2(a), using Eq. (1). Our results are markedly different for ^{3}He and ^{4}He surfaces. The ^{4}He data are dominated by surface relaxation giving rise to an exponentially increasing relaxation with lowering of the temperature. Fitting the data by a straight line, we find $\epsilon_a/k=0.89(6)$ K and $\alpha\langle G_s\rangle(1+16.68/B)^{-2}=3.4(1.0)\times10^{-13}\ \mathrm{cm}^2/\mathrm{sec}$. Here we use *one half* of the area of the pressure cell for reasons to be given later. We assumed the intrinsic surface relaxation rate (G_s) to be temperature independent. As shown by theory[11-13] G_s has a very weak temperature dependence, rather than being proportional to T as assumed by CGK.[8] We note that because of their restricted temperature range and small A/V ratio, $G\equiv G_v+G_s^{\,e}$ is dominated by G_v, whereas our cell emphasizes $G_s^{\,e}$. To compare with the CGK-MIT results we evaluate their data using our value of ϵ_a (which increases their rate by 2.2) to find $1.8\times10^{-13}\ \mathrm{cm}^2/\mathrm{sec}$, or a factor 1.9 smaller than what we find.

The angular brackets on G_s refer to an average over the angle θ in Eq. (2). Defining $\bar\theta$ as the macroscopic value of θ, the CGK-MIT geometry has $\bar\theta=90^\circ$ whereas our geometry has $\bar\theta=0$. Ahn *et al.*[13] have pointed out that the copper surface probably has a roughness of order 1–0.1 μm and it is more appropriate to consider the profile as a "muffin tin" surface. They average Eq. (2) using a section of a spherical surface subtending an angle φ. For $\varphi=90^\circ$, $\alpha=1.17$; G_s is totally dominated by $G_{s,0}$ with $\langle G_s\rangle/G_{s,0}\simeq0.39$ in the CGK-MIT geometry and 0.70 in ours. This provides a factor 1.8 and brings our results and the CGK-MIT results into good agreement. However, the

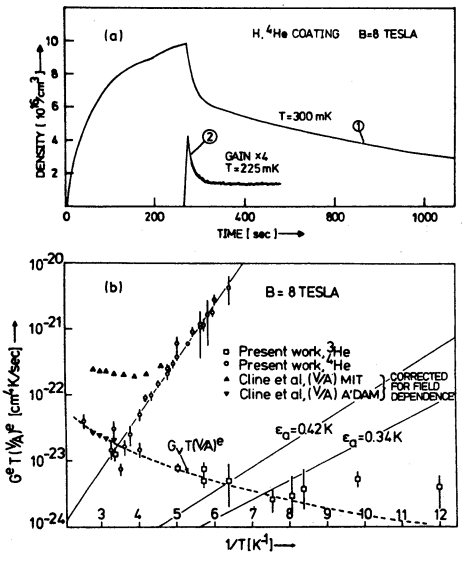

FIG. 2. (a) Decay of hydrogen to H↓T. (b) The effective nuclear relaxation rate times $T(V/A)^e$ as a function of T^{-1}, for H on ^{4}He and ^{3}He-^{4}He surfaces. The data of Cline, Greytak, and Kleppner are corrected to our conditions for comparison. The straight line is a fit to the data; its slope is $2\epsilon_a$. For the ^{3}He surface with a smaller ϵ_a, if surface relaxation were important, the data would rise linearly within the bound given by the two lines rising to the right. However, we only observe bulk relaxation. The dashed line is a fit to the ^{3}He data assuming $G_v \propto \sqrt{T}$.

theoretical value for $\langle G_s\rangle(1+16.68/B)^{-2}$ is 0.57×10^{-14} cm^2/sec for our geometry which is a factor 50 smaller than experiment (using $\alpha=1.17$). A possible explanation is that because of the presence of the helium surface, H-H interactions will be modified so that relative motions are slowed, reducing the "motional narrowing" or increasing G_s.

We have also studied the dependence of G_s [Eq. (2)] on magnetic field and find reasonable agreement with theory.

Now we consider ^{3}He surfaces achieved from a mixture of ^{3}He-^{4}He. ^{3}He forms several monolayers on the ^{4}He as described by van Yperen *et al.*[10] We might now expect a term G_s^i in Eq. (1) due to the ^{3}He. However, this term is probably negligible as can be seen from scaling the dipolar interaction. For H-^{4}He, the H-H electron-nuclear dipole interaction is dominant and $(T_1^s)^{-1} \propto (\gamma_e{}^{\rm H}\gamma_n{}^{\rm H})^2 n_s^2$ whereas for H-^{3}He, the additional term due to ^{3}He is $(T_1{}^{^3\rm He})^{-1} \propto (\gamma_n{}^{^3\rm He}\gamma_n{}^{\rm H})^2 n_s n_{^3\rm He}$, where γ_n and γ_e are the nuclear and electronic gyromagnetic ratios. We find $(T_1{}^{s\,^3\rm He})^{-1}/(T_1{}^s)^{-1} \simeq 10^{-3}$, using $n_{^3\rm He}=6.4\times10^{14}$ cm^{-2} and $n_s=10^{12}$ cm^{-2}. In Fig. 2(b) we also plot our data for G on ^{3}He. Using the relaxation rate on ^{4}He and the measured values of ϵ_a on ^{3}He or ^{3}He-^{4}He mixtures we would expect the data to fall within the limits of the two lines for surface relaxation, contrary to observations. We identify the rate as volume relaxation with $G_v T^{-1/2}=5.6(5)\times10^{-21}$ cm^3/sec K$^{1/2}$ at $B=8$ T, in good agreement with the 5.3×10^{-21} cm^3/sec K$^{1/2}$ of CGK on ^{4}He, scaled to $B=8$ T. To understand why G_s is suppressed for ^{3}He and not for ^{4}He, we note that in the latter case, the ^{4}He film in the pressure gauge will be of thickness ~200 Å due to superflow properties of the film in the presence of gravity and the warmer lower sections of the cell.[10] On the other hand, ^{3}He will be concentrated in the lowest-temperature part of the cell, the pressure gauge. As a result of gravity the ^{3}He will level the surface of the lower (copper) side of the pressure gauge so that it is atomically flat (see Fig. 1, detail). The upper side, made of Kapton, will be covered with a thin (~200 Å) ^{3}He-^{4}He film. The Kapton surface examined by a scanning electron microscope appears flat with our highest spatial resolution of ~100 Å, with a low density of pits (diam $\lesssim 1$ μm) that may be filled by capillary condensation. Evidently the combination of Kapton and He film provides an atomically flat surface. In this case all of the $A_\perp$ is atomically flat so that $\langle G_s\rangle \simeq 0$. This implies that for pure ^{4}He surfaces we should just use the area of the copper, reducing the area of the pressure gauge by a factor 2, as used in the analyses. The maximum density achieved in this run with ^{3}He surfaces was 3×10^{17}/cm^3.

We thank O. H. Höpfner for technical aid and J. Kragten for chemical analyses of our copper. The financial support of the Stichting voor Fundamenteel Onderzoek der Materie is gratefully acknowledged.

[1]I. F. Silvera and J. T. M. Walraven, Phys. Rev. Lett. 44, 164 (1980).
[2]J. T. M. Walraven, I. F. Silvera, and A. P. M. Matthey, Phys. Rev. Lett. 45, 449 (1980).
[3]R. W. Cline, D. A. Smith, T. J. Greytak, and D. Klep-

pner, Phys. Rev. Lett. 45, 2117 (1980).
[4]I. F. Silvera and J. T. M. Walraven, Phys. Rev. Lett. 45, 1268 (1980).
[5]A. P. M. Matthey, J. T. M. Walraven, and I. F. Silvera, Phys. Rev. Lett. 46, 668 (1981).
[6]M. Morrow, R. Jochemsen, A. J. Berlinsky, and W. N. Hardy, Phys. Rev. Lett. 46, 195 (1981), and 47, 455 (1981).
[7]B. W. Statt and A. J. Berlinsky, Phys. Rev. Lett. 45, 2105 (1980); J. M. Greben, A. W. Thomas, and A. J. Berlinsky, Can. J. Phys. 59, 945 (1981).
[8]R. W. Cline, T. J. Greytak, and D. Kleppner, Phys. Rev. Lett. 47, 1195 (1981).
[9]E. D. Siggia and A. E. Ruckenstein, Phys. Rev. B 23, 3580 (1981).
[10]G. H. van Yperen, A. P. M. Matthey, J. T. M. Walraven, and I. F. Silvera, Phys. Rev. Lett. 47, 800 (1981).
[11]A. Legendijk, Phys. Rev. B 25, 2054 (1982).
[12]A. E. Ruckenstein and E. D. Siggia, Phys. Rev. B 25, 6031 (1982); B. Statt, Phys. Rev. B 25, 6035 (1982).
[13]R. M. C. Ahn, J. P. H. W. v.d. Eynde, C. J. Reuver, B. J. Verhaar, and I. F. Silvera, Phys. Rev. B 26, 452 (1982).
[14]J. T. M. Walraven and I. F. Silvera, Phys. Rev. Lett. 44, 168 (1980).

Chapter 4 Volume compression of spin-polarized atomic hydrogen

4.1 Volume compression of H↓↑; an isobaric decay method

Although the double polarization observed in the experiment described in the previous chapters enhances the stability dramatically, the gas densities that are obtained by loading a cell with a (continuous) flux of atoms remain below the densities where the BEC transition should be observable. The density can be increased further by compression of the gas volume. For example, with a starting volume of $\approx 1 cm^3$, a starting density of only $10^{15} cm^{-3}$ and a volume compression ratio of 10^4, the density in the compressed sample volume of $0.1 mm^3$ satisfies the B.E.C. conditions at 100mK. The required compression ratio is in fact higher because recombination occurs during the compression.

Two different schemes were developed to compress the gas and study the high density sample. The first method monitors the density decay in the small volume by using, as in the previous experiment, a pressure gauge. Since the volume remains constant during the decay, one could call this an isochoric measurement; the high density decays very rapidly after the compression has been concluded. Such a scheme was developed by the M.I.T. group.[1-4]

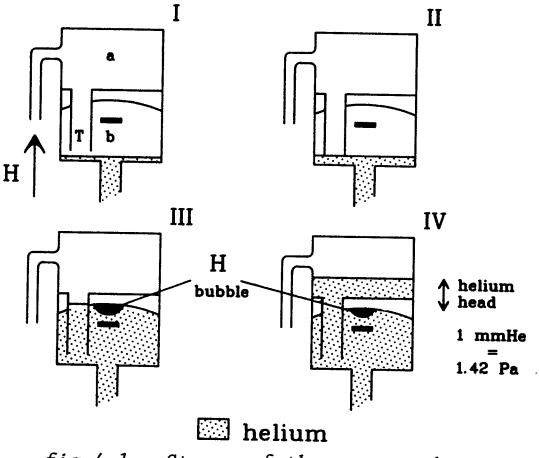

fig.4.1 Stages of the compression.

The second method, which we developed in Amsterdam[5,6] and has also been used in Turku[7,8], starts with the same idea: compression of a large volume, low density gas to smaller volumes. After the compression, the pressure in the gas is maintained nominally constant and the decay of the volume is monitored. The principle of such an 'isobaric' compression technique is schematically drawn in fig.4.1. The cell consists of a storage volume (a) and an lower part (b) connected by a separating tube T. The helium level in

the cell can be varied by adding helium via the bottom tube. In the first stage (fig.4.1.I) of the compression, volume (a) and (b) are loaded with H↓↑ up to densities $\simeq 1 \times 10^{15} cm^{-3}$ and the helium level is gradually raised. Volume compression starts when the rising helium level reaches the rim of tube T and traps the gas in volume (a) (fig.4.1.II) Further (slow) compression will lead to an increase of the density. By raising the helium level beyond the point were the H↓↑ is trapped (fig.4.1.III), the helium column head applies a pressure to the gas (fig.4.1.IV). A column head of 1mm ^4He corresponds with an applied pressure of 1.4Pa (10^{-2}Torr). The pressure for BEC conditions at 100mK corresponds to a column head of 30mm if all other contributions to the pressure in the bubble are ignored. Since the applied pressure in the gas is constant, the volume of this bubble will change as a function of time due to the recombination of the H atoms (the formed H_2 molecules will not contribute to the pressure as they most likely will penetrate the helium liquid and stick to the (metallic) cell walls[9]). In this method the density in the gas remains high during the whole decay in contrast to the previously described isochoric measurement. We choose a straightforward method to move the liquid helium level by building the cell in a U-tube like configuration and lowering a copper block (handled from outside the cryostat) in one of the legs. The helium level is than determined by simple volumetric considerations. More complex schemes have been developed to handle helium levels at low temperatures, e.g. using the fountain effect of liquid helium[10] and decreasing the volume of the cell by compressing a system of bellows.[7,8]

The first measurements with this compression cell were presented in a letter article (chapter 5) and in an extended article (chapter 6). The extended article also treats the analysis of the volume decays in detail. After modification of the HEVAC system, the connection between the compression cell and the higher temperature parts, and the addition of a helium level stabilizer, a new run was made. Although the compression cell could be cooled to lower temperatures than in the first run, the cell again warmed up to ≃700mK after a while. This seems to be caused by droplets of helium falling from the low temperature part on to high temperature parts (4.2K) where they evaporate. The bursts of back streaming hot gas form an excessive heat load on the system. Nevertheless a number of measurements at ≃700mK for low magnetic fields were recorded to complement the data from the first run (see section 4.4). Section 4.3 gives some additonal information of the analyzing method as presented in detail in chapter 6.

The decay of the volume as function of time and the level of the helium are both measured using capacitive methods. In the next sections the gauge to measure the volume is treated in more detail. Also a method to actively stabilize the helium level as well as some of the electronics to measure the various capacitive gauges in the cell are discussed.

4.2 Some technical details of the compression cell

The volume gauge and the helium level detector are two key components of the compression cell; they measure the volume of the compressed hydrogen bubble and the helium column height. In this section more technical details of the construction and use of these vital parts are given. In the last section some methods to displace liquid helium by using magnetic and electric fields are discussed.

4.2.1 The volume gauge

The measurement of the bubble volume by a capacitor is based on the difference in dielectric susceptibility of bulk helium and the atomic hydrogen gas. The relative dielectric constant of helium is determined via the Clausius-Mossotti relation[12] by using the polarizability of the helium atom ($\alpha/(4\pi\epsilon_0)$=0.204956Å^3 [13]) and the density of the liquid (^{3}He or ^{4}He) at the measuring temperature. Below 1.2K the density of liquid ^{4}He is nearly constant ($n_{He}\simeq 2.18\times10^{22}$cm^{-3} [14]) resulting in an overall ϵ_r=1.057. Because of the 'low' density of the hydrogen gas in the bubble and also the low vapor pressure of helium at T<1K, the overall dielectric constant inside the bubble is almost the vacuum value (e.g. for an H density of $1.\times10^{18}$cm^{-3} and with $\alpha/(4\pi\epsilon_0)$=0.666793Å^3 [13] $\epsilon_r-1=8.4\times10^{-6}$). To first approximation the total capacity is easily estimated to be:

$$C=C_H + C_{He} = \epsilon_0 V_H/d^2 + \epsilon_r\epsilon_0 V_{He}/d^2. \qquad (4.2.1)$$

Here V_H and V_{He} are the volume of the H bubble and the helium respectively and d is the distance between the plates. This results in a change of the capacitance (ΔC) that is to good approximation proportional to the bubble volume (V_H):

$$\Delta C/C_{tot} = ((\epsilon_r-1)/\epsilon_r) V_H/V_C, \qquad (4.2.2)$$

with C_{tot} the capacity when the gauge is completely filled with He and V_C the volume of the gauge.

To check the validity of this simple approximation, one would have to solve the problem of the electric field pattern in detail. For arbitrary shape and position of the bubble between the plates, the Maxwell equations should be solved using the proper boundary conditions at the bubble interface, an arduous task. To study qualitatively the influence of the shape of the bubble on the capacitance, consider the volume to be a cylinder with one of the ends in contact with the plate. For the two extreme situations of a slab like cylinder covering one of the plates and a needle like cylinder touching both plates, one can easily show that the relative change of $\Delta C/C_{tot}$ is less than $1 \pm (1/2)(\epsilon_r/\epsilon_0 - 1)$ and the deviation from the simple equation 4.2.2 is always less than ≃3%. For more realistic shape changes, the error is even smaller. The problem is very analogous to the

familiar problem of demagnetization of a sphere in a constant magnetic field.

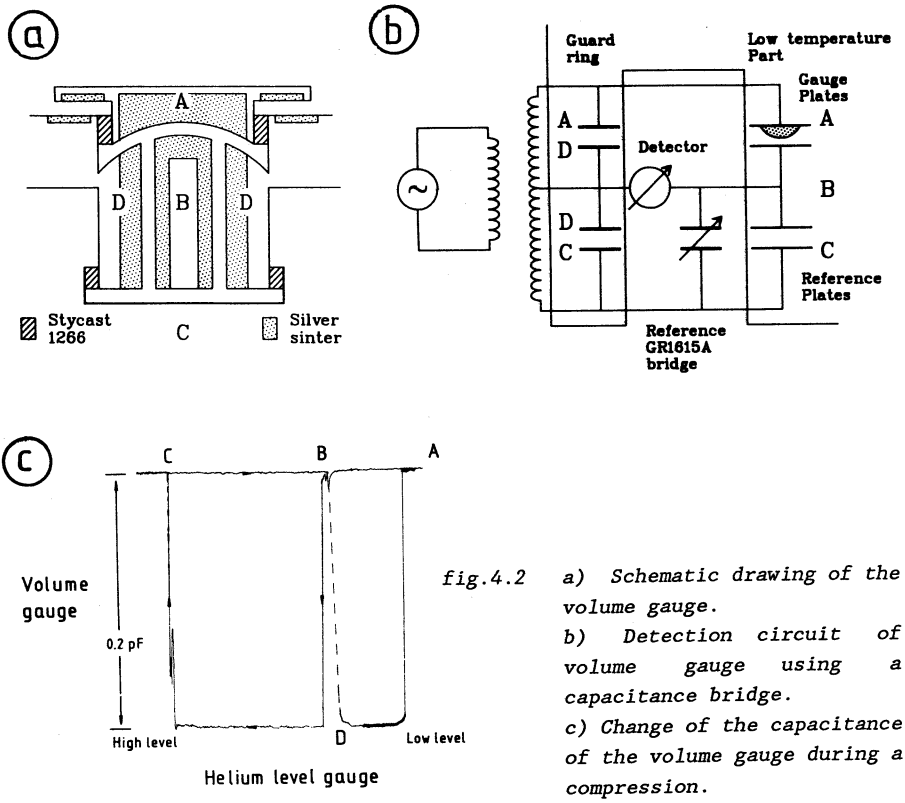

fig.4.2 *a) Schematic drawing of the volume gauge.*
b) Detection circuit of volume gauge using a capacitance bridge.
c) Change of the capacitance of the volume gauge during a compression.

To avoid the problems of the fringe fields near the edge of the capacitor plates, a guard ring system[12] was also included in the volume gauge, as schemetically illustrated in fig.4.2a. Keeping the guard ring and the actual measuring plates at the same potentials results in an undisturbed field pattern at the edges of the measuring capacitor plates.

A further improvement of the volume gauge was obtained by including a reference capacitor that is completely immersed in liquid helium when a bubble of gas is contained between the plates of the gauge. An advantage of such a reference system is that it allows for compensation of a changing ϵ_r of the liquid helium due to temperature, ^3He concentrations in ^4He and other effects.

The capacitance of the volume gauge is measured with a GR1615A capacitance bridge. The bridge also includes the possibility of using the low temperature reference capacitor (see fig.4.2b).

An illustration of the operation of the volume gauge and the reference

plates is given in fig.4.2c, showing the capacitance of the gauge during a compression. At (A) both measuring and reference plates are empty, the first jump (B) occurs when the reference system fills with helium, and finally both the capacitor plates are filled (C). The actual measurement of the bubble volume is on a more sensitive scale near C. On lowering the helium level again, the system shows hysteresis due to the fact that helium remains between the measurement plates and is released rather suddenly at point (D).

As illustrated in fig.4.2a and in chapter 5 the different parts of the volume gauge are covered with silver sinter to provide a high contact area between the helium and the metal body of the cell. This way the Kapitza resistance between the helium and cell body is minimized. However, since the capacitor plates have to float electrically, the heat contact between these plates and the body of the cell is indirect. From both the top plate (A) and the middle plate(B) (fig.4.2a) the heat is coupled again to the helium and then crosses a small gap of liquid helium to sinter that is connected to the cell body. The application of sinter is essential, otherwise the release of about 1μW recombination heat would cause a temperature gradient of as much as 0.1K accross a liquid helium/copper interface with 1cm^2 area (see e.g. Lounasma[15]). Using the data of Frossati[16] (see also Franco et al.[17] and references therein) for the Kapitza resistance between silver sinter and helium, the use of $\approx$200mm^3 silver sinter (grain size 0.1μm) reduces the temperature gradient to <1mK.

Technically the mounting of the silver sinter on the different parts of the volume gauge is rather involved. We use the recipe of Frossati[16] to prepare the sinter (see also[17]). It is produced from silver powder (1μm grain, 'French powder') which is first compressed to about 50% of the bulk density (10g/cm^3). The actual sintering process is done in a vacuum oven at 200^{0}C for about 30 min. During the sintering process the sinter must be kept under pressure. This is done by clamping the parts in a handtightened press. During the sintering, the volume of the sinter reduces to about 60% of the silver bulk density. A sheet of teflon is put between the sinter and the press to maintain the pressure which would otherwise fall due to the different thermal contraction of the metals. All copper parts are first silver plated to get a good bonding of the sinter. The pre-compression of the silver powder in parts where a radial compression is needed, is done by forcing a tapered cylinder on the sinter in such a way that finally the proper compression ratio is achieved. After the sinter is applied the parts are machined to the proper dimensions. Then the surface of the silver sinter is etched in a dilute methanol/nitric-acid mixture to open the pores of the sinter at the surface again and to remove any iron left by the machining.

The total volume of the gauge V_C=17.7mm^3 and a filled capacitance C_{tot}=0.2pF resulted in a sensitivity $\Delta C/\Delta V = 6.59\times10^{-4}$pF/mm^3. The resolution was 10^{-3}mm^3, although we did not pursue attempts to improve the signal-to-noise ratio.

4.2.2 The level gauge

The level gauge is based on the same principle as the volume gauge; the difference in dielectric constant of liquid helium and helium vapor. The coaxial capacitor (C=2pF) is measured by a capacity to frequency conversion technique.[18] This capacitor forms a part of the frequency determining LC circuit in a tunnel diode oscillator (TDO),using a Backward Diode BD6 (General Electric). This diode was chosen because of its low dissipation. The electronic circuit used for the TDO and the various bias components is illustrated in fig.4.3a To obtain a resonance frequency of about 10MHz with C=2pF and an internal capacitance ≈3pF of the TD, the inductance of the solenoid must be L=55μHenry. The solenoid was constructed from 139 windings of copper wire (Φ=0.06mm) on a hollow quartz tube (Φ=6mm) and placed directly under the cell, together with the tunnel diode and a 1200pF silver-mica capacitor. The performance of the oscillator can be improved by choosing a weaker coupling of the tunnel diode with the LC circuit by tapping the solenoid at an intermediate winding.[18] For our purpose this was not needed. The optimum orientation of the tunnel diode in the static magnetic field was found to be parallel (leads along the field direction); the magnetic field dependence of the TDO is than smallest[19] (< -650Hz/T).

The small signal from the TDO is amplified by a 40dB low noise preamplifier (Trontech W50 ATC, see fig.4.3b). Further processing can be done in two different ways. The first, and cheapest, possibility uses a 'tracking filter' based on an integrated circuit (XR215, see fig.4.3c). It acts as a narrow band filter that follows the main frequency component of the incoming rf-signal and gives this frequency at the reference output. Another way is to convert the frequency to about 100kHz by mixing the signal (RF mixer Anzac MD140) with a stable reference frequency near 10MHz (synthesizer HP8660). This 100kHz signal is further amplified by a PAR 114 amplifier. The second method was sometimes preferred because the tracking filter can be disturbed by 'spike' like electric pickup (the phase locked loop is than temporarily thrown 'out of lock'; optimizing the circuitry can suppress this problem). The reference signal from the tracking filter or the amplified output of the mixer is coupled to a counter (HP5300) to determine the frequency. This particular counter has a feature to select a number of digits of the total displayed frequency and to give an analog reference signal of these digits which we used for further processing on a recorder or for storage on the computer (PDP11/40) via a transient recorder (Nicolet 1170). The level gauge had a sensitivity of 2.3kHz/mmHe and a resolution of 10^{-2}mm, which was mainly limited by the noise due to the helium liquid.

The different techniques used in sections 4.2.1 and 4.2.2 to measure capacitances each have merits and disadvantages, which will not all be discussed in detail here. From a cryogenic point of view, the TDO-method has the advantage that at least one of the plates can be thermally anchored to the cell body. However, this precludes the use of a guard ring.

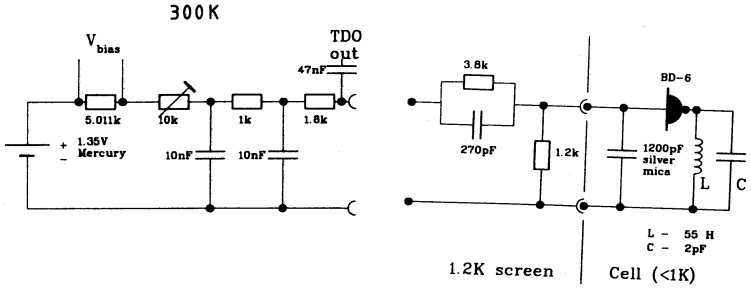

a) Tunnel diode oscillator (TDO) circuit for the level gauge.

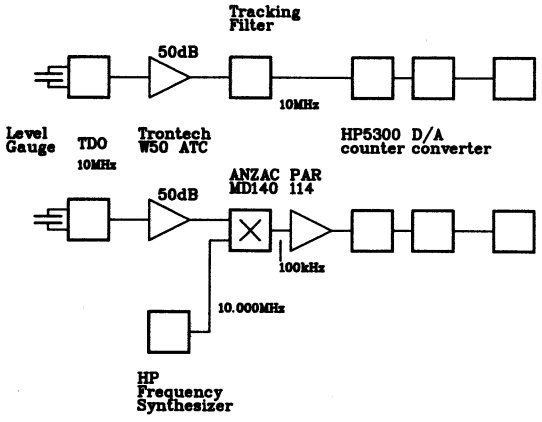

b) Detection schemes for the determination of the TDO frequency.

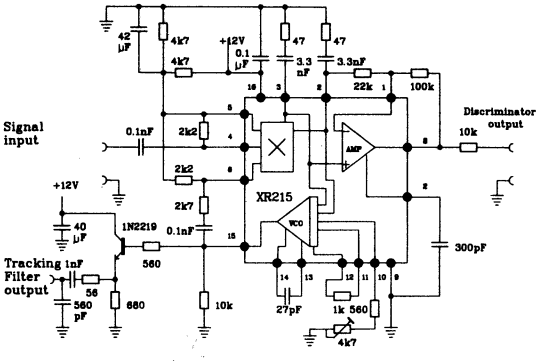

fig.4.3 *c) Tracking filter circuit.*

4.2.3 Displacement of liquid helium by electric and magnetic fields

An additional effect of the difference in ϵ_r of liquid helium and vacuum is the possibility to displace helium in an electric field. It is easily shown that the displacement of helium caused by a voltage difference E accross two capacitor plates d apart is given by:[12]

$$h = (\epsilon_r - 1)\,\epsilon_0\,E^2 / (\rho g d^2), \qquad (4.2.3)$$

where h is the height difference between the level in- and outside the capacitor, ρ=145kgm^{-3} the mass density of ^{4}He liquid and g the gravitational acceleration. The total displaced volume is given by:

$$\Delta V/E^2 = (\epsilon_r - 1)\epsilon_0/(\rho g)\,(w/d)\,n_{pl}, \qquad (4.2.4)$$

with w the width of the plates and n_{pl} the number of plates.

Combining a set of plates (40 plates, d=0.2mm, width w=2cm) results in a total volume displacement of 1.4×10^{-3}mm^{3}V^{-2}. This is not enough to compress the hydrogen gas (displaced amount of helium with the copper block is $\simeq$2cm^3), but can be used for stabilizing and modulating the column height.

Such a stack of plates was added to the part of the compression cell outside the magnet. It was constructed from brass plates (0.1mm thick) with Kapton spacers (0.1mm thick, 2mm wide and 2cm long) and glued together with Stycast 1266. The system could indeed be used to stabilize the pressure (compensate for drift), but because it only displaces minute amounts of helium its applicability was limited. The DC voltage that could be applied was limited to $\simeq$400V ($\simeq1.\times10^6$V/cm); at higher voltages a discharge occurs in the helium.

Analogous to the mentioned displacement of helium by electric fields above, gradients in magnetic fields also result in the displacement of helium. Due to the diamagnetic susceptibility of helium (χ_m=8.7×10^{-7}), the liquid helium is pushed towards the lowest magnetic field (only the absolute value of the field is relevant). For our U-tube configuration with one of the legs outside the magnet, this leads to substantial level differences between inner and outer leg. For a magnetic field difference of 10T, the height difference is about 11mm (this scheme is known as the Quincke method and is applied in measurements of the magnetic susceptibilities of liquids[12]). This effect could in principle also be used to displace considerable amounts of helium. An additional influence of the diamagnetic moment is due to the gradients in our parabolic magnetic field at the center (see chapter 5), it leads to a field dependent calibration of the column height to pressure conversion.

4.3 Bulk third-order recombination

The analysis of the volume decays in a bubble of H↓↕, including the effects of surface tension etc. is treated in detail in chapter 6. That

analysis shows that the decays can be described by the same rate equations as were used for the isochoric decay techniques, even if the occupation of the a-state has to be included. For a simple situation where the decay only depends on second-order processes and where the occupation of the c and d states can be ignored the rate equation for the number of particles in hyperfine state a (A) and b (B) is given by:

(4.3.1)

$$(1/V)\ dA/dt = -\ 2K_{aa}\ a^2 - K_{ab}\ ab + G_{ab}(a+b)(b-a)$$

$$(1/V)\ dB/dt = -\ K_{ab}\ ab - G_{ab}(a+b)(b-a)$$

Eq.4.3.1 is the basis for both the isochoric and isobaric decay. An additional relation between the volume (V), pressure (p), temperature (T) and density (n) determines the character of the decay. Under isothermal conditions; i.e. when the gas remains in thermal equilibrium with the walls of the cell, the conditions become:

(4.3.2)

isochoric: $p(t) = N(t)\ (k_BT/V) = n(t)\ k_BT$

isobaric: $V(t) = N(t)\ (k_BT/p)$

As a result the time dependence of the decay of the a and b density in the isochoric and isobaric case are different, which will have consequences for the role of the degree of polarization in the sample.

An interesting property of the autonomous system eq.4.3.1 is its homogeneous nature (the explicit time dependence in eq.4.3.1 can be eliminated). One can easily show that both for the isobaric and the isochoric case the ratios a/b and c/b go to a well defined asymptotic value as a function of time, independent of the starting conditions. The asymptotic value is determined by the competition between the decay processes that deplete the b-state and produce a or c state atoms and the processes that remove these a and c states. This equilibrium condition is determined by posing the condition:

(4.3.3)

$$d\hat{a}/dt = (1/b)\ (\ \dot{A}/V - \hat{a}\ \dot{B}/V\ ) = 0,$$

for the ratio $\hat{a}=A/B=a/b$. In particular for eq.4.3.1 it results in a third order equation for the asymptotic value $\hat{a}$:

(4.3.4)

$$\Gamma\hat{a}^3 + (\Gamma+2\gamma-1)\ \hat{a}^2 + (1-\Gamma)\hat{a} - \Gamma = 0,$$

where $\gamma=K_{aa}/K_{ab}$ and $\Gamma=G_{ab}/K_{ab}$. The solution of eq.4.3.4 for $\hat{a}$ can be expanded in orders of the usually small parameter Γ. To first order: $\hat{a} \simeq \Gamma/(1-\Gamma) \simeq \Gamma$. Note that the term $(2\gamma-1)\hat{a}^2 \simeq (2\gamma-1)\ \Gamma^2$ and should be included to obtain the solution of eq.4.3.4. to second order in Γ:

$\hat{a} = \Gamma(1 + 2(1-\gamma)\Gamma)$. Simply expanding the solution $\hat{a}=\Gamma/(1-\Gamma)\approx\Gamma(1+\Gamma)$ leads to an incorrect second-order correction.

If first or third order processes are included in eq.4.3.1, the concept of asymptotic values is no longer valid (eqs.4.3.1 are no longer homogeneous). Including some third order recombination rates (see chapter 6) leads to:

(4.3.5)

$$\dot{A}/(Vb^2) = - K^{eff}_{ab}\hat{a} + G^{v}_{ba} - K^{v}_{abb}b\hat{a}$$

$$\dot{B}/(Vb^2) = - K^{eff}_{ab}\hat{a} - G^{v}_{ba} - K^{eff}_{bc}\hat{c} - G^{v}_{bc}\uparrow(1+\hat{c}) + G^{v}_{bc}\downarrow\hat{c} - (2+\xi)K^{v}_{bbb}b - K^{v}_{bbc}b\hat{c} - K^{v}_{abb}b\hat{a}$$

$$\dot{C}/(Vb^2) = - K^{eff}_{bc}\hat{c} + G^{v}_{bc}\uparrow(1+\hat{c}) - G^{v}_{bc}\downarrow\hat{c} + \xi K^{v}_{bbb}b - K^{v}_{bbc}b\hat{c}$$

and summing these three equations gives the rate equation for N:

$$\dot{N}/(Vb^2) = - 2[\, K^{eff}_{ab}\hat{a} + K^{eff}_{bc}\hat{c} + K^{v}_{bbb}b + K^{v}_{abb}b\hat{a} + K^{v}_{bbc}b\hat{c}\,].$$

One can think of replacing $\hat{a}$ and $\hat{c}\equiv c/b$ by a quasi asymptotic value that depends on density. Again using the conditions eq.4.3.3 and assuming the density to be time independent these quasi asymptotic values become up to first order:

(4.3.6)

$$\hat{a} = G^{v}_{ba}/(K^{eff}_{ab} - G^{v}_{ba} - G^{v}_{bc}\uparrow + K^{v}_{abb}b - (2+\xi)K^{v}_{bbb}b)$$

$$\hat{c} = (G^{v}_{bc}\uparrow + \xi K^{v}_{bbb}b)/(K^{eff}_{bc} + G^{v}_{bc}\downarrow + K^{v}_{bbc}b).$$

They depend explicitely on the density. In particular for the isobaric decay the assumption of quasi asymptotic values seems reasonable, because under isobaric conditions the densities are nearly constant. Since this assumption plays an essential role in the data analysis used in chapter 6, the decays under isobaric (and isochoric) conditions were simulated starting from the rate equations. These rate equations include all the relevant processes for decays at the temperatures used in the experiments (see eq.4.3.5).

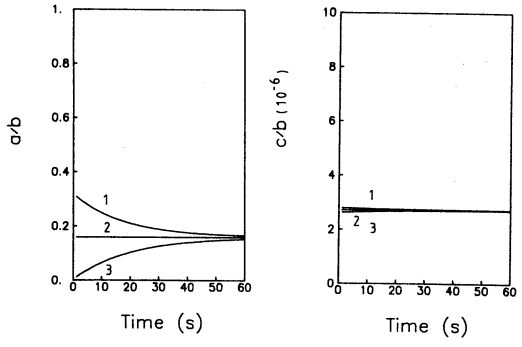

fig.4.4 Simulation of the volume decay under isobaric conditions for different starting polarizations (based on eq.4.3.5): 1) a/b=0.32 2) a/b=0.16 3) a/b=0.0

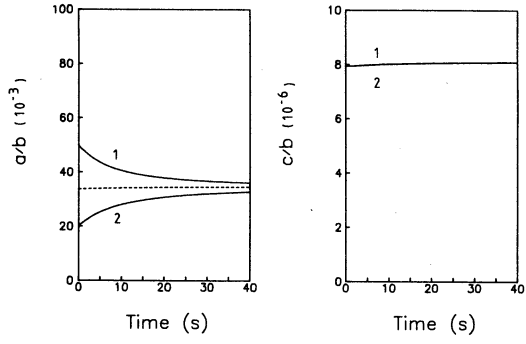

fig.4.5 Simulation of the density decay under isochoric conditions for different starting polarizations. Dotted line indicates the quasi equilibrium condition for that particular density.

Eq.4.3.5 was solved numerically using a Merson integration technique. Some examples of such a simulation with different starting conditions are plotted in fig.4.4. In general, the quasi asymptotic values are reached within 30 seconds if the starting conditions are within 20% of the asymptotic values. Usually these conditions are well fullfilled in the experiments. The dynamics slows down for lower densities as can be expected because the rates are smaller under these conditions. The dynamics of $\hat{c}$ is much faster than that of $\hat{a}$, e.g. in fig.4.4 $\hat{c}$ remains in equilibrium with the changing conditions of $\hat{a}$.

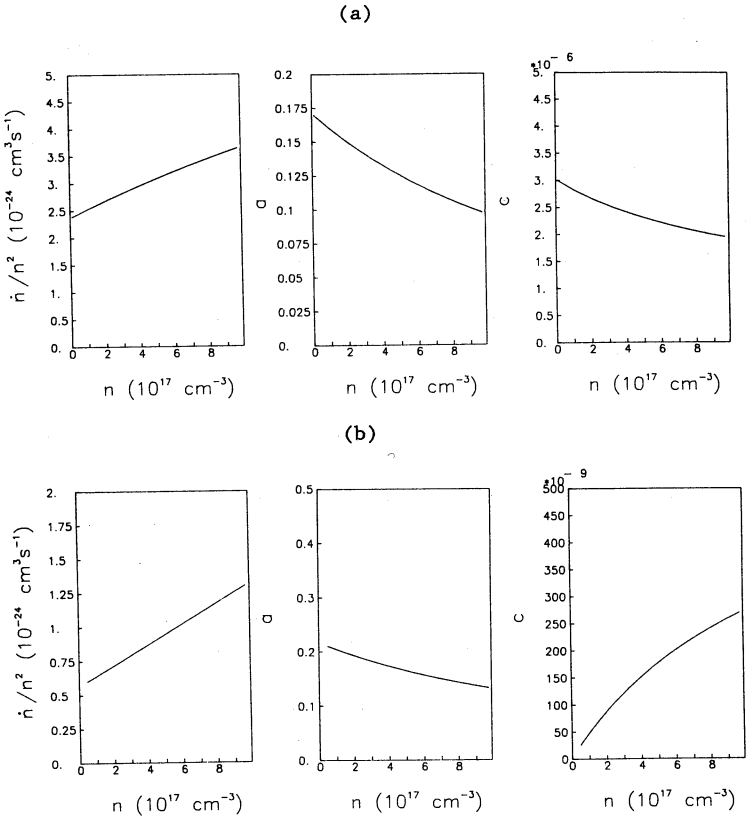

fig.4.6 Quasi equilibrium values for $\hat{a}$ and $\hat{c}$ as function of density. Based on eq.4.3.5. and $d\hat{a}/dt=0$ and $d\hat{c}/dt=0$. The rate $\dot{n}/n^2$ is curved as function of n.
a) 6T, 0.71K b) 9.8T, 0.71K

Fig.4.5 shows the same type of decays under isochoric conditions. For most of the decays, the asymptotic value is only reached when the density is already low. In the interesting high density part of the decay, the polarization depends on the starting conditions. However, if the system is prepared in the quasi asymptotic state (fig.4.5), the decay follows the changing quasi asymptotic values.

In chapter 6, linearized equations for $\dot{n}/n^2$ as function of n are derived using the density dependent quasi asymptotic values for $\hat{a}$ and $\hat{c}$. Due to the explicit density dependence of $\hat{a}$ and $\hat{c}$ the overall function for $\dot{n}/n^2$ does not display a simple linear behavior, but includes (small) higher order terms. This curvature is not an artifact of the linearization. An example of this curvature is displayed in fig.4.6. The calculated rates are

based on eq.4.3.5. In the analysis of the data as presented in chapter 6, the small curvature was ignored, instead effective second order and third order coefficients are used.

4.4 Magnetic field dependence of second- and third-order processes

The magnetic field dependence of the decay rate depends on the specific processes that are contributing. In a doubly-polarized system at low temperature only processes occurring between b states are important: second order relaxation G_{ab} and third order recombination K_{bbb}. At higher temperature or lower field ($B/T \leq 10$) the c state can also be populated and new processes become important: G_{bc} and K_{bbc}. Measurements were done at $B/T<10$ and displayed the contribution of G_{bc} in the second order and K_{bbc} in the third order coefficient (see chapter 6). Additional measurements for $B/T<10$ were obtained in a second run with the same compression cell. These results agree well with the earlier measurements. Fig.4.7a displays τ^{-1}/p vs. p. The lines are a fit through the data points for different fields. The intercept of the line gives $C_2(p)$ and the slope gives $C_3(p)$. The origin of the larger scatter in the data points at B=6.5T is unclear. In fig.4.7b the new and old data are combined in one plot. Within experimental uncertainties the results reproduce.

In a more realistic model for the decays at higher temperatures (Our compression experiments are performed at T≈700mK) one has to account for the fact that the sample is not fully doubly-polarized ($\hat{a} \neq 0$) and other decay processes become important (e.g. K_{ab}, K_{abb} etc.). The decays depend on a combination of the different decay rates and the analysis becomes quite involved (see chapter 6). In particular the field dependence of the decay is very complicated; the predicted field dependence of the exchange driven recombination channels (K_{ab}, K_{abb}, K_{bbc} etc.) decreases, while the predicted dependence of the dipolar driven recombination (K_{bbb}) increases as function of the field.

The field dependence of the third-order rate, even using an extended model, fails to describe the behavior at low fields (see line in fig.4.7). The reason for this discrepancy is not clear. Perhaps the assumption for an equilibrium polarization $\hat{a}$ and $\hat{c}$ as developed in section 4.3 is not correct for the low fields where the decays are very fast. Without further knowledge of $\hat{a}$ and $\hat{c}$ during the decays it is difficult to study this in more detail.

The calculation by Kagan et al.[20] and de Goeij et al.[21] for the dipolar three-body recombination between three b-state atoms shows an increasing rate as a function of field (see chapter 6). The observed third order recombination shows a decrease as function of field which was observed for both the bulk recombination[1-6] and the surface recombination[1-4] at high gas densities and also was obtained from reinterpretation of previously measured decays at low densities (see chapter 2). A complication for the analysis of these third-order processes is the fate of the third outgoing atom.

Depending on its hyperfine state and the condition in the cell it will influence the decay accordingly. In the model for dipolar three-body recombination two outgoing 'channels' are important:

(4.4.1)

$$b + b + b \xrightarrow{L^s} H_2^* + b \qquad \text{single spinflip } (\Delta S=1)$$

$$b + b + b \xrightarrow{L^d} H_2^* + c \qquad \text{double spinflip } (\Delta S=2).$$

fig.4.7

a) Data points from second compression run for different fields. Lines are fits to the data (see also chapter 6).

b) Field dependence of second-order (C_2) and third-order (C_3) coefficients. Filled circles are data points obtained in the first run (see chapter 5,6). Open circles are from the second run. For an explanation of the lines see chapter 6.

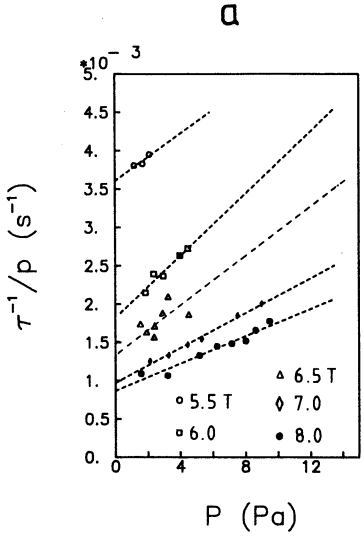

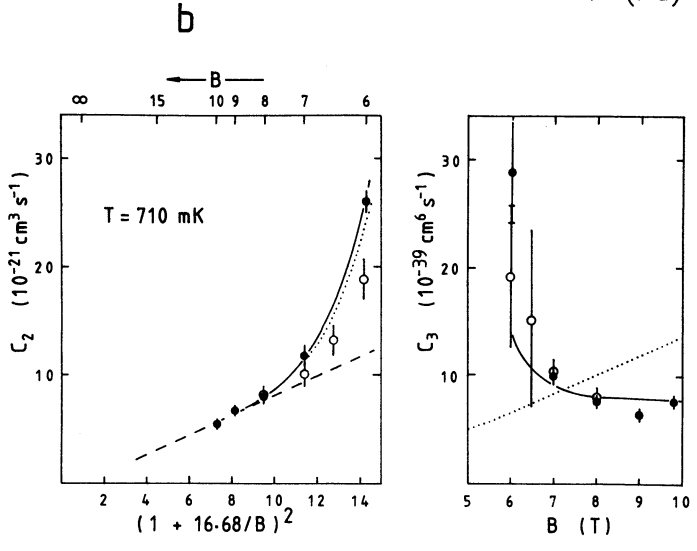

With $L^{s,d}$ the event rates for the specific channel and H_2^* the produced molecule in one of the rotational and vibrational bound states (see chapter 1). The double spin-flip process occurs more frequently than the single spin-flip process. According to the calculations of de Goeij et al.[21] the ratio $\xi \equiv L^d/(L^s + L^d) = 0.91$ (Kagan et al.[20] find $\xi = 0.93$) and is nearly field independent. Furthermore, a simple relation exists between L^d and L^s :[21]

$$L^d(B) = 4\, L^s(2B). \tag{4.4.2}$$

This relation is more general and also applies to other three body b-state recombination mechanisms.[22]

To include these processes in the rate equation for the density of the hyperfine states, one has to account the number of atoms lost or produced in a specific state (see also chapter 6). Let us focus on the b and c state and only take into account the three-body dipolar recombination mentioned above and the processes that determine the fate of the produced c-state atom:

$$\begin{aligned} \dot{b} = &- (2+\xi)\, K_{bbb}\, b^3 \\ &- K_{bc}\, bc - K_{bbc}\, b^2 c \\ &- G_{bc}{\uparrow}\, (b+c)\, b + G_{bc}{\downarrow}\, (b+c)\, c \end{aligned} \tag{4.4.3}$$

$$\begin{aligned} \dot{c} = &+ \xi\, K_{bbb}\, b^3 \\ &- K_{bc}\, bc - K_{bbc}\, b^2 c \\ &+ G_{bc}{\uparrow}\, (b+c)\, b - G_{bc}{\downarrow}\, (b+c)\, c. \end{aligned}$$

The relation between the event rates L^s and L^d and the recombination rate as used in e.g. chapter 6 is given by:

$$\begin{aligned} \xi\, K_{bbb} &= L^d \\ (2+\xi) K_{bbb} &= 2L^s + 3L^d. \end{aligned} \tag{4.4.4}$$

Let us assume for the present discussion that all produced c-state atoms recombine (for low temperature measurements a very plausible assumption, since the c-state atoms are formed on the surface and may recombine via the K_{bc} process). The rate of n=b+c is then given by:

(4.4.5)

$$\dot{n}/n^3 \equiv - L_3 = 2\ (1+\xi)\ K_{bbb} \equiv -2L^s - 4L^d.$$

The observed field dependence of the third order rate is well described by a linear expansion around a magnetic field $B_0 \simeq 8T$ between 5 and 11T (see chapter 2):

(4.4.6)

$$L_3 = \hat{L}\ e^{-\eta(B-B_0)}$$

$$\simeq \hat{L}\ (\ (1.+\eta B_0) - \eta\ B\ ),$$

with $\eta = 0.07$ and $\hat{L} = 1.5(2)\times10^{-24} cm^4 s^{-1}$.

Instead of using the value of ξ as calculated by the Goeij et al. one can try to fit the observed field dependence and extract a value for ξ. Assuming a linear field dependence for L^s: $L^s = c_1 + c_2\ B$, the overall third order rate can be expressed in terms of c_1 and c_2 by making use of the relation eq.4.4.2:

(4.4.7)

$$L^3 = 2L^s + 4L^d = 18c_1 + 34c_2\ B.$$

Comparison between the observed rate (eq.4.4.6) and eq.4.4.7 leads to a value for c_1, c_2:

(4.4.8)

$$c_1/\hat{L} = (1/18)\ (1 + \eta B_0)$$

$$c_2/\hat{L} = (1/34)\ \eta.$$

The ratio between becomes:

(4.4.9)

$$\xi(B) = L^d(B)/(L^s(B) + L^d(B)) \simeq (4 + 0.0475B)/(5 + 0.214B).$$

The ratio $\xi(B)$ is field dependent, between 5 and 11T ξ varies from 0.70 to 0.61.

4.5 Modulation techniques for bubble measurements

In principle some of the thermodynamic properties of the gas can be measured by observing the response of the volume to modulation of the pressure, temperature etc. This modulation can be done in a stepwise manner, or by continuous (sinusoidal) modulation. Some of the modulation techniques will be discussed in this section.

4.5.1 Stepwise modulation

Modulation of the pressure can in principle yield information on the compressibility κ of the gas. The response of the volume of the bubble on a stepwise variation of the applied pressure depends on the nature of the

(de)-compression.

If the compression is slow enough, the temperature will be constant in the bubble. The corresponding volume change is then given by the isothermal-compressibility for small modulations of the pressure:

(4.5.1)

$\kappa_T = - (1/V) (\partial V/\partial p)_T$ (= 1/p for an ideal classical gas).

For larger modulations the volume/pressure change is described by the ideal gas law: $p\ V = N\ k\ T$. At the Bose-Einstein transition the isothermal compressibility will change by a factor of 2. (see chapter 1) and may as such be helpful to indicate the transition.

Fast compressions will tend to be adiabatic ($\Delta S=0.$) and the response is given by the adiabatic compressibility:

(4.5.2)

$\kappa_S = - (1/V) (\partial V/\partial p)_S$ (= (3/5) (1/p) for an ideal classical gas),

or if the modulations are too large, the pressure/volume change is given by the Poisson relation: $p\ V^{\gamma}$ = constant, with $\gamma=C_p/C_v=5/3$ the ratio of the specific heat under constant volume (C_v) and pressure (C_p) condition. The adiabatic compressibility does not change at the B.E.C. transition, indicating that the compressibility measurements are only useful for the detection if the compression is isothermal.

In our measurements we used the stepwise compressions to study the thermal conditions of the gas. In the bubble situation the total pressure p is given by the sum of the column pressure p_k and the pressure due to buoyancy and surface tension p_α (see chapter 6). Thus the response of the volume due to a change Δp_k is given by:

(4.5.3)

$p_1\ V_1^{\gamma} = p_2\ V_2^{\gamma}$, $p_1=p_{\alpha 1} + p_k$, $p_2=p_{\alpha 2} + p_k + \Delta p_k$,

where p_1 and V_1 describe the situation before the step-wise change and p_2 and V_2 the situation after the compression. Exponent $\gamma=1$ for the isothermal case and $\gamma=C_p/C_v$ for the adiabatic case. The pressures $p_{\alpha 1}$ and $p_{\alpha 2}$ depend on V_1 and V_2. In fig.4.8 a number of stepwise compressions is combined in one plot of p_2 $p_{\alpha 1}$ and $p_{\alpha 2}$ depend on
V_1 and V_2. In fig.4.8 a number of stepwise compressions is combined in one plot of p_2/p_1 vs. V_1/V_2. The curved line corresponds to the adiabatic case and the straight line to the isothermal case. Due to the relatively large uncertainties, it is not easy to discriminate between these two cases, although the observed compression ratios seem to be following the straight line for the isothermal compressions. The errors are mainly due to the non-systematic errors in the small volume and pressure changes. The compressibilities do not depend strongly on a systematic error in the pressure.

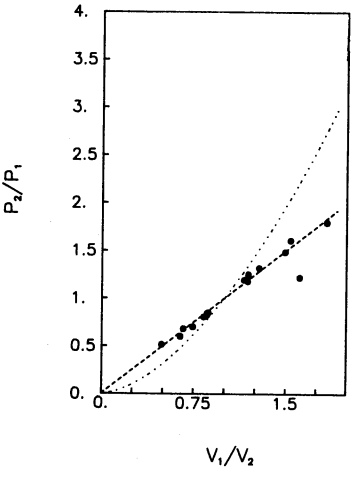

fig.4.8
Stepwise (de)compressions. The dashed line is pure isothermal and the dotted line is pure adiabatic (de)compression.

4.5.2 Continuous modulation

Instead of applying a stepwise compression, the pressure can also be modulated continuously. In our cell this can be done by modulating the level of the helium column. These level modulations can be made by moving the block or by inducing a temperature gradient between the two legs of the U-tube like cell. Due to the fountain effect, these temperature gradients induce a level difference (1mK temperature difference corresponds with[23] 0.24mmHe at 700mK). The response of the system was optimal near a few Hz, which probably corresponds to a resonance mode of the cell system. The volume response to these oscillation was not analyzed quantitatively.

4.5.3 Oscillations in the bubble

A bubble filled with gas submersed in a liquid has a number of oscillatory modes. Such bubble oscillations have been extensively studied in connection with the problem of (acoustic) cavitation.[24] One of these oscillations is associated with volume oscillations of a spherical bubble with (average) radius R_0. In this section the frequency of this volume oscillation is determined for the H-bubble in helium. The time dependence of the radius R of the bubble is described by the differential equation:[24]

$$R\ddot{R} + 3/2\ \dot{R}^2 = 1/\rho\ [\ P_g - 2\sigma/R - P_0\ ], \qquad (4.5.3)$$

with ρ the density of liquid helium, σ the surface tension of liquid helium, P_g the pressure in the gas and P_0 the pressure in the surrounding helium liquid (= column pressure).
For a (classical) ideal gas the pressure in the bubble is described by:

(4.5.4)

$$p\ (4/3)\pi R^3 = N\ kT \quad \text{and} \quad p\ (4\pi/3\ R^3)^{\gamma} = \text{constant},$$

with γ=1 for isothermal case and $\gamma=C_p/C_v$ for the adiabatic case. The gas pressure is in that case given by:

(4.5.5)

$$P_g(R) = (\ P_0 + 2\sigma/R_0)\ (R_0/R)^{3\gamma}.$$

Using these relations in eq.4.5.3 and expanding around R_0 gives a harmonic oscillator like equation with frequency ν:

(4.5.6)

$$\nu = (1/2\pi)\ (\ 2(3\gamma-1)\sigma/(\rho R_0^3)^{1/2}.$$

For $R_0=10^{-4}$m, the frequency is ν=917Hz.

Equation 4.5.3 can also be used to describe the response to a small temperature modulation. Other oscillation modes of the bubbles are given by oscillations which preserve the volume of the bubble ('droplet' oscillations), however they are not very sensitive to the properties of the gas inside the bubble and will not be considered here. In principle these resonance frequencies are also sensitive to the equation of state near the B.E.C. transition.

References

1 H.F. Hess, D.A. Bell, G.P. Kochanski, R.W. Cline, D. Kleppner and T.J. Greytak, Phys.Rev.Lett. 51, 483 (1983).

2 H.F. Hess, D.A. Bell, G.P. Kochanski, D. Kleppner and T.J. Greytak, Phys.Rev.Lett. 52, 1520 (1984).

3 D.A. Bell, G.P. Kochanski, L. Pollack, H.F. Hess, D. Kleppner and T.J. Greytak, Physica (LT-17) , 449 (1984).

4 D.A. Bell, H.F. Hess, G.P. Kochanski, S. Buchman, L. Pollack, Y.M. Xiao, D. Kleppner and T.J. Greytak, preprint , (1985).

5 R. Sprik, J.T.M. Walraven and I.F. Silvera, Phys.Rev.Lett. 51, 479 (1983) ;Erratum 51 (1983) 942.

6 R. Sprik, J.T.M. Walraven and I.F. Silvera, Phys.Rev.B 32, 5668 (1985).

7 T. Tommila, S. Jaakkola, M. Krusius, K. Salonen and E. Tjukanov, Proceedings LT-17 (Karlsruhe) Elsevier Science Publishers, 453 (1984).

8 T.J. Tommila, S. Jaakkola, M. Krusius, I. Krylov and E. Tjukanov, Phys. Rev. Lett. 56, 941 (1986).

9 I.F. Silvera, Phys.Rev.B 29, 3899 (1984).

10 B. Yurke, J.S. Denker, B.R. Johnson, N. Bigelow, L.P. Levy, D.M. Lee and J.H. Freed, Phys.Rev.Lett. 50, 1137 (1983).

11 B.R. Johnson, J.S. Denker, N. Bigelow, L.P. Levy, J.H. Freed and D.M. Lee, Phys.Rev.Lett. 52, 1508 (1984).

12 W.J. Duffin, Electricity and Magnetism McGraw-Hill , (1965).

13 T.M. Miller, B. Bederson, Adv.At.Mol.Phys. 13 1 (1977).

14 J. Wilks, 'The Properties of Liquid and Solid Helium', Clarendon Press (Oxford) 1967.
15 O.V. Lounasma, 'Experimental Principles and Methods Below 1K', Academic Press (New York) 1974.
16 G. Frossati, J.Phys. (Paris) 39 C6-1578 (1978).
17 H. Franco, J. Bossy, H. Godfrin, Cryogenics 24 477 (1984).
18 C.T. Degrift, Rev. Sci. Instrum. 46, 599 (1975).
19 A.P.M. Matthey, private communication.
20 Yu. Kagan, I.A. Vartanyantz and G.V. Shlyapnikov, Sov.Phys.JETP 54, 590 (1981).
21 L.P.H. de Goey, J.P.J. Driessen, B.J. Verhaar and J.T.M. Walraven, Phys.Rev.Lett. 53, 1919 (1984).
22 L.P.H. de Goeij, private communication.
23 D.S. Betts, 'Refrigeration and Thermometry Below One Kelvin', Sussex University Press, 1976.
24 R.E. Apfel, 'Ultrasonics', Methods of Experimental Physics Vol.19, 355 (1981).

Chapter 5

Compression of Spin-Polarized Hydrogen to High Density

R. Sprik, J.T.M. Walraven,
Natuurkundig Laboratorium, Universiteit van Amsterdam,
Valckenierstraat 65, 1018 XE Amsterdam, The Netherlands.

and

Isaac F. Silvera
Lyman Laboratory of Physics, Harvard University, Cambridge, MA 02138, USA, and Natuurkundig Laboratorium, Universiteit van Amsterdam, Valckenierstraat 65, 1018 XE Amsterdam, The Netherlands.

Abstract

A new technique enabled the authors to compress doubly polarized hydrogen by up to five orders of magnitude and study the sample in very small volumes at constant density up to $2 \times 10^{18}/cm^3$. The first determination of the bulk three-body dipolar recombination rate was made, $K_v^{3b} = 4(1) \times 10^{-39} cm^6 s^{-1}$. The authors also identified a new process, bulk electronic dipolar b→c-state relaxation with rate constant $G_v^{bc} \exp(2\mu_B B/k_B T) = 8(4) \times 10^{-16} cm^3 s^{-1}$. Samples were very delicate and too rapid a compression could result in an explosion.

[Physical Review Letters, 51 479-482 (1983)]
[Erratum , 51 942 (1983)]

Compression of Spin-Polarized Hydrogen to High Density

R. Sprik and J. T. M. Walraven

Natuurkundig Laboratorium der Universiteit van Amsterdam, 1018 XE Amsterdam, The Netherlands

and

Isaac F. Silvera

Lyman Laboratory of Physics, Harvard University, Cambridge, Massachusetts 02138, and Natuurkundig Laboratorium der Universiteit van Amsterdam, 1018 XE Amsterdam, The Netherlands

(Received 2 June 1983)

A new technique enabled the authors to compress doubly polarized hydrogen by up to five orders of magnitude and study the sample in very small volumes at constant density up to $2\times10^{18}/\mathrm{cm}^3$. The first determination of the bulk three-body dipolar recombination rate was made, $K_V^{3b}=4(1)\times10^{-39}\ \mathrm{cm}^6\ \mathrm{s}^{-1}$. The authors also identified a new process, bulk electronic dipolar $b\rightarrow c$–state relaxation with rate constant $G_V^{bc}\exp(2\mu_B B/k_B T)=8(4)\times10^{-16}\ \mathrm{cm}^3\ \mathrm{s}^{-1}$. Samples were very delicate and too rapid a compression could result in an explosion.

PACS numbers: 67.40.Fd, 67.40.Kh

Since spin-polarized atomic hydrogen (H↓) was first stabilized there has been an intense effort to obtain high enough densities or low enough temperatures to observe degenerate properties of this boson gas.[1] A prime goal is to observe Bose-Einstein condensation (BEC), which, in the limit of weakly interacting bosons, should occur at $T_c=3.31\hbar^2 n^{2/3}/mk_B$ (=74 mK for a density of $n=10^{19}/\mathrm{cm}^3$; m is the hydrogen mass). H↓ is a gas with atoms in two hyperfine states: the ground state $|a\rangle=|{\downarrow}\,{\downarrow}\rangle-\epsilon|{\uparrow}\,{\uparrow}\rangle$ and the pure spin state $|b\rangle=|{\downarrow}\,{\uparrow}\rangle$ (here ↑ and ↓ denote electron and nuclear spin-$\frac{1}{2}$ projections and $\epsilon=a/4\mu_B B$ is the hyperfine mixing parameter with a the hyperfine constant, μ_B the Bohr magneton, and B the magnetic field). Recently, a gas of hydrogen with almost all atoms in the state $|b\rangle$, called doubly polarized hydrogen (H↓↑), has been produced[2-5] as follows. Collisions involving an atom with a spin-up admixture can result in recombination. Thus, a-a and a-b, but not b-b, collisions can lead to H_2 formation. Because of the slow $b\rightarrow a$ relaxation rate, G^{ba}, a gas of H↓ evolves to H↓↑ by this preferential recombination. The lifetime of H↓↑ is substantially longer than H↓ since it is controlled by G^{ba}, not the recombination rate constant. Densities as high as $10^{17}\ \mathrm{cm}^{-3}$ of H↓↑ have been produced by preferential decay; this gas can potentially be compressed to very high density.

In this Letter, we describe a new experimental approach which has enabled us to increase the maximum densities by more than an order of magnitude to $2\times10^{18}/\mathrm{cm}^3$. The volume of the gas of H↓↑ can be compressed by a factor 10^5. All earlier hydrogen studies have used fixed-volume cells and the decay of the density was studied. Here we have developed a new type of cell which enables us to study high-density samples for periods of order minutes at constant hydrostatic pressure and temperature, observing the volume of the compressed hydrogen "bubble" decay away. We can measure volumes as small as 3×10^{-3} mm^3. Such small volumes have important technical advantages for obtaining BEC. The temperature is limited by the heating rate $\frac{1}{2}D\,dN/dt$ ($D=4.6$ eV is the dissociation energy of H_2, and $N=nV$ is the number of atoms in volume V). For our smallest volume, and densities of $10^{19}/\mathrm{cm}^3$, there are only 3×10^{13} atoms in the bubble, or about 10 μJ of potential recombination energy which can easily be accommodated by a moderate-size dilution refrigerator without excessive warming. Furthermore, the small bubble diameter reduces the thermal gradient which can develop in the bubble as a result of thermal boundary resistance.

A number of new and interesting phenomena were observed by studying the volume decay rate as a function of magnetic field and temperature. This includes the first measurements of previously undetected decay mechanisms: three-body dipolar recombination and bulk electronic dipolar relaxation from the pure $|b\rangle$ state to the electron-spin-reversed state, $|c\rangle=|{\uparrow}\,{\uparrow}\rangle+\epsilon|{\downarrow}\,{\downarrow}\rangle$. The compressed bubbles of hydrogen were very delicate and under certain circumstances their lives were terminated by a spontaneous explosion (rapid recombination). Explosions could also be induced by a rapid compression. A technical cryogenic problem prevented us from obtaining

temperatures lower than 600 mK for pure ^{4}He films. For ~1% mixtures of ^{3}He-^{4}He, measurements were made down to 200 mK. Since these bubbles were susceptible to explosion and possibly out of thermal equilibrium, quantitative results are only given for the pure ^{4}He case. The highest densities achieved were $2\times10^{18}/\text{cm}^3$ for ^{4}He and $1\times10^{18}/\text{cm}^3$ for ^{3}He-^{4}He, under the assumption of equilibrium.

The cell is shown in Fig. 1 and consists of a central cell (CC) in the bore of a superconducting magnet and an outer leg partially filled with liquid helium, containing a weight which can be vertically translated to displace the helium. The CC has upper and lower chambers separated by a midsection. The heart of the cell is a capacitive volume gauge mounted in the bottom of the midsection. The capacitor is made of two concentric spherical sections (radius of curvature, 10 mm) with a spacing of 0.9 mm. A reference capacitor plate was incorporated for added stability. The three sections are electrically isolated and floating with respect to ground. The measurement plates are made of silver sinter (0.1 μm grain size) to carry away the recombination heat. The thermometer is attached to the sinter block. The

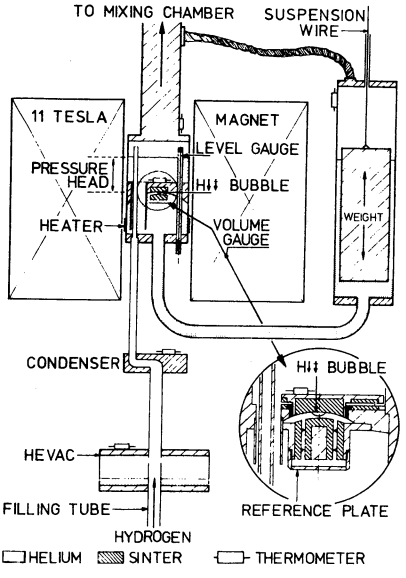

FIG. 1. Schematic diagram of the experimental apparatus.

capacitance of the capacitor increases substantially (5.7%) when it is filled with helium. The volume of an H bubble (assumed to have a negligible dielectric constant) is proportional (for small volumes) to the change of capacitance due to the displaced helium. Hydrogen is loaded into the CC from a room-temperature discharge. (The lower part of the cell is described elsewhere.)[1] With the weight up and the helium level in the CC down, the hydrogen diffuses into both the upper and the lower chambers. As the weight is lowered, the helium rises in the CC until it reaches the bottom of a tube concentric with the H↓ fill tube, sealing the 3-cm^3 volume of the lower chamber from the upper chamber. Any further increase of the He level compresses the hydrogen in the lower chamber. The gas is forced in between the capacitor plates, guided by the curved lower surface of the midsection. The pressure $p = p_s + p_k$ is determined by the hydrostatic head p_k of the helium and a surface-tension contribution p_s. The p_k is measured with a coaxial capacitance level meter. A maximum head of 12 mm was available (1-mm ^{4}He corresponds to $p_k = 1.4$ Pa or $\sim10^{-2}$ Torr) which could be measured with a resolution of 10^{-2} mm. The height of the helium in the CC could be modulated with an ~0.5-Hz ac heating; the thermomechanical effect (fountain effect) of ^{4}He leads to a level (i.e., pressure) and a volume modulation, giving directly the compressibility, providing a method for future detection of BEC.

To analyze the decay of the volume, we must know the shape of the bubble. For large volumes, it will conform to the top capacitor plate and have the shape of a skullcap, whereas for small volumes, the surface tension will dominate the buoyant forces and the shape will approach a sphere. For simplicity, we use the small-volume approximation and shall correct for the resulting systematic error. If we write the decay equation in the form $\dot N = -Vf(n)$, where $f(n)$ is polynomial in n, then since $\dot N = n\dot V + \dot n V$ and $\dot n = \dot n_k - \frac{1}{3} n_s \dot V/V = \frac{1}{3} n_s \dot V/V$ (where $n_k \equiv p_k/k_B T$, $n_s \equiv p_s/k_B T$, and p_s is assumed to scale with $V^{-1/3}$ since the surface tension is inversely proportional to the radius),

$$\dot V/V = -f(n_k + n_s)/(n_k + \tfrac{2}{3} n_s); \quad n_k \gtrsim n_s . \qquad (1)$$

A characteristic decay rate τ^{-1} may be defined for any volume (i.e., any n_s) by plotting V versus time on a semilogarithmic scale and determining the local derivative: $\tau^{-1} = d(\ln V/V_0)/dt = \dot V/V$. In Fig. 2 we show some typical decay curves.

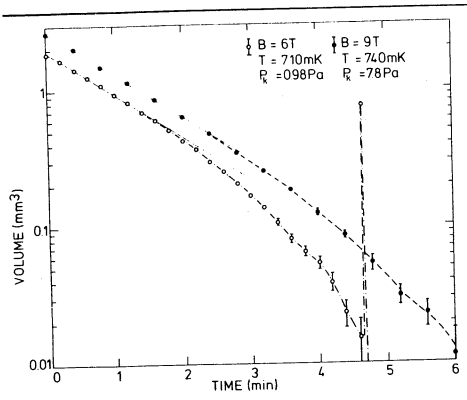

FIG. 2. Typical decay curves for ^{4}He surfaces. The low-field decay shows an explosion. The data points are taken from a recorder trace. The error bars are a measure of the noise. The dotted lines represent a guide to the eye.

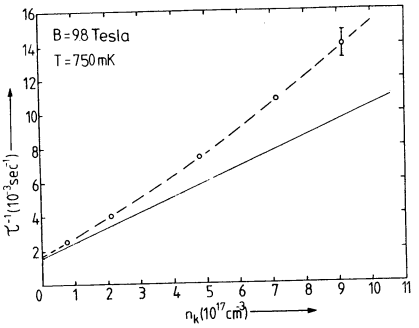

FIG. 3. Decay rate vs density. The dashed curve represents a second-order fit to the data used for extrapolation to zero density. The solid line corresponds to bulk relaxation, G_V.

The curvature for $V < 1$ mm^3 is interpreted as compression due to surface tension. The lower curve is terminated by an explosion. By plotting τ^{-1} as a function of n_k for a fixed volume (1 mm^3) as shown in Fig. 3, we observe curvature, pointing to a new fundamental decay process (third order in n). We first correct all data points for systematic error in the density determination (due to errors in the absolute helium level and the spherical assumption) by fitting with a second-order polynomial in n_k and extrapolating to $\tau^{-1} = 0$ to determine the systematic error Δn, which is used to correct the raw data; i.e., $n \equiv n_k + n_s + \Delta n$. The quantity $f(n)$ must have second- and third-order terms in the density. We assume the second-order term to be nuclear relaxation for a pure b-state gas so that n is the b-state density. In this case, the limiting recombination process is three-body dipolar volume recombination ($\dot{N} = -VK_V{}^{3b}n^3$) predicted by Kagan, Vartanyants, and Shlyapnikov[6] to have a value $K_V{}^{3b} = 4 \times 10^{-39}$ cm^6 sec^{-1} for $B = 10$ T and $T = 0$ K. We then have

$$f(n) = 2G_V{}^{ba}n^2 + K_V{}^{3b}n^3. \qquad (2)$$

A computer fit leads to $G_V{}^{ba}T^{-1/2}(1 + 16.68/B)^{-2} = 6.6(6) \times 10^{-22}$ cm^3 K$^{-1/2}$ s^{-1} in agreement with the double-polarized picture and earlier experiments.[2,3,5] We also find $K_V{}^{3b} = 4(1) \times 10^{-39}$ cm^6 s^{-1} for $T = 750$ mK and $B = 9.8$ T, in agreement with Kagan, Vartanyants, and Shlyapnikov. Here the error bars are statistical and do not include possible deviations from thermal equilibrium, to be discussed later.

A study of the magnetic field dependence of second-order decay (see Fig. 4) shows that the term $G_V{}^{ba}$ alone is inadequate, implying that a new second-order process becomes important at lower fields. As spin exchange cannot relax the $|b\rangle$ state in H↓↑, the most likely candidate is the bulk electronic dipolar $|b\rangle \rightarrow |c\rangle$ relaxation discussed by Kagan, Vartanyants, and Shlyapnikov.[6] In Fig. 4 the solid line corresponds to the quoted value for $G_V{}^{ba}$; the dashed line is obtained from an estimate by Lagendijk[7] for the $G_V{}^{bc}$ process (Kagan, Vartanyants, and Shlyapnikov did not evaluate the energy average of the cross section). This new process has an exponential B/T dependence, as established by temperature variation. From the

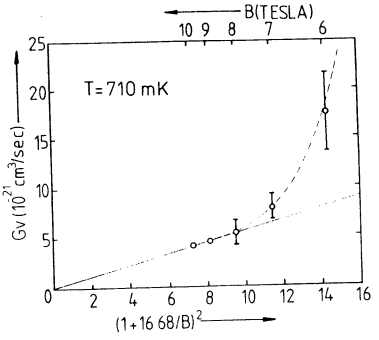

FIG. 4. The bulk relaxation rate constant $G_V = G_V{}^{ba} + G_V{}^{bc}$ (dashed line). The solid line is $G_V{}^{ba}$.

field dependence, we determined $G_V{}^{bc} \exp(1.34B/T) = 8(4)\times10^{-16}$ cm^3 s^{-1}, in good agreement with theory.

At our current high densities, H↓↓ is a very delicate gas and a rapid increase in the pressure can result in an explosion of the bubble. This result is extremely important in relation to future experiments to observe BEC where rapid compressions are required in view of the expected short lifetime of the sample. For $B/T \lesssim 10$ T/K and small volume, the sample explodes spontaneously. However, for $B/T > 10$ T/K, it was possible to follow the decay of the bubble to the minimum detectable volume. The explosions may be understood if we assume the sample to be driven out of equilibrium by too rapid of a compression. Then the exponential temperature dependence of the $b \rightarrow c$ relaxation process can generate the required positive feedback to explain the occurrence of an explosion. "Spontaneous" explosions may possibly result from compression by surface tension in shrinking bubbles. On two occasions, we also observed an explosion to result from a decompression, a phenomenon which does not fit in the proposed picture.

We conclude with a discussion of thermodynamic equilibrium upon which the analysis of decay is based. The gas can be out of thermal equilibrium because of Kapitza resistance, with interfacial temperature differences ΔT_{K1} between H↓↓ and He,[8] and ΔT_{K2} between He and the cell walls. Our experiment and cell were carefully designed to minimize this problem by use of small bubbles, high temperature, and silver sinter. The worst situation is when the bubble volume-to-surface ratio is large; i.e., for large volume. If it is out of thermal equilibrium, then $V \rightarrow V_{eq}$; as the bubble shrinks, $V \rightarrow V_{eq}$ and curvature should be observed in Fig. 2 for large V, instead of the straight line. We estimate $\Delta T_{K2} \ll 1$ mK. For ΔT_{K1} we make a calculation for the highest density in Fig. 3, $n = 10^{18}$ cm^{-3}: $\dot{Q} = D\dot{N}/2 = \alpha(nvA/4) \times 2k\Delta T_{K1}$. Using the low-temperature (conservative) value of Salonen *et al.*[9] for the accomodation coefficient, $\alpha = 0.2$, we find the $\Delta T_{K1} \approx 3$ mK or $\Delta T_{K1}/T \lesssim 4\times10^{-3}$, supporting our contention that samples are close to thermal equilibrium.

We thank A. Lagendijk and G. Fossati for a number of stimulating discussions, A. Mattheij for building the tunnel diode electronics, O. Höpfner for technical support, and H. van Zwol, J. Berkhout, and E. Salomons for help with the measurements. The financial support of the Stichting voor Fundamenteel Onderzoek der Materie is gratefully acknowledged.

[1]I. F. Silvera, Physica (Utrecht) 109&110B, 1499 (1982).

[2]R. W. Cline, T. J. Greytak, and D. Kleppner, Phys. Rev. Lett. 47, 1195 (1981).

[3]R. Sprik, J. T. M. Walraven, G. H. van Yperen, and I. F. Silvera, Phys. Rev. Lett. 49, 153 (1982).

[4]G. H. van Yperen, I. F. Silvera, J. T. M. Walraven, J. Berkhout, and J. Brisson, Phys. Rev. Lett. 50, 53 (1983).

[5]B. Yurke, J. S. Denker, B. R. Johnson, N. Bigelow, L. P. Lévy, D. M. Lee, and J. H. Freed, Phys. Rev. Lett. 50, 1137 (1983).

[6]Yu. Kagan, I. A. Vartanyants, and G. V. Shlyapnikov, Zh. Eksp. Teor. Fiz. 81, 1113 (1981) [Sov. Phys. JETP, 54, 590 (1981)].

[7]A. Lagendijk, private communication.

[8]B. Castaing and M. Papoular, to be published.

[9]K. T. Salonen, I. F. Silvera, J. T. M. Walraven, and G. H. van Yperen, Phys. Rev. B 25, 6002 (1982).

ERRATA

COMPRESSION OF SPIN-POLARIZED HYDROGEN TO HIGH DENSITY. R. Sprik, J. T. M. Walraven, and Isaac F. Silvera [Phys. Rev. Lett. 51, 479 (1983)].

The following final paragraph was inadvertently left off:

Note added.—After our measurements were completed we were informed that the MIT group (see following Letter) had independent evidence for the three-body recombination process (T. J. Greytak, private communication).

Chapter 6

Compression experiments with spin-polarized atomic hydrogen

R. Sprik, J.T.M. Walraven,
Natuurkundig Laboratorium, Universiteit van Amsterdam,
Valckenierstraat 65, 1018 XE Amsterdam, The Netherlands.

and

Isaac F. Silvera
Lyman Laboratory of Physics, Harvard University,
Cambridge, MA 02138, USA.

Abstract

Doubly polarized atomic hydrogen has been produced up to densities of $2x10^{18}cm^{-3}$ with the use of a compression technique. Samples were compressed up to five orders of magnitude into small bubblelike volumes under a column of liquid helium. This technique enabled us to study the volume decay of a bubble at almost constant gas density for minutes. The analysis of the volume decay of such a bubble is discussed. A bulk three-body recombination process was observed with a rate constant $C_3=[7(2)]x10^{-39}cm^6s^{-1}$, as well as bulk electronic b→c relaxation with rate constant $G_{bc}^{v}\downarrow = [12(4)]x10^{-16}cm^3s^{-1}$. The nature of the three-body process is analyzed with a set of extended rate equations. The samples were very delicate and rapid compressions could result in explosions.

[Physical Review B, 32 5668-5682 (1985)]

PHYSICAL REVIEW B VOLUME 32, NUMBER 9 1 NOVEMBER 1985

Compression experiments with spin-polarized atomic hydrogen

R. Sprik and J. T. M. Walraven
Natuurkundig Laboratorium, Universiteit van Amsterdam, Valckenierstraat 65, 1018 XE Amsterdam, The Netherlands

Isaac F. Silvera
Lyman Laboratory of Physics, Harvard University, Cambridge, Massachusetts 02138
(Received 13 May 1985)

Doubly polarized hydrogen has been produced up to densities of 2×10^{18} cm^{-3} with the use of a compression technique. Samples were compressed up to five orders of magnitude into small bubble-like volumes under a column of liquid helium. This technique enabled us to study the volume decay of a bubble at almost constant gas density for minutes. The analysis of the volume decay of such a bubble is discussed. A bulk three-body recombination process was observed with rate constant $C_3=[7(2)]\times10^{-39}$ cm^{6}s^{-1}, as well as bulk electronic $b\rightarrow c$ relaxation with rate constant $G^v_{bc}\downarrow=[12(4)]\times10^{-16}$ cm^{3}s^{-1}. The nature of the three-body process is analyzed with a set of extended rate equations. The samples were very delicate and rapid compressions could result in explosions.

I. INTRODUCTION

In the rapidly developing field of spin-polarized atomic hydrogen (H↓), one of the principal experimental goals is to achieve high densities of H↓ at low temperatures.[1–3] Under these conditions many-body effects and phenomena of quantum degeneracy of the gas become important. Hydrogen in its atomic form is a composite boson consisting of an electron (spin $S=\frac{1}{2}$) and a proton (spin $I=\frac{1}{2}$). A gas of H↓ is believed to behave as a weakly interacting Bose gas and one expects the system to undergo a phase transition to a Bose-Einstein condensed (BEC) state, possibly exhibiting superfluid behavior.[4] For example, to observe the transition at $T_c=100$ mK, the gas has to be stabilized to densities $n=1.6\times10^{19}$ cm^{-3} ($T_c=3.31\hbar^2n^{2/3}/mK_B$).

In this paper we report on experiments in which we have extended the experimentally accessible density regime by an order of magnitude to $n=2\times10^{18}$ cm^{-3}. A short report of this work was published earlier.[5] Hess *et al.*[6–8] developed a different technique for the same purpose and achieved densities $n\simeq4.5\times10^{18}$ cm^{-3}. At these high densities one observes interesting new phenomena such as three-body recombination, spontaneous explosion of gas samples, and relaxation to electron spin-reversed states. However, the densities are not sufficiently high or the temperature sufficiently low to observe BEC. Before we discuss the specific aspects of our experiment, we briefly review the conditions that enable manipulation of H at high densities.

In its atomic form H is unstable against recombination to the $^1\Sigma_g^+$ electronic singlet state of the hydrogen molecule. Experimentally, recombination is suppressed by electron-spin polarizing the gas (H↓) with a strong magnetic field, forcing the atoms to interact pairwise via the nonbinding "triplet" potential associated with the $^3\Sigma_u^+$ electronic state of the H-H system. An important aspect in stabilizing H↓ is that the recombination not only has to be suppressed in the bulk, but also for atoms adsorbed on the walls of the sample cell. This is done by coating the walls of the cell with liquid helium which has a very low binding energy (ε_a) for H atoms (e.g., for ^{4}He, $\varepsilon_a/k_B\simeq1$ K). Therefore at moderately low temperatures the surface density of H atoms, which depends exponentially on ε_a/k_BT, remains relatively low and the recombination on the surface is suppressed.

The electronic-spin polarization of the gas and the related stability is limited by the presence of the hyperfine interaction. The "well-known" hyperfine level diagram of hydrogen in a magnetic field is shown in Fig. 1. The two lower states $|a\rangle=-|{\downarrow}{\ddagger}\rangle+\varepsilon|{\uparrow}{\ddagger}\rangle$ and $|b\rangle=|{\downarrow}{\ddagger}\rangle$ are the spin states occupied in an H↓ sample. Here ↓ and ‡ denote the electron- and proton-spin projections, respectively, and $\varepsilon=a/4\mu_BB$ is the hyperfine mixing coefficients; a is the hyperfine coupling constant, and μ_B is the Bohr magneton. The upper states, $|c\rangle=|{\uparrow}{\ddagger}\rangle+\varepsilon|{\downarrow}{\ddagger}\rangle$ and $|d\rangle=|{\uparrow}{\ddagger}\rangle$, are thermally depopulated at low temperature. Due to the hyperfine coupling between proton and electron spin, $a\mathbf{I}\cdot\mathbf{S}$, there is an intrinsic difference in recombination probability between atoms in the a state and the b state. The a state atoms have a small admixture (ε) of electron spin-up, limiting the electronic polarization to $1-\varepsilon^2$ and giving rise to singlet behavior during collisions with other atoms. Atoms in the b state are in a "pure," fully-polarized Zeeman state. Consequently a-state atoms have a higher probability to recombine than atoms in the b state, leading to a faster depletion of the a state than the b state and to a gas of predominantly b-state atoms: nuclear and electron-spin ("doubly") polarized hydrogen (H↓‡).[9,10] Historically the decay of H↓‡ was first attributed to a magnetic relaxation mechanism[10–13] and more recently to dipolar recombination.[6,7,14,15,13] Remarkably, many properties that are known for H↓ were obtained by studying the density decay due to recombination, showing that although recombination is detrimental if one aims at the highest densities,

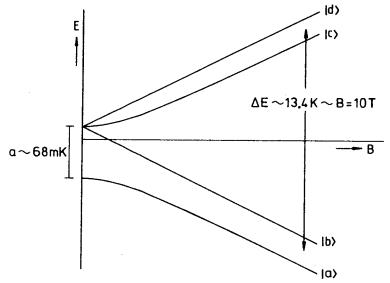

FIG. 1. Hyperfine level diagram of a hydrogen atom in a magnetic field B.

it in fact facilitates the study of many of the properties of H↓.

In earlier experiments H↓ was fed into a sample cell until a steady state was achieved between filling flux and the dominant decay process. In this way H↓↑ has been produced at densities up to $3\times10^{17}\text{cm}^{-3}$ and estimated polarizations of 99.9%.[10,11] When the filling stage is terminated, the decay of the density is observed, using a convenient probe, ranging from calorimetric tools in the early days of H↓ experiments to sophisticated resonance probes to observe the NMR and ESR in the gas.[16,1,2,3] One of the intrinsic difficulties with such an approach is that the gas density decays fastest in the interesting high-density regime, so that high densities are observable only during the very short initial period, just after terminating the filling procedure when uncertainties about thermal equilibrium are largest.

In this paper we expand our earlier report[5] on experiments in which we maintain the system under nominally constant pressure conditions while the effects of recombination are studied by observing the decay of the sample volume. This novel approach enables us to observe the system during periods of minutes at densities 10 times higher than previously possible for periods of seconds. In these experiments a gas of H↓↑ is compressed to densities up to 2×10^{18} cm^{-3}; new destabilization processes are observed which will be discussed in the following sections. Other compression experiments in which H↓↑ was studied up to densities $n\simeq4.5\times10^{18}$ cm^{-3} were done at the Massachusetts Institute of Technology (M.I.T.).[6,7,14,15,8] Apart form a large overlap with our results, these measurements also provide information on surface related phenomena.

II. EXPERIMENTAL APPARATUS

Before describing the details of the sample cell used in the present measurements, we give a short general description of the experimental configuration.

A. General cryogenic system

The experiments are carried out in an Oxford Instruments (1000-μmole/s circulation) dilution refrigerator with access from the bottom (Fig. 2). The sample cell is placed in the center of a 11-T superconducting magnet (Thor Cryogenics, 2.5-cm bore), which creates a parabolic field profile in the cell region.[17] The cell is thermally connected to the mixing chamber by a 1.5-cm-diam. copper rod. The atoms are fed into the cell from the bottom and are produced in a room temperature H_2-discharge operated at 2.45 GHz.[18] The discharge pressure is stabilized to 1–2 Torr using a simple gas handling system with a zeolite-filled cold trap at liquid-N_2 temperature, which purifies the hydrogen and provides a buffer of H_2 gas. The gas handling system is also used to introduce helium into the cell. After dissociation the atoms flow through a constriction in the discharge tube into a teflon-covered 6-mm-diam. transport tube.[18] Before it enters the cryostat the gas passes through a teflon valve, which enables us to isolate the cryogenic part from the rest of the system. The atoms are cooled down in a few stages by heat ex-

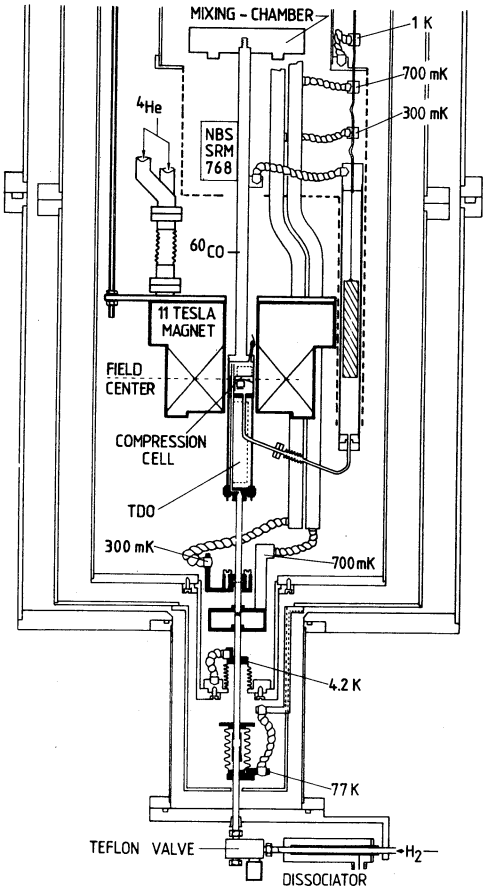

FIG. 2. Schematic diagram of the H↓↑ compression experiment in a ^{3}He-^{4}He dilution refrigerator.

change with the walls of the filling line (see Fig. 2) as has been described elsewhere.[1,18] Thermal pinning points for this purpose are derived from intermediate temperature available in the dilution refrigerator. The a- and b-state atoms are localized in the high-field region by magnetic compression.[17]

B. Compression cell

The general arrangment of our compression cell is shown in Fig. 3. The heart of the cell, located inside of the magnet bore, is separated into two chambers, the upper part (UP) and the lower part (LP) which are connected by tubes extending almost to the bottom of the LP. Entering the bottom of the cell are two tubes: the H↓ fill tube and a tube leading to a large liquid-helium reservoir outside of the magnet. Due to a U-tube arrangement, the helium is distributed over the inner and outer chambers.

The gas may be compressed by up to 5 orders of magnitude in four stages. With the helium level low (stage 1), H↓ fed into the cell fills both the UP and LP to a density of about 10^{15} cm^{-3}. By lowering a large copper block in the outer leg (OL), the He level rises until it seals the bottom of the tubes connecting the UP and LP, isolating the LP region ($\simeq$1.5 cm^3, stage 2). Then the helium level is gradually (in about 1 min) raised by lowering the block further, compressing the gas to smaller volumes (stage 3), in which an equilibrium of the polarization is achieved (see Sec. IV C). Eventually (stage 4) the hydrogen is compressed into a small "bubblelike" volume ($V \geq 2\times10^{-3}$ mm^3) completely immersed in the liquid at the curved top of the LP and is detected by a volume gauge. Since the helium level is above the bubble, there is a hydrostatic pressure on the bubble proportional to the helium column head (1 mm He at $T<1$ K$\simeq$1.42 Pa$\simeq10^{-2}$ Torr). The recombination of atoms results in the decay of the volume of the bubble under nearly constant hydrostatic pressure.

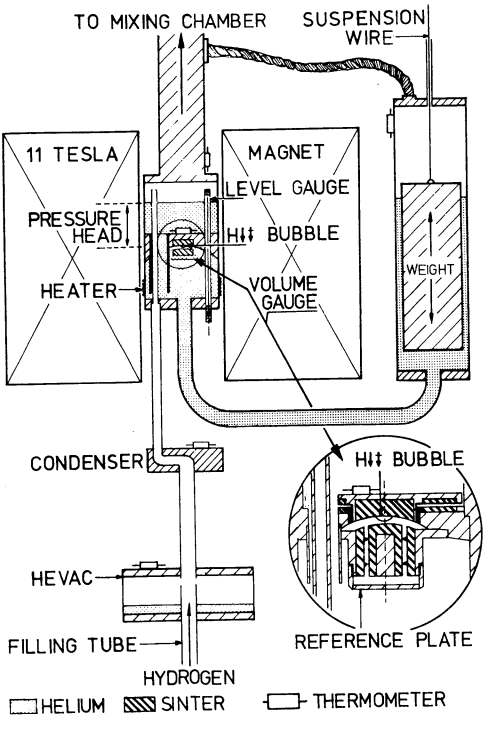

FIG. 3. H↓↑-compression cell (schematic).

The volume of the bubble of compressed H↓↑ is measured with a capacitance gauge. The capacity reaches its maximum value when the gauge is completely filled with liquid helium. The capacitance change due to displacing He with a bubble of H↓↑($\varepsilon=\varepsilon_0$) is a direct measure of the sample volume. Calibration of the volume gauge is done by measuring the relative change in capacitance when filling an empty gauge completely with helium. This gives $\Delta C/C=(1-\varepsilon_r)/\varepsilon_r(\Delta V/V)$ ($\varepsilon_r=1.057$ for pure ^{4}He at temperatures <1 K).[19] The volume of the gauge is 17.7 mm^3 and $\Delta V=6.59\times10^{-4}$ pF/mm^3. The resolution is approximately 10^{-3} mm^3.

The helium level is detected by a coaxial capacitance level gauge, based on the same principle as the volume gauge. Inside the cell, on top of the volume gauge we mounted a resistance thermometer (Matsushita, 200Ω, covered with 1266 Stycast epoxy) to measure the temperature of the plate. These three devices make it possible to follow the decay of the volume under a known hydrostatic pressure and a known ambient temperature. Furthermore, the system includes a membrane-pressure gauge for vapor-pressure thermometry and to monitor the loading of the cell with hydrogen, as well as a trigger bolometer[20] to enable complete removal of the sample.

The construction of the volume gauge is sketched in more detail in Fig. 4(a). It consists of the measuring capacitance (plates A–B, 0.9 mm apart and 6 mm wide, radius of curvature 10 mm), a reference capacitance (plates B–C) and a guard ring D. The difference in capacitance between A–B and B–C is measured with a General Radio 1615A capacitance bridge. This scheme compensates for temperature effects, etc. The plates of the volume gauge are covered with 200-mm^3 silver sinter (0.1-μm grain size) to minimize Kapitza resistance between the helium and the plates. The sinter is filled with liquid helium through capillary action and cannot be penetrated by the H↓↑ gas. Since plates A, B, and C have to be electrically floating, the removal of the heat from these plates is somewhat indirect. The heat of recombination once coupled to the liquid, is extracted via plates A and B and via a small gap filled with liquid helium towards a sinter covered part of the body of the cell (D). The heat exchange between the H↓↑ gas and the helium will be discussed in Sec. IV D.

The level gauge is shown in more detail in Fig. 4(b). The capacitance of this gauge is measured with a capacitance to frequency conversion technique.[21] The coaxial capacitor is the frequency determining element in the LC

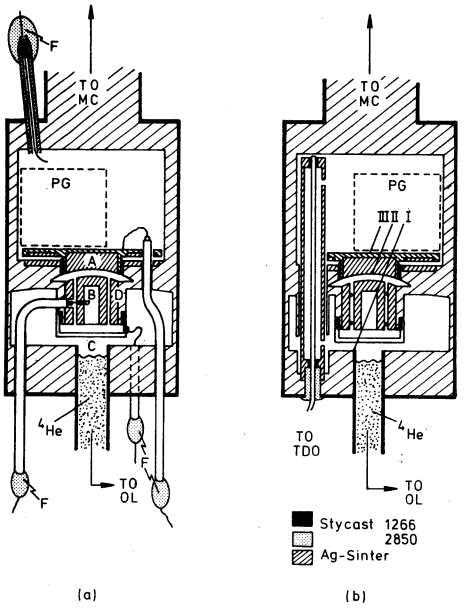

FIG. 4. Detailed cross section of the compression cell inside the magnet. (a) Volume gauge. (b) Level gauge. PG represents pressure gauge, F represents electrical feedthrough, TDO represents tunnel-diode oscillator, and MC represents mixing chamber. The ^{4}He tube connects to the outer leg (OL) of the cell. The H↓ filling line is not shown in this drawing; it would require a third cross section

circuit of a tunnel diode oscillator (TDO) operating at 10.6 MHz. The coil, the tunnel diode (General Electric backward diode BD6) and a feedback capacitor are directly mounted under the cell (see Fig. 2); bias resistors are placed on a 1-K post nearby. The calibration of the level gauge is fixed by determining the frequency when the helium is at the lowest point in the cell [level I, Fig. 4(b)] and at the point just above the volume gauge (level III). The location of these points is determined by inducing U-tube oscillations, sweeping the helium level across levels I and III. The change in cross section at I and III shows up as a change in oscillation amplitude. Using ^{4}He, oscillations are easily generated with a small periodically varying temperature gradient between the legs. The varying fountain pressure then leads to the oscillations. Using the known distance between I and III [12.4(2) mm] and the distance between III and the top of the volume gauge [level II, 2.8(3) mm], the zero column height level is determined and also the sensitivity (about 2.3 kHz/mm He with a resolution of 10^{-2}mm). This calibration had to be done for each field setting, due to a slight field dependence of the characteristics of the tunnel-diode circuit ($\simeq$0.4 kHz/T).

The column height measured this way is not directly proportional to the applied pressure on the bubble. An additional effect is caused by the gradients in our parabolic magnetic field. Due to the diamagnetic susceptibility of ^{4}He, the column tends to be pushed out from the magnet and thus gravity is partially compensated. One can easily show that in the parabolic field the overall resulting pressure at the field center is[22]

$$p_k = p_{\text{gravity}} + p_{\text{diamagnetic}}$$
$$= \rho g z + \tfrac{1}{2}(\chi_m/\mu_0)[B^2(x,z) - B^2(0,0)]$$

with

$$B^2(x,z) = B_0^2\{[1-(z/z_m)^2 + \tfrac{1}{2}(x/z_m)^2]^2 + (xz/z_m^2)^2\},$$

where χ_m is the diamagnetic susceptibility of liquid helium ($\chi_m = 8.7\times10^{-7}$),[23] $\mu_0 = 4\pi\times10^{-7}$ Hm^{-1} is the permeability of vacuum, and x,z is the radial position and height of the helium meniscus. For our magnet $z_m = 5.1\times10^{-2}$ m. This effect is especially important when z becomes large (e.g., for $B_0 = 10$ T, $r = 0$, and $h = 10$ mm the pressure is reduced to 75% of the value in a homogeneous field).

In an earlier paper[5] these diamagnetic effects on the column pressure were not taken into account. Therefore our present value for the third-order coefficient C_3 is substantially larger than in Ref. 5 and in better agreement with the results of Hess *et al.*[6,7] Note that the same diamagnetic effect also causes a difference in level positions between the cell part inside and outside the magnet.

Level oscillations can also be used to study the compressibility of H↓↑ gas. The pressure (Δp) and volume (ΔV) variations associated with the oscillations may be measured with the level and volume gauge, respectively, and should be related through the compressibility κ: $\Delta V/V = \kappa\,\Delta p$. One expects κ to be isothermal [$\kappa_T = -1/V(\partial V/\partial p)_T = 1/p$ for an ideal classical gas] as long as the heat contact between the H gas and the liquid helium is good. In the absence of thermal contact, κ is the adiabatic compressibility [$\kappa_S = -(1/V)(\partial V/\partial p)_S = \frac{3}{5}(1/p)$ for an ideal monatomic classical gas]. Also a stepwise change of p gives information on the compressibility. This method may ultimately lend itself to the observation of BEC where a factor of 2 change in κ_T is predicted at T_c.[3]

C. Thermometry

To measure the temperature of the various parts in the cell, several carbon resistance thermometers were used (Fig. 3). Although most of these thermometers were previously calibrated, a numer of calibration devices were also mounted on the cell to check the calibration. For the low-temperature regime ($T = 20$–300 mK) the calibration was done in zero-field against a National Bureau of Standards (NBS) fixed-points device (SRM 768) and a ^{60}Co nuclear orientation thermometer. For the regime at $T = 300$–900 mK the calibration was done against the ^{3}He and ^{4}He vapor pressures, making use of the internal pressure gauge and an external gauge (Barocel 1173) to measure the vapor pressure. The resistance thermometers are field dependent and must be calibrated *in situ* for each

magnetic field setting. Since the nuclear orientation thermometer and the fixed-points device are no longer useful once the field has been turned on, the calibration in field is done by transferring the zero-field calibration to the higher fields by cycling the field up and down. The calibration reproduced within 2% of previous ones.

III. ANALYSIS OF THE VOLUME DECAY

To analyze our data we use a simple rate equation to describe the decrease of the total number of particles N in a doubly polarized gas:

$$dN/dt = -F(n)N \ , \tag{3.1}$$

where $F(n)$ is a polynomial in the density n. Under the appropriate conditions the polynomial coefficients may be compared with decay coefficients provided by theory (see Sec. IV C). For instance, allowing only for two-body $b \rightarrow a$ volume relaxation (rate constant G^v_{ba} which bottlenecks rapid a-b recombination) and three-body volume recombination (rate constant K^v_{bbb}) one may write

$$F(n) = C_2 n + C_3 n^2 \ , \tag{3.2}$$

where $C_2 = 2G^v_{ba}$ and $C_3 = 2K^v_{bbb}$.

Using the ideal gas law, $pV = Nk_BT$, gives for the decay rate under isothermal condition:

$$\tau^{-1} \equiv \dot{V}/V = -F(n)[1 + (V/p)dp/dV]^{-1} \ . \tag{3.3}$$

In general the gas pressure $p = p_k + p_\gamma$ is the sum of the pressures due to the helium column height, p_k, measured with respect to the top of the bubble and corrected for the diamagnetic susceptibility of helium p_{diam} and a bubble volume and shape-dependent part p_γ. The latter term $p_\gamma \equiv p_\alpha + p_\beta$ has a contribution due to the surface tension of the liquid-helium surface, p_α, and the buoyancy pressure, $p_\beta = \Delta\rho g h$, where $\Delta\rho$ is the difference in mass density between liquid and gas, g is the acceleration of gravity, and h is the height of the bubble (see Fig. 5). p_γ increases during the decay of the volume.

Before addressing ourselves to the case of a nonspherical bubble at arbitrary pressure, we first consider two important limiting regimes for the volume decay; the isobaric regime and the surface tension dominated regime. In the isobaric regime p is predominantly determined by the hydrostatic pressure head ($p_k \gg p_\gamma$) and the volume decay rate (τ^{-1}) is constant:

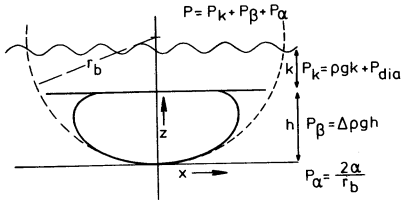

FIG. 5. Definition of symbols used in calculation of the shape of a sessile bubble. The column pressure p_k is also influenced by the gradient in the magnetic field (p_{diam}, see the text).

$$\tau^{-1} = -F(p_k/k_BT) \ . \tag{3.4a}$$

Hence, the volume decays exponentially:

$$V(t) = V_0 \exp(-F[p_k/k_BT]t] \ . \tag{3.4b}$$

This regime is characteristic for most of our experiments with bubbles in the 0.5–2.0 mm^3 range. A typical decay for this regime is illustrated in Fig. 6.

For small bubbles the buoyant forces are negligible ($p_\beta \ll p_\alpha$) so that the bubble is spherical. Then $p_\gamma \simeq p_\alpha = 2\alpha/r \equiv \hat{\alpha}/V^{1/3}$,[24] where r is the radius of the bubble, α the surface tension of helium and $\hat{\alpha} = 2\alpha(4\pi/3)^{1/3}$ (for ^{4}He at $T < 1.2$ K; $\alpha = 3.7 \times 10^{-4}$ Nm^{-1}).[25] Hence Eq. (3.3) reduces to

$$\tau^{-1} = -F(p/k_BT)[p/(p - \tfrac{1}{3}p_\alpha)] \ , \tag{3.5}$$

with $p = p_k + p_\alpha$. Furthermore, if $p_k \ll p_\alpha$, which holds for very small bubbles, surface tension effects are dominant and τ^{-1} becomes

$$\tau^{-1} = -\tfrac{3}{2}F(p_\alpha/k_BT) \ . \tag{3.6}$$

The transition to the surface tension dominated regime is illustrated in Fig. 7 for a bubble under small applied pressure where the decay is approximately second order in nature and τ^{-1} approaches a $V^{-1/3}$-like behavior. One notes that even at 10^{-2} mm^3 the observed decay still deviates from a decline according to Eq. (3.6).

An accurate relation between p_γ and V, taking into account the detailed shape of the bubble, may be derived starting from the Young and Laplace equation for the surface pressure of a curved surface:[24]

$$\alpha(1/R_1 + 1/R_2) = p - p_l(x,z) \ . \tag{3.7a}$$

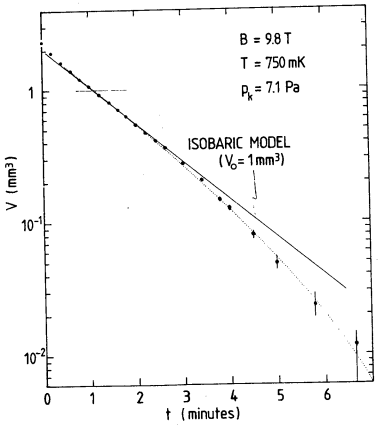

FIG. 6. Example of a decay at relatively high column pressure ($p_\gamma \ll p_k$). The solid line represents the exponential approximation for an isobaric decay, the dotted line is the fit of the decay using the calculated pressure p_γ. For $V > 1.4$ mm^3 the volume gauge is no longer linear.

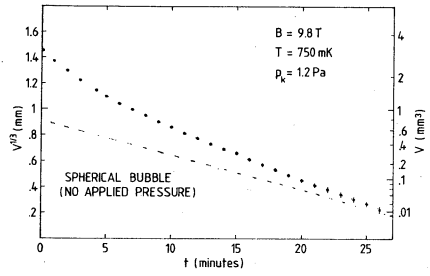

FIG. 7. Example of a decay at relatively low column pressure ($p_\gamma \gg p_k$). The dashed line represents an approximation with $p_k=0$ and p_γ the surface tension of a spherical bubble, the dotted line is the fit of the decay using the calculated pressure p_γ. For $V>1.4$ mm^3 the volume gauge is no longer linear.

Here R_1 and R_2 are the local radii of curvature of the bubble surface, p is the gas pressure in the bubble, and p_l is the pressure in the liquid at the evaluation point (x,z). The result of the model is illustrated in Fig. 5. We show the bubble deformed by the buoyant forces, which push the bubble against a flat plate. The contact angle between bubble and plate is zero, the limit of complete wetting of the surface. To describe the bubble shape we choose the x,z coordinate system with the origin at the lower apex of the bubble. At the origin, where $R_1=R_2\equiv r_b$, Eq. (3.7a) reduces to

$$p=p_l(0,0)+2\alpha/r_b\equiv p_k+p_\gamma\ . \tag{3.7b}$$

Combining Eqs. (3.7a) and (3.7b) and using $p_l(0,0)-p_l(x,z)=\Delta\rho gz$ one finds

$$\alpha(1/R_1+1/R_2)=\Delta\rho gz+2\alpha/r_b\ . \tag{3.7c}$$

In principle, the shape of the bubble depends on the presence of magnetic field gradients, but these effects are negligible since the bubble is very small and located in the center of the magnetic field. Exploiting the axial symmetry of the bubble with respect to the z axis one finds from differential geometry for R_1 and R_2:[24]

$$1/R_1=\ddot{z}(1+\dot{z}^2)^{-3/2} \tag{3.8a}$$

and

$$1/R_2=\dot{z}[x(1+\dot{z}^2)^{1/2}]^{-1}\ , \tag{3.8b}$$

where R_1 is the radius of curvature of the meridian,

$$\dot{z}\equiv(dz/dx)\equiv\tan(\Phi)$$

and

$$\ddot{z}\equiv d^2z/dx^2\equiv\cos^{-2}(\Phi)(d\Phi/dx)\ .$$

The bubble problem may be reformulated in terms of a set of differential equations in x,z as a function of Φ which may be solved numerically once the curvature r_b at the apex is chosen:

$$dx^*/d\Phi=\cos(\Phi)/f(x^*,z^*)\ , \tag{3.9a}$$

$$dz^*/d\Phi=\sin(\Phi)/f(x^*,z^*)\ , \tag{3.9b}$$

where $x^*\equiv x/r_b$, $z^*\equiv z/r_b$, and

$$f(x^*,z^*)=[\Delta\rho g/(\alpha r_b^2)]z^*+2-\sin(\Phi)/x^*\ . \tag{3.9c}$$

The required relation between p_γ and V, taking into account the bubble shape, then follows from a numerical integration procedure. The results of the calculation for the case of ^{4}He are illustrated in Fig. 8. These are slightly different when using a curved top surface of the bubble instead of the flat top shown in Fig. 5. For the curvature used in the experiment, the difference between the results for a flat top and the actual curved top are less than 2%. The bubble model only applies for $V<1.4$ mm^3, beyond which the bubble contacts both capacitor plates.

In principle, information on the second-order and third-order decay coefficients can be derived from one volume decay curve, provided p_k, T and B are known, with the use of this bubble model. The dotted lines in Figs 6 and 7 are fits to the data, obtained by numerical integration of Eq. (3.3) for an optimum choice of C_2 and C_3. The fit demonstrates that the bubble model enables

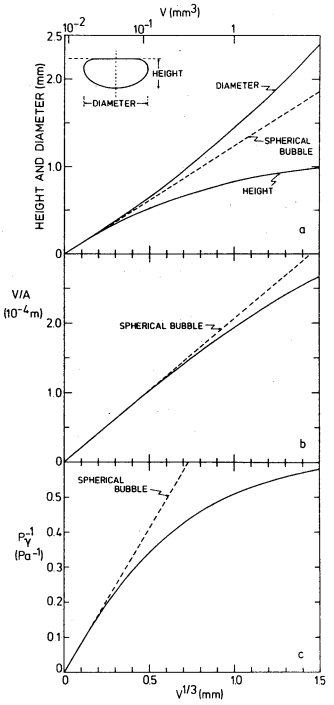

FIG. 8. Calculated properties of a sessile bubble in ^{4}He ($\alpha=3.7\times10^{-4}$ Nm). Dashed line is a spherical bubble approximation.

an accurate description of the decay. However, the results depend very critically on the exactness of the bubble model and furthermore one neglects the influence of a changing A/V ratio on the coefficients C_2 and C_3. A more attractive approach, which is less sensitive to this problem, involves the combination of decay curves obtained for different p_k. This is done by measuring $\tau^{-1} \equiv \dot{V}/V$ at one specific volume V_0 (e.g., 1 mm^3) for different decay curves. The additional pressure $p_{\gamma 0} \equiv p_\gamma(V=V_0)$ and its volume derivative $(dp_\gamma/dV)_{V=V_0}$ are then the same for each density curve, independent of the exact shape of the bubble as long as this shape reproduces for each temperature and magnetic field. With the use of Eq. (3.3), τ^{-1} is

$$\tau^{-1} = -F[(p_k + p_{\gamma 0})/k_B T]/\mathscr{C}_{\rm cor}(V_0) , \qquad (3.10)$$

with

$$\mathscr{C}_{\rm cor}(V_0) = 1 + [V_0/(p_k + p_{\gamma 0})](dp_\gamma/dV)_{V=V_0} .$$

All corrections due to the change of the pressure as function of the volume are contained in the factor $\mathscr{C}_{\rm cor}$. This factor is close to unity as long as $p_k > p_{\gamma 0}$, which is the case for our $V_0 = 1$-mm^3 data, as illustrated in Fig. 9.

The analysis of our experimental data is presented in Sec. IV and was done by measuring τ^{-1} at $V_0 = 1$ mm^3 in the volume decays for different values of p_k. Using the correction factor $\mathscr{C}_{\rm cor}$ and $p_{\gamma 0}$ for $V_0 = 1$ mm^3, $\tau^{-1} \times \mathscr{C}_{\rm cor}$, and $p = p_k + p_{\gamma 0}$ were obtained. Fitting $\tau^{-1}\mathscr{C}_{\rm cor}$ versus p to a second-order polynomial through the origin gives the coefficients C_2 and C_3 in $F(p)$. To illustrate the consistency of the model for p_γ, Fig. 10 shows the data at 9.8 T and 750 mK analyzed for different volumes and combined in one plot. For the range of volumes considered (0.02–1.0 mm^3), p_γ changes about 4 Pa and the data points follow approximately a common parabola, although at small volumes (dotted line) a systematic deviation from the curve is observed in a detailed analysis. In Sec. IV C we will show that the deviation can be explained by the effect of a changing A/V ratio and its influence on the effective surface decay rates.

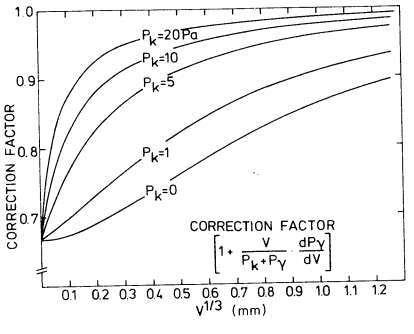

FIG. 9. Correction factor $\mathscr{C}_{\rm cor}$ as a function of column pressure p_k and volume $V^{1/3}$ [Eq. (3.10)].

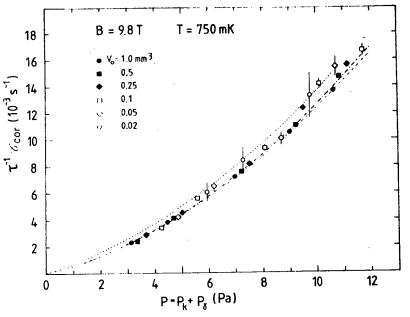

FIG. 10. Five decays at $B = 9.8$ T and $T = 750$ mK analyzed for different volumes V_0. The dashed line is a second-order fit to $V_0 = 1$ mm^3. The dashed-dotted line is a curve based on Eqs. (4.9) using the decay-rate constant from Table I. The dotted line idem but for $V_0 = 0.02$ mm^3 ($A/V = 150$ cm^{-1}). The deviation between the dashed-dotted and dotted line is attributed to the difference in the A/V ratio.

IV. RESULTS

A. General features

The highest pressure we could apply, using the compression scheme of Sec. II B, corresponds to $\simeq$12-mm helium column ($\simeq$15 Pa at 8 T) as limited by the dimensions of the sample cell. At the lowest ambient temperatures employed in this experiment ($T \simeq 700$ mK, using ^{4}He as compression fluid) this implies a density of $n \simeq 2 \times 10^{18}$ cm^{-3}. The assumption of thermal equilibrium will be discussed in Sec. IV D. The highest densities were achieved in bubbles with a volume $V = \simeq 0.1$ mm^3 and in an 8 T magnetic field.

High densities could only be obtained by compressing the sample at a relatively slow rate ($\simeq$1 min) to the final pressures. Too rapid a compression was found to lead to a short (<1 s) transient phenomenon in which the bubble disappeared after a sudden increase in volume (by as much as a factor of 10). These transients were accompanied by small spikes on the level gauge and on the internal thermometer of the cell, and were interpreted as the occurrence of an explosion in the gas. The explosions could always be induced by compressing sufficiently fast, even when the gas was carefully precompressed (stage 3, see Sec. II B) to induce double polarization. In a typical experiment we observed the decay of the volume over at least 1 order of magnitude from $\simeq$2 mm^3 to 0.1 mm^3. This process was quite slow, especially at low densities, requiring termination of the decay by rapid compression to obtain a "zero-volume" reference measurement (Fig. 11). An attractive aspect of the explosions is that they enabled us to do such a zero-volume measurement at will, when useful. In this sense the explosions replace the use of the "trigger bolometer" in pressure decay measurements.

Under appropriate conditions ($B/T < 10$ T/K) the explosions were observed to occur "spontaneously" (Fig. 12). This is associated [5,26] with a new destabilization process that we identified: electronic dipolar ($b \rightarrow c$) relaxation

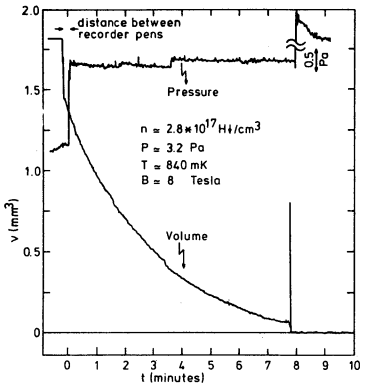

FIG. 11. Typical volume decay terminated by rapid compression, inducing an "explosion" of the gas.

which will be discussed in more detail in Sec. IV C. Recently, the explosions have been studied in more detail by Tommila *et al.*[27]

Perhaps the most significant result of the quantitative analysis of the decay curves was evidence for a third-order decay process with rate constant $C_3=[7(2)]\times10^{-39}\text{cm}^6\,\text{s}^{-1}$ ($B=9.8$ T, $T=750$ mK) and in good agreement with the result of Hess *et al.*[6,7] This process represents a very important barrier for obtaining high-gas densities since the decay rate is proportional to the cube of the density.

Although a quantitative analysis will only be given for the ^{4}He case, we also obtained some results ^{3}He/^{4}He mixtures as compression fluid. Due to a cryogenic problem we could not measure below 650 mK with ^{4}He liquid in the cell. Apparently the film flow of the superfluid helium out of the cell, and the back-fluxing helium vapor gave rise to an excessive heat load (estimated to be $\simeq$2 mW). With a small admixture of ^{3}He (1%) this problem was suppressed and the cell could be cooled below 100 mK.

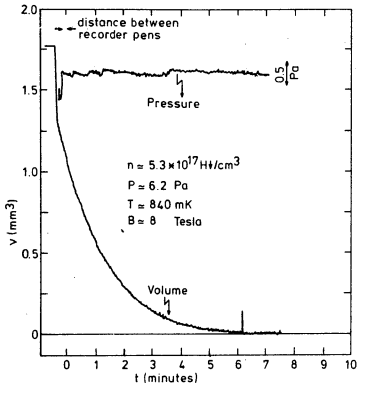

FIG. 12. Typical volume decay terminated by a spontaneous "explosion."

The reported data on ^{4}He cover the 650–900 mK temperature regime, where destabilization processes in the bulk gas dominate the surface processes. As such, this temperature regime is well suited to study the bulk destabilization processes of the sample. Compression data for ^{3}He/^{4}He mixtures were observed for temperatures ranging from 300–500 mK. Under those conditions the H↓ samples turned out to be much more susceptible to explosions than when using ^{4}He as a compression fluid. Although we could produce densities of the same order of magnitude as in the ^{4}He case, irreproducibilities in the data, which were likely due to poor thermal equilibrium, caused us to focus on the ^{4}He data.

B. Analysis of the decay rates

We used the procedure in Sec. III to analyze the observed rate of change of the volume (τ^{-1}) as function of pressure, taking into account the correction factor $\mathscr{C}_{\text{cor}}$, p_γ, and the influence of the diamagnetic correction of p_k. In Fig. 13 we show $(1/p)\tau^{-1}\times\mathscr{C}_{\text{cor}}(V_0=1\text{ mm}^3)$ versus p for magnetic fields $B=9.8$, 9, 8, 7, and 6 T obtained for a temperature of $\simeq$710 mK. The lines in Fig. 13 are fits of $\tau^{-1}\times\mathscr{C}_{\text{cor}}$ versus p to a second-order polynomial through the origin, where (C_2/k_BT) is the intercept and $[C_3/(k_BT)^2]$ the slope [see Eqs. (3.2) and (3.10)]. For some fields the number of data points and the dynamic range of the density was quite limited (due to a rapidly decaying sample). The results for the field dependence of the second-order coefficient (C_2) are presented in Fig. 14(a), and for the third-order coefficient (C_3) in Fig. 14(b).

The results for the temperature dependence of the rates $(1/p)\tau^{-1}\times\mathscr{C}_{\text{cor}}$ versus p at $B=8$ T are shown in Fig. 15. For 680 and 840 mK reliable data for C_2 and C_3 could be obtained. For 733 and 925 mK only one decay was recorded, which is not enough to deduce C_2 and C_3 independently. These data will be used only for an estimate of C_2, correcting for C_3, resulting in relatively large error bars.

C. Discussion of the decay results

To interpret our results, we consider the known recombination and relaxation processes in doubly polarized gas ($n_b \gg n_a$) where the a state is depleted due to preferential

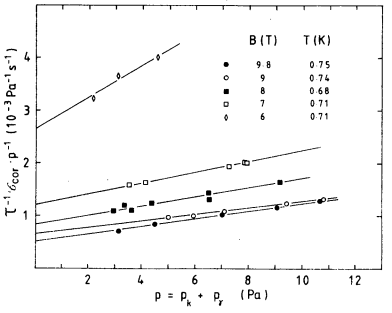

FIG. 13. Field dependence of the decay rates at $\simeq$710 mK. The lines are fits to the data for different fields.

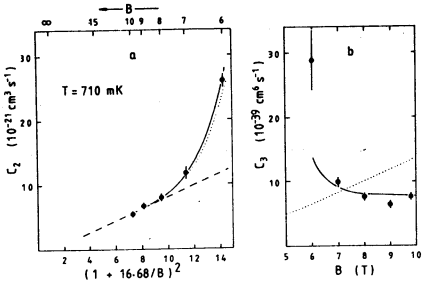

FIG. 14. Field dependence of (a) second-order (C_2) and (b) third-order (C_3) decay rates. (a) The dashed line is the contribution of volume relaxation: $G^v_{ba}T^{-1/2}(1+16.68/B)^{-2}=6.9(6)\times10^{-22}$ cm^{3}s^{-1}. The solid line is the sum of G^v_{ab} and $G^v_{bc}\uparrow$ contribution (see text). Dotted line idem, but with $G^v_{bc}\downarrow$ the value obtained by Lagendijk *et al.* (Ref. 36). (b) The dotted line is the calculated volume recombination rate K^v_{bbb} (Ref. 29) multiplied by $2\theta_b=3.27$. The solid line is a fit to the data with $K^v_{bbb}=2.0(5)\times10^{-39}$ cm^{6}s^{-1} and $K^v_{bbc}=3(1)\times10^{-33}$ cm^{6}s^{-1} (see text).

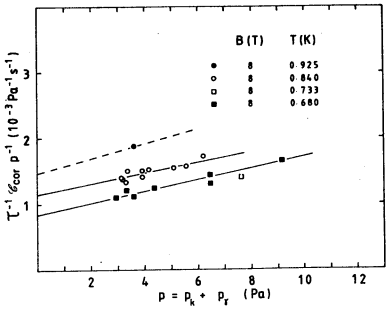

FIG. 15. Temperature dependence of the decay rates at $B=8$ T. For $T=733$ mK and $T=925$ mK only one data point is available. Dashed lines are fits to the data.

recombination.[6] As our experiments were done at relatively high temperatures and/or low magnetic fields, we also considered the occupation of the c and d levels. In that case the evolution of the system is described by a set of four coupled rate equations. For simplicity we only retain the leading terms, assuming $n_d \ll n_c \ll n_a < , n_b$. As we will discuss later, the degree of double polarization may not be sufficiently high to neglect all processes where two or more a-state atoms participate. The rate equations are

$$\begin{aligned}
\dot{A}/V &= -K^{\rm eff}_{ab}ab + G^v_{ba}(a+b)(b-a) + G^{\rm eff}_E(bd-ac) \\
&\quad -K^{vv}_{abb}ab^2 , \\
\dot{B}/V &= -K^{\rm eff}_{ab}ab - G^v_{ba}(a+b)(b-a) - G^{\rm eff}_E(bd-ac) \\
&\quad -K^{\rm eff}_{bc}bc - G^v_{bc}\uparrow(b+c)b + G^v_{bc}\downarrow(b+c)c \\
&\quad -K^{\rm eff}_{bd}bd - (2+\xi)K^v_{bbb}b^3 - K^v_{bbc}b^2c - K^v_{abb}ab^2 , \\
\dot{C}/V &= -K^{\rm eff}_{bc}bc - G^v_{bc}\downarrow(b+c)c + G^v_{bc}\uparrow(b+c)b \\
&\quad +G^{\rm eff}_E(bd-ac) + \xi K^v_{bbb}b^3 - K^v_{bbc}b^2c , \\
\dot{D}/V &= -K^{\rm eff}_{bd}bd - G^{\rm eff}_E(bd-ac) .
\end{aligned} \tag{4.1}$$

Adding all terms yields

$$\begin{aligned}
\dot{N}/V = -2(&K^{\rm eff}_{ab}ab + K^{\rm eff}_{bc}bc + K^{\rm eff}_{bd}bd \\
&+K^v_{abb}ab^2 + K^v_{bbb}b^3 + K^v_{bbc}b^2c) .
\end{aligned}$$

Here capital letters represent numbers of particles and lower case letters represent number densities in a specific hyperfine level. The contributing rate constants at higher temperatures can be grouped in four classes. (a) The second-order rates $K^{\rm eff}_{ab}$, $K^{\rm eff}_{bc}$, etc., correspond to three-body recombination processes where a third body other than hydrogen enables conservation of energy and momentum. Helium atoms of the helium surface can provide this third body for H atoms adsorbed on the helium film (K^s_{ab}). These surface processes are proportional to the surface coverage and hence exponentially dependent on the binding enregy (ε_a) of an H atom to the surface. At higher temperatures, where the helium vapor pressure becomes appreciable, the third body can also be a helium atom from the vapor [$K^v_{ab}(n_{\rm He})$]. Both bulk and surface processes are included in $K^{\rm eff}_{ab}$,$K^{\rm eff}_{bc}$, etc.:

$$K^{\rm eff}_{ab} = (A/V)K^s_{ab}[\lambda_{th}\exp(\varepsilon_a/k_BT)]^2 + K^v_{ab}(n_{\rm He})$$

with

$$\lambda_{th} = (2\pi\hbar^2/mk_BT)^{-1/2} .$$

(b) G^v_{ba} describes the two-body nuclear dipole-dipole relaxation in the bulk and $G^v_{bc}\uparrow$, $G^v_{bc}\downarrow$ the electronic dipolar relaxation. The ratio of $G^v_{bc}\uparrow$ and $G^v_{bc}\downarrow$ is determined by the Boltzmann factor:

$$G^v_{bc}\uparrow/G^v_{bc}\downarrow = \exp(-2\mu B/k_BT) \simeq \exp(-1.35B/T) .$$

Surface relaxation can be ignored at high temperatures. (c) $G^{\rm eff}_E$ relates to the spin-exchange process between a,c and b,d levels. All other spin-exchange processes are suppressed in high magnetic fields. Spin-exchange tends to maintain $a/b=d/c$. (d) K^v_{bbb}, K^v_{abb}, and K^v_{bbc} describe three-body hydrogen recombination processes in the bulk. K^v_{bbc} yields the recombination rate with one of the atoms in the c state. It is driven by the exchange recombination mechanism described by Kagan *et al.*[28] Similarly K^v_{abb} is associated with the exchange recombination with one of the atoms in the a state. Note that we introduced K^v_{abb} and K^v_{bbc} in the equations in spite of the fact that the only available theory for exchange recombination by Kagan *et al.*[28] implies $K^v_{abb}=\varepsilon^2K^v_{bbc}=0$ for $T\to0$. K^v_{bbb} is the three-body dipolar-recombination rate.[28] For each K^v_{bbb} event, a hydrogen molecule and an atom in the c state [fraction $\xi=0.91$ (Ref. 29)] or in the b state (fraction $1-\xi$) is produced. This c-state atom can relax to the b state ($G^v_{bc}\downarrow$) or recombine either on the surface (K^s_{bc}) or in the gas phase (K^v_{bbc}).[15] In the latter two cases one event of K^v_{bbb} finally results in the production of two molecules

and a total loss of four b-state atoms. In the former case, only two atoms disappear from the b state. The dominant scenario is determined by the temperature, field and density conditions. Again surface three-body effects are ignored because at higher temperatures the surface coverage is too low.

To illustrate some features of this set of rate equations, assume that the density is sufficiently low to exclude third-order processes and that the temperature and/or field conditions are such ($B/T < 10$ T/K) that the c level is partially populated, while $n_d \ll n_c \ll n_b$ due to preferential recombination and spin-exchange. Then, Eqs. (4.1) reduce to

$$\begin{aligned}
\dot{A}/(Vb^2) &= -K_{ab}^{\rm eff}\hat{a} + G_{ba}^{v}(1-\hat{a}^2) + G_E^{\rm eff}(\hat{d}-\hat{a}\hat{c}) , \\
\dot{B}/(Vb^2) &= -K_{ab}^{\rm eff}\hat{a} - G_{ba}^{v}(1-\hat{a}^2) - G_E^{\rm eff}(\hat{d}-\hat{a}\hat{c}) \\
&\quad -K_{bc}^{\rm eff}\hat{c} + G_{bc}^{v}\downarrow(1+\hat{c})\hat{c} - G_{ab}^{v}\uparrow(1+\hat{c}) - K_{bd}^{\rm eff}\hat{d} , \\
\dot{C}/(Vb^2) &= -K_{bc}^{\rm eff}\hat{c} - G_{bc}^{v}\downarrow(1+\hat{c})\hat{c} + G_{bv}^{v}\uparrow(1+\hat{c}) \\
&\quad + G_E^{\rm eff}(\hat{d}-\hat{a}\hat{c}) , \\
\dot{D}/(Vb^2) &= -K_{bd}^{\rm eff}\hat{d} - G_E^{\rm eff}(\hat{d}-\hat{a}\hat{c}) ,
\end{aligned} \tag{4.2}$$

with $\hat{a} \equiv a/b$, $\hat{c} \equiv c/b$, and $\hat{d} \equiv d/b$.

For the doubly polarized gas $\hat{a}$, $\hat{c}$, and $\hat{d}$ go to well-defined limit values for $t \to \infty$, $\hat{a}_0$, $\hat{c}_0$, and $\hat{d}_0$, which are independent of the history of the sample. Retaining only terms up to first order in $\hat{a}$, $\hat{c}$, and $\hat{d}$, this results in ratios

$$\begin{aligned}
\hat{a}_0 &= G_{ba}^{v}/(K_{ab}^{\rm eff} - G_{bc}^{v}\uparrow) , \\
\hat{c}_0 &= G_{bc}^{v}\uparrow/(K_{bc}^{\rm eff} + G_{bc}^{v}\downarrow) ,
\end{aligned} \tag{4.3}$$

and $\hat{d}_0 = 0$. These relations are obtained by setting $\dot{\hat{a}}$, $\dot{\hat{c}}$, and $\dot{\hat{d}}$ equal to zero. Here $\hat{a}_0$ is a measure for the double polarization in the gas [the polarization is usually defined as $(b-a)/(b+a) = (1-\hat{a})/(1+\hat{a})$]. The ratio $\hat{c}_0$ expresses the competition between the relaxation of b-state atoms to the c-state atoms ($G_{bc}^{v}\uparrow$) and the subsequent recombination ($K_{bc}^{\rm eff}$) or relaxing back ($G_{bc}^{v}\downarrow$) of this c-state atom. Which process is dominant depends on temperature and on the geometry of the cell. If the recombination is much slower than the relaxation ($K_{bc}^{\rm eff} \ll G_{bc}^{v}\downarrow$), $\hat{c}_0$ equals the ratio of the b and c level in thermal equilibrium. In the other limit ($K_{bc}^{\rm eff} \gg G_{bc}^{v}\downarrow$) the ratio $\hat{c}_0$ is analogous to the bottlenecked situation of the b and a level. The relaxation rates $G_{bc}^{v}\uparrow$ and G_{ba}^{v} are then the stability determining rates for the decay of b atoms. For example, for a bubble of $V = 1$ mm^3, $A/V = 50$ cm^{-1}, $K_{bc}^{\rm eff} \simeq G_{bc}^{v}\downarrow$ at 0.8 K (using the numerical values given in Table I).

Combining Eqs. (4.2) and (4.3) the number decay is given by

$$\dot{N}/(Vb^2) = -2[\zeta_0 G_{ba}^{v} + \eta_0 G_{bc}^{v}\uparrow] \tag{4.4}$$

with $\zeta_0 \equiv k_{ab}^{\rm eff}/(K_{ab}^{\rm eff} - G_{ba}^{v} - G_{bc}^{v}\uparrow)$ and $\eta_0 \equiv k_{bc}^{\rm eff}/(K_{bc}^{\rm eff} + G_{bc}^{v}\downarrow)$. The decay is thus bottlenecked by nuclear and electronic relaxation as long as $K_{bc}^{\rm eff} \gg G_{bc}^{v}\downarrow (\eta_0 \simeq 1)$ and $K_{ab}^{\rm eff} \gg G_{ba}^{v} (\zeta_0 \simeq 1)$.

When third-order effects are included in Eqs. (4.2), the rate equations become, up to first order in $\hat{a}$ and $\hat{c}$ (ignoring the small contribution of $\hat{d}$):

$$\begin{aligned}
\dot{A}/(Vb^2) &= -K_{ab}^{\rm eff}\hat{a} + G_{ba}^{v} - K_{abb}^{v} b\hat{a} , \\
\dot{B}/(Vb^2) &= -K_{ab}^{\rm eff}\hat{a} - G_{ba}^{v} - K_{bc}^{\rm eff}\hat{c} - G_{ab}^{v}\uparrow(1+\hat{c}) + G_{bc}^{v}\downarrow\hat{c} \\
&\quad -(2+\xi)K_{bbb}^{v} b - K_{bbc}^{v} b\hat{c} - K_{abb}^{v} b\hat{a} , \\
\dot{C}/(Vb^2) &= -K_{bc}^{\rm eff}\hat{c} + G_{bc}^{v}\uparrow(1+\hat{c}) - G_{bc}^{v}\downarrow\hat{c} \\
&\quad + \xi K_{bbb}^{v} b - K_{bbc}^{v} b\hat{c} .
\end{aligned} \tag{4.5}$$

Summing results, we find a rate equation for N:

TABLE I. Some rate constants used in the analysis. Rate constants G_{ba}^{v}, G_{bc}^{v}, and K_{bbb}^{v} follow from the analysis of our data.

	Rate constants	Reference
Two-body recombination	$K_{ab}^{\rm eff} = A/V[\lambda_{th}\exp(\varepsilon_a/k_BT)]^2 2.5\times10^{-8}T^{1/2}B^{-2} + K_{abHe}$ cm^3 s^{-1}	11
	$K_{aa}^{\rm eff} = 2.2K_{ab}^{\rm eff}$	11
	$K_{bc}^{\rm eff} = A/V[\lambda_{th}\exp(\varepsilon_a/k_BT)]^2 3.9\times10^{-5}T^{1/2} + K_{bcHe}$ cm^3 s^{-1} with $E_a = 1.15$ K	31 and 32
	$K_{bcHe} = 2.8(3)\times10^{-33} n_{He}$ cm^3 s^{-1}	33
	$K_{abHe} = \varepsilon^2 K_{bcHe}$, $n_{He} \simeq 4.65\times10^{13}\exp(10.1T)$ cm^{-3}	33
Two-body relaxation	$G_{ab}^{v} = T^{1/2}(1+16.68/B)^2 6.9(6)\times10^{-22}$ cm^3 s^{-1}	This work[a]
	$G_{bc}^{v}\downarrow = 12(4)\times10^{-16}$ cm^3 s^{-1}	This work[a]
	$G_{bc}^{v}\uparrow = G_{bc}^{v}\downarrow \exp(-1.35B/T)$ cm^3 s^{-1}	This work[a]
Three-body recombination	$K_{bbb}^{v} = 2.0(5)\times10^{-39}$ cm^6 s^{-1} at $B = 9.8$ and 9 T	This work
	$K_{bbc}^{v} = 3(1)\times10^{-33}$ cm^6 s^{-1}	This work[a] and 14
	$K_{abb}^{v} = \varepsilon^2 K_{bbc}^{v}$ cm^6 s^{-1}	This work[a] and 14

[a]We use $T^{1/2}$ behavior for G_{ba}^{v} near 700 mK to scale data.

$$\dot{N}/(Vb^2) = -2(K_{ab}^{\rm eff}\hat{a} + K_{bc}^{\rm eff}\hat{c} + K_{bbb}^{v} b + K_{abb}^{v} b\hat{a} + K_{bbc}^{v} b\hat{c}) . \quad (4.6)$$

Here $\hat{a}$ and $\hat{c}$ do not go to a well-defined limit value, but change as a function of density due to the presence of third-order terms in Eqs. (4.5). An estimate of the equilibrium value of $\hat{a}$ and $\hat{c}$ is found by assuming $\hat{a}$ and $\hat{c}$ to be small. Under the nearly isobaric conditions of our bubble measurements this is a plausible assumption. One then finds b-density-dependent ratios

$$\hat{a} = G_{ba}^{v}/[K_{ab}^{\rm eff} - G_{ba}^{v} - G_{bc}^{v}\uparrow + K_{abb}^{v} b - (2+\xi)K_{bbb}^{v} b] , \quad (4.7)$$

$$\hat{c} = (G_{bc}^{v}\uparrow + \xi K_{bbb}^{v} b)/(K_{bc}^{\rm eff} + G_{bc}^{v}\downarrow + K_{bbc}^{v} b) .$$

At low densities Eqs. (4.7) reduce to Eqs. (4.3). The influence of the three-body terms on $\hat{c}$ is substantial, even for the experimental conditions reported here: e.g., $B = 9.8$ T, $T = 0.75$ K and $b = 5\times10^{17}$ cm^{-3} gives $\hat{c} = 6\times10^{-9}$ without and $\hat{c} = 1\times10^{-7}$ with three-body terms. This shows that the production of c-state atoms is mainly due to three-body recombination (K_{bbb}^{v}) events and not to electronic relaxation ($G_{bc}^{v}\uparrow$). As a consequence the c-state occupation is a factor of 5 larger than one expects for thermal equilibrium ($\hat{c} \simeq 2\times10^{-8}$). At lower temperatures the factor may become substantially larger than 5.

Substituting Eqs. (4.7) into Eq. (4.6) and arranging the equation in order of b density gives

$$\dot{N}/(Vb^2) = -2(\zeta G_{ba}^{v} + \eta G_{bc}^{v}\uparrow) - 2[(1+\xi\eta)K_{bbb}^{v} + K_{abb}^{v}\zeta(G_{ba}^{v}/K_{ab}^{\rm eff}) + K_{bbc}^{v}\eta G_{bc}^{v}\uparrow/K_{bc}^{\rm eff}]b - 2[(K_{bbc}^{v}K_{bbb}^{v}/K_{bc}^{\rm eff})\xi\eta]b^2 , \quad (4.8)$$

with

$$\eta = K_{bc}^{\rm eff}/(K_{bc}^{\rm eff} + G_{bc}^{v}\downarrow + K_{bbc}^{v} b) ,$$

and

$$\zeta = K_{ab}^{\rm eff}/[K_{ab}^{\rm eff} - G_{ba}^{v} - G_{bc}^{v}\uparrow + K_{abb}^{v} b - (2+\xi)K_{bbb}^{v} b] .$$

Note that arranging in order of b density is not completely adequate, because η and ζ depend on the b density and also that there is a small term proportional to the fourth power of the density due to cross terms. We emphasize that this fourth-order (and higher-order) term contributes to the decay, although a four-body term is not explicitly included in the rate equations.

One would like to compare expression (4.8) with the experimentally observed C_2 and C_3 [see Eq. (3.2)]; it is virtually impossible to extract the small fourth-order term from the experiment. Good agreement with a numerical solution of the equilibrium values of $\hat{a}$, $\hat{c}$, and $\hat{d}$ from an extended equation including all rate constants is obtained by expansion of η, ζ, etc., into a density-independent part $\eta_0 = \eta(b=0)$, $\zeta_0 = \zeta(b=0)$ and a small density-dependent part

$$\eta = \eta_0\{1 - [K_{bbc}^{v}/(K_{bc}^{\rm eff} + G_{bc}^{v}\downarrow)]b + [K_{bbc}^{v}/(K_{bc}^{\rm eff} + G_{bc}^{v}\downarrow)]^2 b^2 - \cdots\}$$

and

$$\zeta = \zeta_0\{1 - [K_{abb}^{v}/(K_{ab}^{\rm eff} - G_{ba}^{v} - G_{bc}^{v}\uparrow)]b + [(2+\xi)K_{bbb}^{v}/(K_{ab}^{\rm eff} - G_{ba}^{v} - G_{bc}^{v}\uparrow)]b + \cdots\}$$

and using only terms up to first order in b density. This approach is valid as long as $K_{bbc}^{v} b \ll K_{bc}^{\rm eff} + G_{bc}^{v}\downarrow$, etc. This results in

$$C_2 = 2(\zeta_0 G_{ba}^{v} + \eta_0 G_{bc}^{v}\uparrow)/(1+\hat{a}_0)^2 ,$$
$$C_3 = 2(\theta_b K_{bbb}^{v} + \theta_c K_{bbc}^{v} - \theta_a K_{abb}^{v})/(1+\hat{a}_0)^3 , \quad (4.9)$$

with

$$\theta_b \equiv 1 + \xi\eta_0 + (2+\xi)\zeta_0^2(G_{ba}^{v}/K_{ab}^{\rm eff}) \simeq 1 + \xi\eta_0 ,$$
$$\theta_c \equiv \eta_0^2(G_{bc}^{v}\downarrow/K_{bc}^{\rm eff})^2 \exp(-1.35B/T) ,$$
$$\theta_a \equiv (1 + G_{v}^{bc}\uparrow/G_{ba}^{v})(\zeta_0 G_{ba}^{v}/K_{ab}^{\rm eff})^2 ,$$

and $\hat{a}_0$ defined by Eqs. (4.3).

The second-order coefficient C_2, [i.e., the linear coefficient of $F(n)$ in Eq. (3.1)], has contributions from the nuclear and electronic relaxation. The third-order coefficient C_3 consists of three terms. (a) The K_{bbb}^{v} term. The number of b-state atoms lost per K_{bbb}^{v} event is expressed by the proportionality factor, $2\theta_b$, in front of the K_{bbb}^{v} coefficient. In the limit that $\eta_0 \to 1$ and $\zeta_0 \to 1$ (i.e., $K_{bc}^{\rm eff}$ and $K_{ab}^{\rm eff}$ dominating), the effective loss increases to $2\theta_b = 2(1+\xi) = 3.82$ b atoms per K_{bbb}^{v} event. Physically this means that in one K_{bbb}^{v} event, two atoms are lost directly and 2ξ atoms are lost by the third body flipping to the c state followed by $K_{bc}^{\rm eff}$ recombination. (b) The K_{bbc}^{v} term arises from the population of the c level.[30] The θ_c is orders of magnitude smaller than θ_b. However, it has to be taken into account since K_{bbc}^{v} is much larger than K_{bbb}^{v}. (c) Likewise the K_{abb}^{v} term arises from population of the a level. One might wonder why a minus sign appears in front of the K_{abb}^{v} term in Eqs. (4.9). However, this sign follows quite logically from Eq. (4.6). It originates in the influence of K_{abb}^{v} on the polarization [Eqs. (4.7)]. Increase of K_{abb}^{v} decreases $\hat{a}$, with the overall result that the negative third-order contribution (third order in b) of the $K_{ab}^{\rm eff}\hat{a}$ term slightly overcompensates the positive third-order contribution of the $K_{abb}^{v} b\hat{a}$ term. At this point it is also useful to note that in the doubly-polarized gas even a dramatic increase in K_{abb}^{v} does not lead to a significant increase in recombination. The recombination rate is dominated by the relaxation processes (G_{ba}^{v}) and (G_{bc}^{v}) and the dipolar mechanism (K_{bbb}^{v}).

The analysis as presented above is only valid for a doubly-polarized gas ($\hat{a} \ll 1$) and thus one would like to have a good estimate of $\hat{a}$ to check the applicability of Eqs. (4.1)—(4.9). As follows from Eq. (4.7), $\hat{a}$ depends on the ratio of G_{ba}^{v} and $K_{ab}^{\rm eff}$. Measurements of $K_{ab}^{\rm eff}$ are available up to 500 mK.[31–33,10,11,13] To obtain $K_{ab}^{\rm eff}$ at the temperatures used in this experiment ($\simeq$700 mK) one has to extrapolate from low temperature. Although the observed $K_{ab}^{\rm eff}$ in the as yet experimentally accessed temperature range give agreement between the different authors within a factor of 2, extrapolation of these measurements gives differences as large as a factor of 4. To allow analysis of our data we choose a typical value (see Table I)

$K^s_{ab}B^2T^{-1/2}=2.5\times10^{-8}$ cm^{2}s^{-1} (with $\varepsilon_a=1.15$ K).[34] Using these values leads to a rather poor double polarization ($\hat{a}\simeq0.15$) and thus Eqs. (4.5) cannot be used for a rigorous analysis of our experiment. One has to include contributions from processes involving two or more a-state atoms [e.g., $K^s_{aa}\simeq2.2K^s_{ab}$ (Refs. 11, 35, and 13), K^v_{aab}, K^v_{aaa} and processes of combinations of a-state atoms with c- and d-state atoms] and solve this extended form of Eqs. (4.1) numerically to obtain the density-dependent equilibrium values for $\hat{a}$, $\hat{c}$, and $\hat{d}$ and the resulting rate $\dot{N}/n^2$. C_2 and C_3 are then determined from fits to the calculated overall rates as a function of n. Such a procedure does not allow explicit differentiation between contributions of the different processes (K^v_{bbb}, K^v_{abb}, etc.). However, qualitatively the linearized expressions (4.1)—(4.9) are still valid and can guide the understanding of the system.

As an illustration we show in Fig. 10 the full numerical solution (dashed-dotted line, based on Table I) and one based on a second-order fit to the data (dashed line). It is impossible to discriminate between these two approaches within experimental accuracy. The dotted line in Fig. 10 is the numerical solution for a volume of $V_0=0.02$ mm^3 ($A/V=150$ cm^{-1}). This illustrates the influence of the A/V ratio on the decay. As follows from Fig. 8 the A/V ratio increases for smaller bubbles and subsequently $K^{\rm eff}_{ab}$ and $K^{\rm eff}_{bc}$ increase, resulting in a larger C_2 and C_3 [see Eqs. (4.9)].

Using the approach of Eqs. (4.9), one can interpret the data presented in Sec. IV B. The results for the field dependence of C_2 [Fig. 14(a)] give for high fields, where $G^v_{bc}\uparrow$ is suppressed, a bulk nuclear relaxation constant corresponding to $G^v_{ba}(1+16.68/B)^{-2}=6.9(9)\times10^{-22}$ cm^3 s^{-1} at 710 mK [dashed line in Fig. 14(a)]. This is in agreement with the previous lower temperature measurements[10–12] and theory.[36–38] The error in G^v_{ba} includes a systematic error in the reference height as measured by the level gauge of about 0.3 mm helium. Note that the dashed line does not simply scale according to $(1+16.68/b)^2$. Such a relationship is only to be expected if the contribution of the $K^{\rm eff}_{aa}$ term is negligible and the equilibrium value of $\hat{a}$ is independent of magnetic field. In our measurements we estimate a $\simeq30\%$ of $K^{\rm eff}_{aa}$ relative to $K^{\rm eff}_{ab}$, while $\hat{a}$ varies from $\hat{a}=0.17$ for $B=6$ T to $\hat{a}=0.21$ for $B=10$ T. The dashed lines are given by the expression

$$(2\hat{a}_0K^{\rm eff}_{ab}+2\hat{a}_0^2K^{\rm eff}_a)/(1+\hat{a}_0)^2\ ,$$

note that

$$2\hat{a}_0K^{\rm eff}_{ab}/(1+\hat{a}_0)^2\simeq2\xi_0G^v_{ba}\ .$$

For low fields an/or high temperatures ($B/T<10$ T/K) the contribution of the electron-spin relaxation, $2\eta_0G^v_{bc}\uparrow$, becomes important. This is shown in Fig. 14(a) as a deviation from the dashed line. The full line in this figure shows the sum of both contributions with a best value

$$G^v_{bc}\uparrow=12(4)\times10^{-16}\exp(-1.35B/T)\ \text{cm}^3\text{s}^{-1}\ ,$$

in agreement with the calculation of Lagendijk *et al.*[36]

$$G^v_{bc}\uparrow=9.7\times10^{-16}\exp(-1.35B/T)\ \text{cm}^3\text{s}^{-1}\ .$$

This value is also in good agreement with the value of Bell *et al.*,[14]

$$\eta_0G^v_{bc}\downarrow=10(1)\times10^{-16}\ \text{cm}^3\text{s}^{-1}\ ,$$

when using $\eta_0=0.85(8)$, a typical value for the M.I.T. geometry. The exponential character of $G^v_{bc}\uparrow=G^v_{bc}\downarrow\exp(-1.35B/T)$ is illustrated in Fig. 16, where

$$C_2-(2\hat{a}_0k^{\rm eff}_{ab}+2\hat{a}_0^2K^{\rm eff}_{aa})/(1+\hat{a}_0)^2\simeq2\eta_0G^v_{bc}\uparrow$$

is plotted versus B/T. This corresponds to the deviation from the dashed line in Fig. 14(a). The dotted line in Fig. 16 is based on the theoretical value of Lagendijk *et al.* About 30% of the difference between the dotted line and the data points can be explained by an additional contribution to C_2 from b,d recombination.

Our measurements of C_3 [Fig. 14(b)] are most reliable for high fields. For $B\geq9$ T, $C_3\simeq2\theta_bK^v_{bbb}=7(2)\times10^{-39}$ cm^{6}s^{-1}. Excluding any explicit field dependence of K^v_{bbb} and taking into account a small correction due to θ_c and θ_a we find $k^v_{bbb}=2.0(5)\times10^{-39}$ cm^{6}s^{-1} and $2\theta_b=3.27$. For low magnetic fields C_3 increases due to the contribution of the K^v_{bbc} term in Eqs. (4.9). The solid line in Fig. 14(b) is calculated with a value of $K^v_{bbc}=3(1)\times10^{-33}$ cm^{6}s^{-1} (see Table I), derived from the value of Bell *et al.*[30,15] Hardy *et al.*[16] found $K_{\rm HH^4He}=2.8(3)\times10^{-33}$ cm^{6}s^{-1} and $K_{\rm HH^3He}=1.2\times10^{-33}$ cm^{6}s^{-1} for bulk recombination rates in $B=0$. The systematic errors in pressure p do not permit a useful fit for K_{bc} from our data points. However, the measured value of C_3 seems to be systematically higher than the calculated one. Choosing a substantially larger value for K^v_{bbc} increases C_3 at low fields, but not sufficient to obtain a fit for the third-order rate at 6 and 7 T. For example, increasing K^v_{bbc} by a factor of 10 increases C_3 only by $\simeq15\%$. This problem was checked extensively both by numerical solution of the extended form of Eqs. (4.9) and by direct calculation of

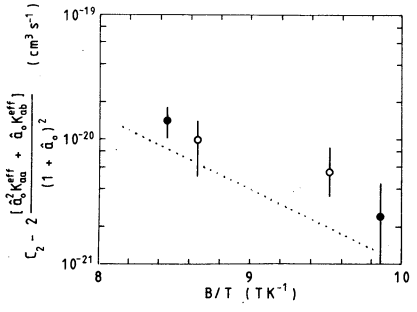

FIG. 16. Exponential dependence of the $G^v_{bc}\uparrow$ contribution to C_2 on B/T (see text). The dotted line is the calculated relaxation by Lagendijk *et al.* (Ref. 36) (see text). Solid circles are data points at different field and $T=710$ mK. Open circles are at $B=8$ T and different temperatures.

the decay curves, both in the isobaric and isochoric case. The problem originates from the change of the c population due to K^v_{bbc} recombination [see Eq. (4.7)] and the subsequent influence on $\eta G^v_{bc}\uparrow$. The calculation of the decay show that $\hat{a}$ and $\hat{c}$ remain close to the density-dependent equilibrium values, even if the starting conditions are different. For densities between 10^{17}–10^{18} atoms /cm^{-3} this equilibrium is achieved under isobaric conditions within 20 s, much faster than the time used for precompression of the gas (see Sec. II B).

Our results for the bulk three-body recombination rates are best compared to the measurements of Bell *et al.*[14,8] at 600 mK between 4 and 8 T. These authors find a K^v_{bbc} contribution[30] for the three-body rate at low field that is suppressed exponentially for increasing field and a contribution of K^v_{bbb} that slightly decreases for increasing magnetic field. This is in contradiction with theory for K^v_{bbb} (Refs. 28 and 29) [dotted line in Fig. 14(b)] showing a rate increasing with field. At 600 mK, Bell *et al.*[14,8] found $2\theta_b K^v_{bbb}=7.9(4)\times10^{-39}$ cm^{6}s^{-1} from a fit to the field dependence between 4 and 8 T. For their conditions $2\theta_b=3.7$, which implies $K^v_{bbb}=2.1(1)\times10^{-39}$ cm^{6}s^{-1}, in good agreement with our results.

The field dependence of the three-body term is of importance to decide if the stability of the gas is increased by going to higher fields than used up to now ($B<11$ T). We cannot reliably separate the K^v_{bbb} contribution from other three-body contributions to the field dependence of C_3. As long as $\hat{a}<1\%$, one can apply the set of Eqs. (4.1) and the subsequent analysis resulting in Eqs. (4.9). At high fields the contributions due to thermal population of the c state are suppressed, leaving only the K^v_{ab} and K^v_{bbb} contributions to C_3. The denominator $1+\hat{a}_0$ in Eqs. (4.9) increases as a function of magnetic field due to the intrinsic field dependence of G^v_{ba} and $K^{\rm eff}_{ab}$. Thus $2\theta_b/(1+\hat{a}_0)^3$ decreases, resulting in a decreasing C_3 if K^v_{bbb} were constant. However, one has to take into account the K^v_{abb} term as well since $\hat{a}_0\neq0$, resulting in a complicated overall field dependence of C_3 which is a function of the intrinsic field dependence of K^v_{bbb} and K^v_{abb}. As mentioned, the dipolar K^v_{bbb} rate constant is predicted to increase by a factor of 2 for $B=6$ to 10 T.[28,39] The exchange recombination rate K^v_{abb} is presumably proportional to ε^2 ($\varepsilon=a/4\mu_B B$ the hyperfine mixing parameter, $K^v_{abb}\simeq\varepsilon^2K^v_{bbc}$). According to Kagan *et al.*[28] at $T=0$ K the K^v_{abb} exchange recombination vanishes due to quantum interference. At finite temperatures, where the experiments are done, the K^v_{abb} exchange rate does not vanish and may contribute to C_3. However, setting $K^v_{bbb}=0$ and using $K^v_{abb}=\varepsilon^2K^v_{bbc}$ underestimates the measured C_3 at the high fields, indicating that K^v_{bbb} cannot be ignored.

D. Thermal equilibrium

The major concern in the analysis is the thermal equilibrium of the gas; the gas should have the same temperature as the body of the cell and liquid helium, and should have a uniform internal temperature distribution. Let us discuss the possibility that the deviation of the decay rate from two-body behavior at high density, which we attribute to three-body effects, could be explained by heating of the gas and two-body effects. In particular, at 9.8 T, 750 mK we would have to explain that the rate $\tau^{-1}=14\times10^{-3}$ s^{-1} at $n=10^{18}$ cm^{-3} is about a factor of 2 larger than expected from two-body relaxation G^v_{ba}. Only above 950 mK the $G^v_{bc}\uparrow$ contribution to the relaxation would make the relaxation sufficiently fast to account for this effect. However, this implies a temperature gradient of 200 mK.

There are three stages in the thermal conduction of the recombination heat to the body of the cell that can be bottlenecking, thus causing a difference between measured body temperature and the gas temperature. The first source for a gradient is the finite heat conductivity of the H$\downarrow\uparrow$ gas ($\kappa=3.5\times10^{-3}$ W/K m)[40] at these densities. For a gas of $n=10^{18}$ cm^{-3}, the mean free path $\lambda=3\kappa/(nC_v\bar{v})\simeq4$ μm at 700 mK, a factor 250 smaller than the typical bubble diameter (1 mm), allowing us to treat the conductivity problem in the hydrodynamic regime:[26] $\nabla\kappa\nabla T=-q$, where q is the (local) heat production per unit volume per unit time. The recombination heat is produced by atoms recombining on the wall. ($K^{\rm eff}_{bc}$) or, if we include three-body effects, in the bulk [K^v_{bbb} and K^v_{bbc} term in Eqs. (4.9)]. The energy transfer between the highly excited molecule produced in the recombination reaction and the H$\downarrow\uparrow$ gas is not known in detail. Assume for simplicity that half of the produced recombination energy is transferred in such a way that q is uniform over the sample. In the limit of small gradients, the average temperature variation, $\langle\Delta T\rangle=(1/V)\int_V(T-T_0)dV$, where T_0 is the surface temperature, is then easily estimated, noting that κ is essentially temperature independent[40] and using $q=(\frac{1}{2})DdN/dt=(\frac{1}{2})Dn\tau^{-1}$, where $D=7.2\times10^{-19}$ J is the dissociation energy of H_2. For a 1-mm^3 spherical bubble (radius $R=0.6$ mm) at 9.8 T, $\tau^{-1}=14\times10^{-3}$ s^{-1} and $n=10^{18}$ cm^{-3}, we find $q=5$ μW mm^{-3} and $\langle\Delta T\rangle=(\frac{1}{15})qR^2/\kappa=30$ mK. Although this is substantial, it is not sufficient to explain the deviation from two-body behavior, because G^v_{ba} is only weakly dependent on temperature and the field is still sufficiently high to suppress electron-spin relaxation $G^v_{bc}\uparrow$. For the true bubble shape (Fig. 8) the larger A/V ratio and the flat geometry of the bubble will lower $\langle\Delta T\rangle$. To describe the situation in the gas for larger temperature gradients, including the three-body effects, one has to use a temperature and density-dependent function for q. Kagan *et al.*[26] investigated this problem for a plane geometry by assuming either strictly local or global heat production (i.e., averaged over the temperature-density distribution). In both cases there is a critical density (n_c) depending on the distance (L) between the planes, above which there is not a stable solution to the problem ($n_c\simeq2\times10^{18}$ cm^{-3} for $L=1$ mm). The main source of this instability is the K^v_{bbc} term that depends on $G^v_{bc}\uparrow$ and thus increases exponentially with temperature.

The second stage in the heat conduction that can cause temperature gradients is the thermal boundary resistance (Kapitza resistance) between the H$\downarrow\uparrow$ gas and the liquid helium. Using simple gas-kinetic arguments, one can estimate the heat transfer across a helium surface:

$\dot{Q}=\frac{1}{4}n\bar{v}A\alpha(T)\Delta E$, where $\bar{v}=(8k_BT/\pi m)^{1/2}$ is the average thermal velocity, A is the helium surface area, $\alpha(T)$ is the energy accommodation coefficient, and $\Delta E=2k_B\Delta T$ is a measure for the energy transfer during a collision with the wall. Using $\alpha(T)=0.2$ from Salonen *et al.*,[41] one finds $\Delta T=4$ mK in a spherical bubble of 1 mm^3 at 9.8 T and $n=10^{18}$ cm^{-3}, again too small to explain the deviations from two-body behavior.

The final stage in the heat conduction is the heat transport through the ^{4}He liquid ($\kappa=100$ W/K m for pure ^{4}He at 700 mK)[42] and the thermal boundary resistance between helium and the silver sinter. For pure ^{4}He in our geometry the typically $\dot{Q}<5$ μW recombination heat can easily be conducted and coupled to the 1-m^2 silver sinter surface. For ^{3}He-^{4}He mixtures, the heat conductivity decreases as a function of the ^{3}He concentration rather drastically (at 300 mK, $\kappa=15$ W/K m for pure ^{4}He and $\kappa=0.2$ W/K m for 1.3% ^{3}He in ^{4}He).[42] This may explain the irreproducibility and thermal problems we had with our measurements on mixtures.

V. CONCLUSIONS

In this paper a new experimental technique based on volume compression up to 5 orders of magnitude and observation of the volume decay under quasi-isobaric conditions was used to study H↓↑ at high densities. The main difference between this technique and the usual isochoric technique is the possibility to study a small sample of gas at high density (up to 2×10^{18} cm^{-3}) for a period of minutes. In addition to the column head of helium used to apply the pressure on the gas, surface tension increases the total gas pressure. This surface tension can be accounted for by a simple model for the bubble shape.

With this technique we identified the two-body electronic relaxation rate $G_{bc}^v\downarrow=G_{bc}^v\uparrow\exp(1.35B/T)=12(4)\times10^{-15}$ cm^{3}s^{-1} at $T=710$ mK, a thermally activated process that becomes noticeable at high temperature and/or low fields ($B/T\lesssim10$ T/K). At high densities dipolar recombination becomes an important destabilization process; $K_{bbb}^v=2.0(5)\times10^{-39}$ cm^{6}s^{-1} at 9.8 T and 750 mK. Also for three-body rates the thermal population of the c level becomes observable at $B/T\lesssim10$ T/K. The magnetic field dependence of the three-body process, especially interesting at high fields, is not clear from our measurements; more data at higher fields are required. An additional complication is the degree of double polarization in the gas, leading to a contribution from K_{abb}^v to the three-body rate. At high densities the gas appears to be susceptible to explosions, especially in large bubbles.

The new technique has good prospects in increasing the maximum density obtainable in the gas by going to very small bubbles and thus reducing the problems of out-of-thermal equilibrium in the gas.

Note added. After submission of our manuscript we received a copy of an extensive paper by Bell *et al.*[8] which gives a detailed account of the experiments done at the Massachusetts Institute of Technology. In view of the importance of this paper, we have added some references to this work in the present text.

ACKNOWLEDGMENTS

We thank A. Lagendijk, B. J. Verhaar, and G. Frossati for a number of stimulating discussions, A. Matthey for building the tunnel-diode electronics, O. Höpfner for technical support, and H. van Zwol, J. Berkhourt, and E. Salomons for assistance with the measurements. The financial support of the Stichting voor Fundamenteel Onderzoek der Materie is gratefully acknowledged. One of us (I.F.S.) acknowledges support from the U.S Department of Energy Contract No. DE-FG02-85ER45190.

[1] I. F. Silvera, Physica **109&110B**, 1499 (1982).
[2] J. T. M. Walraven, in *Proceedings of the International Conference of Low-Temperature Physics, LT-17,* edited by U. Eckern, A. Schmid, W. Weber, and H. Wühl [Physica **126B+C**, 176 (1984)].
[3] T. J. Greytak and D. Kleppner, in *New Trends in Atomic Physics,* edited by G. Grynberg and R. Stora (North-Holland, Amsterdam, 1984), Vol. II, p. 1125.
[4] T. D. Lee, K. Huang, and C. N. Yang, Phys. Rev. **106**, 1135 (1957).
[5] R. Sprik, J. T. M. Walraven, and I. F. Silvera, Phys. Rev. Lett. **51**, 479 (1983); **51**, 942(E) (1983).
[6] H. F. Hess, D. A. Bell, G. P. Kochanski, R. W. Cline, D. Kleppner, and T. J. Greytak, Phys. Rev. Lett. **51**, 483 (1983).
[7] H. F. Hess, D. A. Bell, G. P. Kochanski, D. Kleppner, and T. J. Greytak, Phys. Rev. Lett. **52**, 1520 (1984).
[8] D. A. Bell, H. F. Hess, G. P. Kochanski, S. Buchman, L. Pollack, Y. M. Xiao, D. Kleppner, and T. J. Greytak, Phys. Rev. B (to be published).
[9] B. W. Statt and A. J. Berlinsky, Phys. Rev. Lett. **45**, 2105 (1980).
[10] R. W. Cline, T. J. Greytak, and D. Kleppner, Phys. Rev. Lett. **47**, 1195 (1981).
[11] R. Sprik, J. T. M. Walraven, G. H. van Yperen, and I. F. Silvera, Phys. Rev. Lett. **49**, 153 (1982).
[12] B. Yurke, J. S. Denker, B. R. Johnson, N. Bigelow, L. P. Levy, D. M. Lee, and J. H. Freed, Phys. Rev. Lett. **50**, 1137 (1983).
[13] B. W. Statt, A. J. Berlinsky, and W. N. Hardy, in *Proceedings of the International Conference on Low-Temperature Physics, LT-17,* Ref. 2, p. 467; Phys. Rev. B **31**, 3169 (1985); M. W. Reynolds, I. Shinkoda, W. N. Hardy, A. J. Berlinsky, F. Bridges, and B. W. Statt, Phys. Rev. B **31**, 7503 (1985).
[14] D. A. Bell, G. P. Kochanski, L. Pollack, H. F. Hess, D. Kleppner, and T. J. Greytak, in *Proceedings of the International Conference on Low-Temperature Physics, LT-17,* Ref. 2, p. 449.
[15] D. A. Bell, G. P. Kochanski, D. Kleppner, and T. J. Greytak, in *Proceedings of the International Conference on Low-Temperature Physics, LT-17,* Ref. 2, p. 541.
[16] W. N. Hardy, M. Morrow, R. Jochemsen, and A. J. Berlinsky, Physica **109&110B**, 1964 (1982).
[17] J. T. M. Walraven and I. F. Silvera, Phys. Rev. Lett. **44**, 168 (1980).

[18]J. T. M. Walraven and I. F. Silvera, Rev. Sci. Instrum. **53**, 1167 (1982).

[19]The relative dielectric constant ϵ_r is obtained by using the Clausius-Mossotti relation $(\epsilon_r-1)/(\epsilon_r-2)=np/3\epsilon_0$, where $p/(4\pi\epsilon_0)=0.2044\times10^{-24}$ cm^3 the polarizability for ^{4}He [C. E. Chase, E. Maxwell, and W. E. Millet, Physica **27**, 1129 (1961)], and $n=2.182\times10^{22}$ cm^{-3} the density of ^{4}He below 1 K [E. C. Kerr and R. P. Taylor, Ann. Phys. **26**, 292 (1964)].

[20]I. F. Silvera and J. T. M. Walraven, Phys. Rev. Lett. **44**, 164 (1980).

[21]C. T. van Degrift, Rev. Sci. Instrum. **46**, 599 (1975).

[22]W. J. Duffin, *Electricity and Magnetism* (McGraw-Hill, New York, 1965).

[23]*Handbook of Chemistry and Physics,* edited by R. C. Weast (Chemical Rubber, Cleveland, 1971).

[24]A. W. Adamson, *Physical Chemistry of Surfaces* (Wiley, New York, 1976).

[25]J. R. Eckardt, D. O. Edwards, S. Y. Shen, and F. M Gasparini, Phys. Rev. B **16**, 1944 (1977).

[26]Yu. Kagan, G. V. Shlyapnikov, and I. A. Vartanyantz, Phys. Lett. **101A**, 27 (1984).

[27]T. Tommila, S. Jaakkola, M. Krusius, K. Salonen, and E. Tjukanov, *Proceedings of the International Conference on Low-Temperature Physics, LT-17,* Ref. 2, p. 453.

[28]Yu. Kagan, I. A. Vartanyantz, and G. V. Shlyapnikov, Zh. Eksp. Teor. Fiz. **81**, 1113, (1981) [Sov. Phys.—JETP **54**, 590 (1982)].

[29]Note that Bell *et al.* (Ref. 15) extracted $\xi=0.93$ for $B=10$ T from Kagan *et al.* (Ref. 28). We use the value $\xi=0.91$, which was obtained by de Goeij and Verhaar and checked to be independent of magnetic field within the range of experimental interest [$5<B<10$ T; B. J. Verhaar (private communication)].

[30]Note that our expression for the K^v_{bbc} contribution to C_3 is proportional with $(G^v_{bc\downarrow}/K^{\text{eff}}_{bc})$ (Ref. 2) in contrast to the expression used by Bell *et al.* (Ref. 15).

[31]A. P. M. Matthey, J. T. M. Walraven, and I. F. Silvera, Phys. Rev. Lett. **46**, 668 (1981).

[32]A. P. M. Matthey (unpublished).

[33]M. Morrow, R. Jochemsen, A. J. Berlinsky, and W. N. Hardy, Phys. Rev. Lett. **46**, 195 (1981); **47**, 455 (1981).

[34]The values for K^s_{ab} and ε_a are strongly coupled. Our particular choice gives a reasonable fit for K^{eff}_{ab} in the experimentally accessed regime (Refs. 31—33, 10, and 12).

[35]G. H. van Yperen, I. F. Silvera, J. T. M. Walraven, J. Berkhout, and J. G. Brisson, Phys. Rev. Lett. **50**, 53 (1983); G. H. van Yperen, J. T. M. Walraven, and I. F. Silvera, Phys. Rev. B **30**, 2386 (1984).

[36]A. Lagendijk, G. H. van Yperen, and J. T. M. Walraven, J. Phys. (Paris) Lett. **45**, L929 (1984).

[37]R. M. C. Ahn, J.P.H.W. v. d. Eynde, and B. J. Verhaar, Phys. Rev. B **27**, 5424 (1983).

[38]E. D. Siggia and A. E. Ruckenstein, Phys. Rev. B **23**, 3580 (1981).

[39]L. P. H. de Goeij, J. P. J. Driessen, B. J. Verhaar, and J. T. M. Walraven, Phys. Rev. Lett. **53**, 1919 (1984).

[40]C. Lhuillier, J. Phys. **44**, 1 (1983).

[41]K. Salonen, S. Jaakkola, M. Karhunen, E. Tjukanov, and T. Tommila, in *Proceedings of the International Conference on Low-Temperature Physics, LT-17,* Ref. 2, p. 543; K. T. Salonen, I. F. Silvera, J. T. M. Walraven, and G. H. van Yperen, Phys. Rev. B **25**, 6002 (1982).

[42]R. L. Rosenbaum, J. Landau, and Y. Eckstein, J. Low Temp. Phys. **16**, 131 (1974).

Chapter 7 Production and transport of heat in H↓(↕) at high density

7.1 Limitations to reach high densities

The highest densities obtained up to now were realized in compression experiments in very small sample volumes (see chapter 4-6). At these high densities the three-body recombination limits the stability of the sample as was discussed in the previous chapters. One of the major problems is perhaps not the short life time of the sample, but the thermal conditions in the H system that lead to heating and ultimately to explosive recombination of the sample. In this chapter some of the processes contributing to the thermal conditions in the sample are discussed.

The following quantitative example will illustrate these limitations under B.E.C. conditions. At the transition the density in the gas is determined by: $n_c=\Lambda^{-3}g_{3/2}(1)$ (see chapter 1.2.3). Before the density in the gas has reached n_c, the surface coverage has already reached its saturation value: $\sigma_{sat}\simeq 1\text{x}10^{14}\text{cm}^{-2}$ on ^{4}He and $3.5\text{x}10^{15}\text{cm}^{-2}$ on ^{3}He surfaces (see chapter 1.3.2). Only taking into account third order processes and using the observed rates for three-body surface recombination and three-body bulk recombination in H↓↕ (see chapters 4-6): $L_3^s = 2.\text{x}10^{-24}\text{cm}^4\text{s}^{-1}$ and $L_3^v = 7\text{x}10^{-39}\text{cm}^6\text{s}^{-1}$, the total rate under BEC conditions for a bubble of $V=1\text{mm}^3$ in ^{4}He at T=100mK and B=10T is $\dot{n} = 9.6\text{x}10^{19}\text{m}^3\text{s}^{-1}$. The associated half-lifetime τ is very short: $\tau\simeq 72$msec (see capter 1.4). In principle such a short lifetime could be sufficient to study the BEC transition in the gas. However, the heat production due to recombination is gigantic if all the energy remained in the sample. The potential recombination energy per atom ($(1/2)D=3.6\text{x}10^{-19}$J with $D=7.2\text{x}10^{-19}\text{J}\simeq 52000\text{x}k_B$ the dissociation energy of H_2) could heat up the gas to $T\simeq D/(3k_B)\simeq 9000$K (only using the specific heat at constant volume for a classical ideal gas). For example, the mentioned conditions would result in a heat production: $q = 56\mu$W and the temperature difference in the sample with respect to the ambient temperature of the cell cannot be ignored. The heating of the sample will ultimately activate electron spin transitions ($G_{bc}{}^{\uparrow}=G_{bc}{}^{\downarrow}\exp(-1.34B/T)$, $G_{bc}{}^{\downarrow}\simeq 12(4)\text{x}10^{-16}\text{cm}^3\text{s}^{-1}$) and cause explosive conditions in the H gas (see chapter 4-6).

7.2 Heat production and conduction through the gas

The heat production and the heat conduction can be divided into a few stages. Each is important in maintaining the temperature in the gas as close as possible to the ambient temperature of the cell body:

a - Release of recombination energy.
b - Heat conduction in the H↓↕ gas.
c - Boundary resistance H↓↕ - helium film.
d - Heat conduction of the helium liquid.
e - Boundary resistance helium - (metallic) cell walls and further conduction through the body of the cell.

Stages a,b,c depend on the properties of the hydrogen gas. Stages d,e mainly depend on the properties of liquid helium. It will be shown that the processes in the H gas (a,b,c) are limiting and not the conduction through the helium (d,e) if the design of the experimental cell is optimal. Stage d may play a more important role if mixtures of $^3He/^4He$ are used instead of pure ^4He, since the heat conduction of mixtures is worse than the heat conduction of ^4He (see e.g. ref. 1) for a temperature > 30mK which is relevant for the experiment. In the following sections stages a,b and c will be discussed successively.

7.2.1 Release of recombination energy

Recombination is likely to lead to molecules in the highest rotational and vibrational bound states. Further relaxation occurs when these molecules collide with H atoms, helium atoms in the bulk or the helium surface. Little is known about these relaxation processes and the energy transfer of the recombination energy to the H gas. Ultimately the hydrogen molecules will end in the vibrational and rotational groundstate. Silvera[2] observed that these H_2 molecules will submerse into the helium liquid in the form of small 'snow' flakes, rather than float on the helium liquid interface.

In the context of the heating of the hydrogen gas, the fraction of the recombination energy that is actually released into the H sample during the relaxation of the molecules is especially important. A part of this energy may be transferred directly to the helium liquid and will not contribute to the temperature rise of the H sample. To our knowledge this problem is barely addressed in the literature. In the following paragraphs we would like to study this problem in some length. Mainly to identify the physical processes that are relevant in this problem. More quantitative results can only be obtained if more is known about the detailed processes.

Recombination is always a three-body event. At low densities the third body is predominantly a He atom from the vapor (at 'high' temperature) or the helium surface (at low temperature, see chapter 1). The associated recombination rates were studied in detail, both experimentally and theoretically (see chapter 1). According to theory, the formation of the molecules occurs to the highest rotational and vibrational bound states. The calculations by Greben et al.[3] show that the molecules are formed in the ortho (I=1) and para (I=0) states in a ratio:

$$f_{I=0} = [\ (n_a^2 + n_c^2)\sin^2 2\theta \ + \ 2n_a n_c \cos^2 2\theta \ + \ 2n_b n_d\ ]\ /\ 4$$

$$f_{I=1} = [\ 1 - n_a^2 - n_b^2 - n_3^2 - n_4^2 - 2\cos(2\theta)(n_a - n_c)(n_b - n_d)\ ]\ /4,$$

where the ortho molecules are mainly formed in the (v=14,j=3) bound state and the para molecules in the (v=14,j=2) state.

At higher density the three-body hydrogen recombination is dominant. If

we focus on the three-body recombination by the dipolar mechanism, a single recombination event results in the production of an H_2 molecule in a highly rotational and vibrational state and a third hydrogen atom with a relatively high kinetic energy. For example in the simple model by Kagan et al.[4] for the dipolar three-body recombination this molecule is predominantly produced in the vibrational v=14 and rotational j=3 state, with an energy ≃71K below the dissociation limit (see chapter 1). At B=10T the distribution of the energies expressed in units of Kelvin in the reaction are:[4,5]

(7.2.1)

$$b + b + b \xrightarrow{0.9} H_2(I=1,j=3,v=14,E_k\simeq 33K) + c\ (E_k\simeq 66K) \quad \text{'double'}$$

$$b + b + b \xrightarrow{0.1} H_2(I=1,j=3,v=14,E_k\simeq 28K) + b\ (E_k\simeq 56K). \quad \text{'single'}$$

The difference in kinetic energy E_k between the double and single spinflip process is caused by the extra zeeman energy needed to 'flip' an additional electron spin. In the energy balance the small thermal energies of the incoming atoms may be ignored with respect to the released recombination energy of ≃71K. In the simple model one does not include hyperfine coupling. As a consequence, the total nuclear spin is conserved and only molecules in the ortho-state (I=1) are formed. The rest of the potential recombination energy ($\Delta E \simeq$ D - 71K) is still present in the molecule.

Subsequent relaxation of $H_2(j=3,v=14)$ ($\equiv H_2^*$) to lower bound states will occur during collisions with atoms in the gas or with the helium surface. It is important to note the high relative kinetic energy of these subsequent collisions (≃ 30K). They occur at relative energies much higher than those associated with the ambient temperature of the gas.

The fate of the 'hot' molecules produced in the gas can be studied in some detail using a simple model based on classical gas kinetics for the diffusion and relaxation of these molecules in a background of H gas. First of all a number of cross sections will be introduced to describe this diffusion and the relaxation. Assume that the kinetic energy of the H_2^* that was gained in the recombination is transferred to the H gas close to the point of formation with an associated cross section σ_{rk}, i.e. the kinetic energy of the hot molecules is strongly coupled to the surrounding H gas. Based on estimates of σ_{rk}, this seems a plausible assumption.[6] The rotational and vibrational relaxing collisions of H_2 will then occur with a relative energy corresponding with the gas temperature T. The second important cross section in the problem is the (elastic) cross section for the scattering of H_2^* molecules with H atoms: σ_d. It will determine the diffusion of the molecules through a background of H gas. The cross section

σ_d is in the order of $10^{-15}cm^2$ (see table 7.1), which can be estimated from the extrapolation of the data of binary diffusion in the H-H_2 system.[6] The associated mean free path, using the simple gas kinetic relation,[7] is $\lambda_d=1/(\sqrt{2}\ n_H\ \sigma_d)$. The last cross section that will be used to describe the problem is the cross section determining the relaxation σ_r of the H_2^* molecule to a lower bound state. As already remarked by Kagan et al.[8], this cross section is much smaller than σ_d. Some of these relaxation processes have been studied in other fields, but usually under different conditions. The relaxation cross sections $\sigma_{j\to j-2}$ have been studied in connection with the recombination rates at higher temperatures. One of the important mechanisms for recombination is via long-lived meta stable states H_2' (see chapter 1.3.1). Roberts et al.[9,10] and Pack et al.[11] calculate a number of these transition probabilities for the meta stable states, using a simple exponentially repulsive form for the interaction potential between the molecule and the third body. Roberts et al.[9] introduced the gas kinetic cross section:

$$\sigma^{GK} = \pi\ |r_{TP} + (1/2)\langle R^2\rangle^{1/2}\ |^2. \qquad (7.2.2)$$

Where r_{TP} a parameter describing the classical turning point of the interaction potential ($r_{TP}\simeq 2.1$Å) and $(1/2)\langle R^2\rangle^{1/2}$ the mean square size of the (meta stable) molecule. Cross section σ^{GK} gives an upper limit for the relaxation cross section as confirmed by a more elaborate solution of the scattering equation.[9] Cross section σ^{GK} starts to deviate from the more advanced calculations for low relative kinetic energy (T<40K). In the case that the third body is a hydrogen atom, an exchange reaction is also possible:

$$H_2 + H \to H + H_2.$$

For the meta stable states this exchange reaction is very important (see Whitlock et al.[10]). In table 7.1 the total cross section for the lowest meta stable state (v=14,j=4) is listed at a relative energy of $50k_B$.

The same arguments that apply to the meta stable states probably also hold for the highly excited rotational and vibrational bound states (e.g. the (j=3,v=14) state mentioned above). In principle the non-elastic scattering equations for these bound states can be solved in detail using a coupled channel approach and the known ab initio potential energy surfaces (for H-H-H[12] and for H-H-He[13]). Since such a detailed calculation does not exist and since the present discussion is concerned with the order of magnitudes of effects, we can just apply the simple model mentioned above to get an estimate of the gas kinetic cross sections. It results for the highest vibrational and rotational states in a typical cross-section of $\simeq 50Å^2$.

The vibrational and rotational relaxation processes have also been the

topic of a number of papers in connection with the problem of rainbow scattering in molecular beam experiments at relatively high energy (>2000k_B, see ref. 14). The calculations in these papers deal with the relaxation cross sections for the lower vibrational and rotational states ($0<j<6$, $0<v<10$) and are based on precise three-particle potential surfaces. The typical cross sections for the lower states are given in table 7.1. The relaxation cross sections for collisions between H_2 and He atoms have been studied in relation to the rotational relaxation in H_2/He gas mixtures.[15] Again for the lower excited rotational states (see table 7.1).

Collision process	Elastic/ Inelastic	typical cross section ($Å^2$)	remarks	ref.
H_2 + H	Elastic	22	extrapolated to low temperature	6
H_2 + H	Inelastic	≃0.3		14
	"	70	meta stable state at T≃50K (j=4, v=14)	9-11
H + H	Elastic	4.3		22
H_2 + He	Inelastic	0.05	para rotational	15
		0.02	ortho "	
H + He	Elastic	40		17

Table 7.1 Some typical cross sections for the diffusion of (molecular) hydrogen through a back-ground of H (and He) gas.

To simplify the following discussion, we will use a typical value for the cross sections: $\sigma_d=10^{-15}cm^2$ and $\sigma_r=10^{-17}cm^2$ taken independent of temperature. They merely provide us with an order of magnitude for these cross sections. We would like to emphasize that a more accurate value can only be obtained by a detailed analysis of the (in)elastic scattering problem at low relative energy using the accurate potentials for the interactions.

With the use of the mentioned values for σ_d and σ_r and gas kinetic arguments the rate equation for the density of excited H_2 molecules (n_2) which also includes the diffusion of these molecules in H gas with a density n_H, becomes:

(7.2.4)

$$\dot{n}_2 = + (1/2)\ L_3\ n_H^3 - k_r\ n_H\ n_2 + D(n_H)\ \nabla_r^2\ n_2,$$

where $k_r \equiv \sigma_r\ \bar{v}_r$, the rate for the relaxation of the molecule to a lower state, $D(n_H) \equiv \bar{v}_r/(\sqrt{2}\ n_H\ \sigma_d)$ the diffusion coefficient for the molecules in the H gas, and the first term describes the production of molecules by three-body recombination in the bulk (rate constant L_3). The relative velocity $\bar{v}_r$ is given by:

(7.2.5)

$$\bar{v}_r = ((8k_BT)/(\pi\ \mu))^{1/2}$$

with reduced mass:

$$\mu = (2/3)\ m_H,$$

and T the temperature of the gas. Under steady state conditions $\dot{n}_2=0$ and eq.7.2.4 reduces to a diffusion equation with additional source and sink terms.[7] Using the definitions for k_r and $D(n_H)$ this diffusion equation becomes:

(7.2.6)

$$\nabla_r^2\ n_2 - C_1(r)\ n_2 + C_0(r) = 0$$

with

$$C_0(r) = (1/2)\ L_3\ n_H^4\ \sqrt{2}\ \sigma_d\ /\ \bar{v}_r$$

and

$$C_1(r) = \sqrt{2}\ \sigma_d\ \sigma_r\ n_H^2.$$

In principle the density profile for n_H due to temperature gradients in the sample (see the next section) could be used in the solution of eq.7.2.6. To simplify the analysis, assume n_H to be constant for the present discussion. In a homogeneous system the gradient term vanishes and the density of molecules is:

(7.2.7)

$$n_2 = C_0\ /\ C_1,$$

e.g. using the cross sections of table 7.1, a density $n_H=1\text{x}10^{18}\text{cm}^{-3}$ and a temperature T=300mK, the equilibrium density of molecules is $n_2=3.6\text{x}10^{10}\text{cm}^{-3}$, indicating that the molecules are very dilute in the background gas.

To study the influence of the finite diffusion velocity of the molecules, consider a spherical bubble with a radius R and assume as an additional boundary condition that the density of molecules vanishes at the

surface. The assumption for the boundary conditions is probably too restrictive in a real situation, since a fraction of the molecules will reflect from the surface and reenter the H gas. Nevertheless, the model will indicate what the important length-scales are in the problem.

The solution of eq.7.2.6 in a spherical bubble is given by:

$$n_2(r) = (C_0/C_1)\ (\ 1 - \cosh(C_1^{1/2}\ r)\ /\ \cosh(C_1^{1/2}\ R)\ ), \tag{7.2.8}$$

which can easily be verified by substitution. Solution eq.7.2.8 shows that at the origin, r=0, the density of molecules deviates from the equilibrium value in a homogeneous system. This deviation is determined by: $1./\cosh(C_1^{1/2}\ R)$. Using again the mentioned cross sections, we see that n_2 deviates significantly from the equilibrium value for a radius smaller than $R \approx C_1^{-1/2} \simeq 84\mu m$. This implies that for very small bubbles the effective mean-free-path for the molecules is larger than the bubble size and the molecule will collide with the helium surface before the vibrational and rotational energy is released to the H gas.

The efficiency of the relaxation in the model can be estimated by calculating the flux F of molecules through the boundary:

$$F = \int_S D(n_H)\ \nabla_r\ n_2\ .\ \vec{n}\ dS\ = \pi\ R^2\ D(n_H)\ (dn_2/dr)|_{r=R}. \tag{7.2.9}$$

and comparing this with the total number of molecules that are produced in the volume:

$$\epsilon \equiv F/((1/2)L_3 n_H^3\ V) = (3/R)\ \tanh(\ C_1^{1/2}R)/C_1^{1/2}, \tag{7.2.10}$$

where the second equality is obtained by making use of solution eq.7.2.8. The ratio ϵ expresses the fraction of the molecules that collide with the helium surface before they are able to relax and deposit some of the energy in the H gas, e.g. at a density $n_H = 1x10^{18} cm^{-3}$ at 300mK in a $1mm^3$ bubble, $\epsilon = 0.4$ and about half of all molecules formed relax to a lower bound state before the helium surface is reached.

Eq.7.2.4 describes the rate equation for the molecule that is produced in the three-body recombination. If we assume the relaxation process of the H_2 molecule to occur via a cascade of well determined small steps in j and v, one of such steps from state q^- to the next state q, can be described by the rate equation:

$$\dot{n}_{2,q} = -\ k_r^{q,q+}\ n_{2,q}\ n_H + D(n_H)\ \nabla_r^2\ n_{2,q} + k_r^{q-,q}\ n_{2,q-}\ n_H, \tag{7.2.11}$$

with $n_{2,q}$ and $n_{2,q-}$ the density in level q and in the previous level q- respectively, $k_r^{q,q+}$ the relaxation rate for a transition from level q to the next level q+ and analogously $k_r^{q-,q}$ for the transition from the previous level q- to q.

Analogously as for eq.7.2.6, one can show that under homogeneous conditions the ratio for the density in neighboring levels is given by:

(7.2.12)

$$n_{2,q^-}/n_{2,q} = \sigma^{q,q+} / \sigma^{q^-,q},$$

where the cross section for a particular molecular relaxation process are defined analogously as above. Unfortunately, these cross section are not known in detail. Furthermore the assumption for step-wise relaxation (climbing down the stairs[16]) is also restrictive. A further detailed analysis of eq.7.2.11 will therefore not be done here. Just to indicate the qualitative behavior, assume all the relaxation cross sections in eq.7.2.11 to be equal. Successive relaxations are then described by identical type of equations that can be solved. Fig.7.1 shows the solution of the first step (eq.7.2.6) and subsequent steps using the very restrictive assumptions mentioned above. The solutions were obtained by numerical integration of eq.7.2.11 with $\dot{n}_{2,q}=0$.

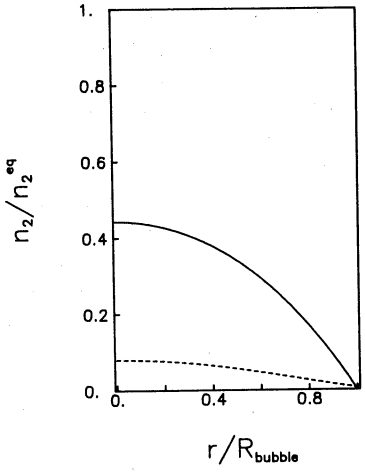

fig.7.1

Profile of H_2^* molecules in a spherical bubble using $\sigma_d=10^{-15}cm^2$ and $\sigma_r=10^{-17}cm^2$. The solid line is the density of singly de-excited molecules. Dashed line, that of doubly de-excited molecules.

The qualitative results of the previous discussion showed that for very small bubbles the energy release of the molecules always involves collisions with the helium surface. For the molecules formed at or near the interface there is a probability to shoot directly into the helium film and release (part of) its energy directly in the helium. If we want to consider the energy release near the surface or for hydrogen molecules produced on the surface the situation becomes very complex. The relaxation may be accompanied by the ejection of 'hot' helium atoms from the surface, becoming an indirect source for heating of the gas. For example in the first step of

the recombination the released energy of ≃71K is enough to desorb ≃10 He atoms from the liquid. The scattering cross section between these 'hot' He atoms and the H atoms in the gas is relatively large (40Å^2 see ref. 17) and the He atoms will thermalize rapidly with the hydrogen gas. The processes in the system become very complicated and it is difficult to say anything quantitative about the actual energy released to the H gas. A further analysis of these processes will not be carried out here.

7.2.2 Heat conduction in the H↓↑ gas.

Kagan et al.[18] analyzed the influence of the finite thermal conductivity of the H-gas. This model was also used by Tommila et al.[19] to analyze their measurements of the critical pressure at which the bubble explodes. The basis of the model is the Fourier heat equation:[20]

$$\nabla\kappa(T)\nabla T(\vec{r}) = - q(\vec{r}). \qquad (7.2.13)$$

With $\kappa(T)$ the thermal conductivity in the gas, $T(\vec{r})$ the temperature at position $\vec{r}$ and $q(\vec{r})$ the heat produced per volume element at position $\vec{r}$. Eq.7.2.13 is valid in the hydrodynamic regime; i.e. mean-free-path λ_{mf} of H atoms in the H gas is much smaller then the size of the sample. In the balistic regime or in the Knudsen regime the validity of eq.7.2.13 is limited.[21] At a density where the thermal instabilities are observed ($n\simeq 1x10^{18}cm^{-3}$) $\lambda_{mf}\simeq 4\mu m$, much less than the typical size of the bubbles ($r<0.5mm$). This justifies the application of the hydrodynamic limit.

The thermal conductivity $\kappa(T)$ in the doubly-polarized gas has been calculated by Lhuillier.[22] In the temperature regime of interest (T=100-700mK) the thermal conductivity κ is nearly temperature independent ($\kappa\simeq 3.5x10^{-3}WK^{-1}m^{-1}$) (Kagan et al.[18] assumed $\kappa\simeq T^{1/2}$ in their model). The calculated value is in agreement with the value observed by Bell et al.[23] extracted from the analysis of the temperature gradients in their compression experiments. The thermal conductivity $\kappa(T)=3.5x10^{-3}WK^{-1}m^{-1}$ will be used in the following discussion.

The particular choice of $q(\vec{r})$ depends on the included decay processes and on the place where the recombination energy is released. The relevant decay processes in H↓↑ are the bulk and surface three-body recombination and the bulk electron spin relaxation:

$$\dot{n}_H = [\ L_3^V + L_3^S\ (A/V)\ (\sigma/n_H)^3\ ]\ n_H^3 + G_{bc\uparrow}\ n_H^2. \qquad (7.2.14)$$

If H↓↑ is not fully double-polarized, exchange recombination and other decay processes also have to be included in the rate (see chapter 4-6). The precise location where the recombination energy is released is not clear (see previous section). Part of this energy will be released near the site where the recombination occurs , part of it will be released at some orther site in the gas and part will be dumped directly into the helium. Kagan et

al.[18] used two limiting conditions in their model. One limit is to assume that all the energy will be released at the recombination site (further referred to as 'local' heat production):

(7.2.15a)

$$q_l(\vec{r}) = (D/2)\ \dot{n}\ (\vec{r}).$$

The other limit is to assume that all the liberated recombination energy is homogeneously spread over the sample, ignoring the energy release directly to the helium (further referred to as 'global' heat production).

(7.2.15b)

$$q_g = \left(\int_V (D/2)\ \dot{n}\ dV \right) / V.$$

From the discussion in the previous section it is clear that neither of the two limits are accurate. Nevertheless they will provide a good qualitative description that does not depend very critically on the particular choice.

Eq.7.2.13 can be simplified by making use of the symmetry in the system. Kagan et al.[18] analyzed a flat plate geometry and eq.7.2.13 reduces then to:

(7.2.16a)

$$\kappa\ d^2T/dz^2 = -\ q,$$

with z the distance to the symmetry plane. Similarly for a spherical bubble:

(7.2.16b)

$$\kappa d^2T/dr^2 + (2\kappa)/r\ dT/dr = -\ q,$$

with r the radial distance.

For the global heat production limit (eq.7.2.15b), the resulting temperature profile is described by a parabolic dependence, both for a flat plate geometry (eq.7.2.16a):

(7.2.17a)

$$T/T_s = 1 - (1/2)\ (q_0 / (T_s L^2))\ (\ (z/L)^2 - 1\ )$$

and for a spherical volume (eq.7.2.16b):[19]

(7.2.17b)

$$T/T_s = 1 - (1/6)\ (q_0 / (T_s R^2))\ (\ (r/R)^2 - 1\ ).$$

These solutions can easily be verified by substitution. The averaged heat production q_0 is obtained by iterating eq.7.2.17(a or b) and eq.7.2.15b until they are consistent.

For a local heat production model (eq.7.2.15a) the solution of the problem is more difficult, but can be done numerically. Fig.7.2 shows the temperature profile in spherical bubbles with different volumes. The center temperature is fixed at T_c and the curves give the radius at which a certain temperature is reached.

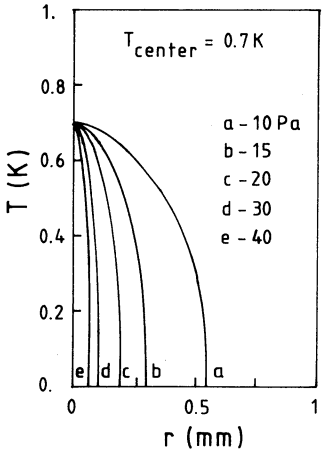

fig.7.2

Thermal gradients in a spherical bubble due to the limited thermal conductivity in the H gas.

The heat flow through the interface is important for the problem of thermal boundary resistance that will be discussed in the next section. The heat flux per unit area through the interface (W) is obtained by a surface integral over the heatflow:

$$W = (1/A) \int_S (\kappa \nabla_r T(\vec{R})) \cdot \vec{n}\, dS \qquad (7.2.18)$$

$$= (1/A) \int_V (\nabla_r \cdot (\kappa \nabla_r T(\vec{r}))\, dV$$

$$= (V/A)\, q_0.$$

This can be derived by application of the Gauss theorem, the global heat production eq.7.2.15b and eq.7.2.13.

The explosive conditions are reached when eq.7.2.13 does not have a solution with a finite central temperature. If only the third order term is included in eq.7.2.4, the system always has a solution, although the central temperature may be outside the physical regime where the model holds. The addition of the exponentially-growing electron spin relaxation term causes the explosive instability.

We did observe that the explosions in the gas occur especially under conditions where $B/T < 10TK^{-1}$ (see chapter 5,6). The analysis presented above displays such a behavior. This is illustrated in fig.7.3, where the calculated critical bubble volume at a pressure p=5Pa is given as a function

of B/T for some temperatures in a range where only volume processes are important. The stability of the sample decreases indeed very rapidly for B/T<10. The criterion stems mainly from the exponential dependence of the electron spin relaxation ($G_{bc}\uparrow$, see chapter 4-6).

Tommila et al.[19] made an extensive set of measurements of these explosions and used a similar analysis as sketched above for their observed explosions in the gas. They made measurements between 0.24-0.6K in fields from 5.5-7.5T and critical bubble volumes as small as $0.001mm^3$ (R=62μm). The model agrees within reasonable limits for temperatures T>0.3K. For T<0.3K the observed stability of the bubble is higher than predicted by the theory. One of the reasons may be that not all the recombination energy is released in the H gas. For example, as was discussed in the previous section, for these small bubbles the mean-free-path of the hot molecules becomes comparable with the size of the bubble and the molecule will collide many times with the helium surface before it relaxes to the groundstate. The enhanced stability leaves some hope to be able to study the BEC transition in very small bubbles (see also next chapter).

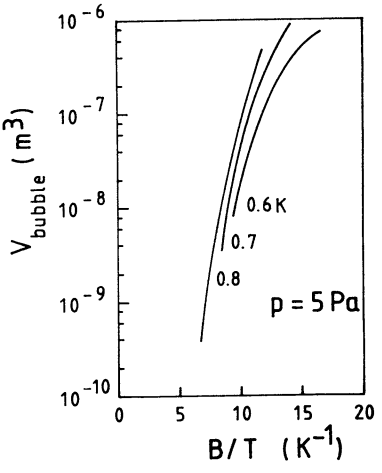

fig.7.3

Critical pressure in a spherical bubble as function of B/T. The decrease at B/T<10TK^{-1} is due to the electron spin relaxation $G_{bc}\uparrow$.

7.2.3 Boundary resistance H↓‡ - helium film.

Eq.7.2.18 from the previous section indicates that the heatflow through the interface can become considerable, hence the thermal boundary (Kapitza) resistance between the H gas and the helium surface should be included in the analysis. First some concepts that are relevant to the energy transfer will be introduced.

The hydrogen atoms are able to transfer energy during collisions with

the helium surface. In principle two different types of inelastic collisions with the helium surface are important.[21] In the non-sticking process (NS) the hydrogen atom immediately leaves the surface after the impact. The efficiency of the NS process is much smaller than the process where the H atom after impact 'sticks' to the surface in a bound state, and (partially) thermalizes before evaporating from the surface (SE process). The energy transfer is defined in terms of an accommodation coefficient:[21]

$$a=(Q_i-Q_r)/(Q_i-Q_s), \qquad (7.2.20)$$

where Q_i the incident energy flux, Q_r the reflected energy flux and Q_s the energy flux if all reflected particles are thermalized with the surface. The accommodation coefficient expresses the efficiency of the colliding hydrogen atoms to transfer energy to the helium surface. For example, if each collision results in a thermalization than: $Q_r=Q_s$, and consequently a=1. In the other extreme, absence of thermalization, the reflected flux equals the incident flux ($Q_i=Q_r$), hence a=0.

For the SE process it is useful to define the sticking probability s. The sticking coefficient s expresses the probability for an atom to stick to the helium surface and remain in the bound state for a while before desorbing. It does not include per sé thermalization of the atom with the wall. Although at best, the accommodation coefficient for the SE process $a^{SE} = s$.

Goldman[24] obtains a simple relation between the sticking coefficient s and accommodation coefficient a^{SE} for small differences between the gas temperature T and the surface temperature T_s:

$$a^{SE}(T) = s(T) \left(1 + (1/2)\, \beta^2 \, (\partial^2 \ln(s(T))/\partial\beta^2) \right), \quad \beta=1/(kT). \qquad (7.2.22)$$

The boundary resistance R_k per unit area is related to the accommodation coefficient through:

$$R_k\,(T,T_s) \equiv W / (T-T_s) = 2\, k_B\, \nu(T)\, a(T,T_s), \qquad (7.2.23)$$

where W the heat flux per unit area from the gas to the surface and $\nu(T)=(1/4)\, n\, \bar{v}$ the familiar gaskinetic collision rate per unit area, with $\bar{v}=(8k_BT/(\pi m))^{1/2}$ the average velocity in the gas (assuming the energies in the gas to be Boltzmann distributed).

Until now a limited number of experiments on the accommodation coefficient are available. The first measurements of Salonen et al.[25] using a technique involving ballistic propagation of 'hot' hydrogen atoms give a result: a=0.2(1) for 0.2K<T<0.5K. Experiments by Salonen et al.[26] based on cooling rate of a bolometer give: 0.2<a<0.3 for T=0.4K. From the analyses of the temperature gradients in their compression experiments Bell et al.[23] find that the accommodation coeffiecient varies between a=0.8 at 0.6K and

a=0.4 at 0.3K. However, this is for a high density gas of H, compared to the dilute cases of Salonen et al.[26] All these values seem to be in reasonable agreement with each other, although the temperature dependence differs.

The sticking coefficient has been studied by the U.B.C. group with the use of NMR and ESR resonance techniques.[27] From the detailed line shape they obtain directly information about s. The sticking coefficient is found to be s=0.035 on ^{4}He and s=0.016 on ^{3}He in a temperature range 0.06<T<0.5K. Surprisingly this is much lower than the accommodation coefficients quoted above. This discrepancy is still puzzling.

A detailed discussion of the theoretical studies of the accommodation coefficient and the sticking coefficient lays outside the scope of this thesis. Only a short review of the results will be given here. The theoretical results do not agree with the quoted experimental values. Kagan et al.[28] find in the low temperature limit $a^{SE} \simeq 0.06T^{1/2}$. This is also the result of a different analysis by Statt[29] for the SE-accommodation coefficient. Castaing and Papoular[30] find for the NS process: $a^{NS}=0.11T^2$. Statt finds for the NS process: $a^{NS} \simeq 0.011T^2$, and also that $a^{NS} \ll a^{SE}$ for the low temperature range. Zimmerman and Berlinsky[31] calculate the sticking coefficient. They find $s=0.049T^{1/2}$. Goldman[24] did an extensive study of the influence of the particular choice for the H-He surface potential. At high T (>200mK) he finds agreement for all potentials with the sticking coefficient as obtained by Zimmerman and Berlinsky[31]. The associated accommodation coefficient is substantially larger than the result of Kagan et al.[28], but still lower than the experimentally observed one. At low T (<200mK) the results are strongly dependent on the particular choice for the interaction potential between the surface and the H atom, casting doubt on the validity of the other results.

All these theoretical results are much smaller than the observed accommodation coefficients. Many of these calculations are only valid in the low temperature regime (T<10mK) and may not be applicable at the temperatures where the experiments are done (T>100mK). Recent developments (see chapter 8) aim at the production of atomic hydrogen at very low temperatures (T<10mK) and one needs an estimate of the energy accommodation to study the feasibility of cooling H atoms to very low temperatures by wall collisions.

The observed values for a (a≃0.2) enable an estimate of the thermal gradients ΔT at the helium interface. Using the estimated energy flux through the helium interface (see eq.7.2.18) the temperature gradient (ΔT) becomes:

$$\Delta T \simeq W / (1/2\ k_B\ \dot{N}\ (A/V)\ \bar{v}\ a). \qquad (7.2.24)$$

For example, in a bubble with $V=1mm^3$ at 700mK and B=9.8T develops a temperature gradient ΔT=30mK.

7.3 Self compression of a bubble of H↓↑ gas

The surface tension of liquid helium dominates the compression of very small bubbles (see chapter 6). For volumes $V<0.1mm^3$ the shape of the bubble is nearly spherical and the pressure, ignoring the pressure due to a helium column, is given by: $p=2\sigma/R$, with σ the surface tension and R the radius of the bubble. The dynamics of the decay are then completely determined by the compression due to surface tension. The compression rate $\dot{V}/V$ under isothermal conditions is given by

$$\tau^{-1} \equiv \dot{V}/V = - (3/2)\, f(N,V,A,T), \tag{7.3.1}$$

where f(N,V,A,T) describes the decay rate and is given by:

$$f(N,V,A,T) = L_3\, (N/V)^2, \tag{7.3.2}$$

if only three-body bulk recombination is included in the decay. The compression rate τ^{-1} diverges in the limit of V=0, since $(N/V)\to\infty$ and one might wonder if the isothermal assumption remains valid. The following discussion deals with this problem. For the present discussion the thermal gradients due to the finite thermal conductivity of the gas as discussed in section 7.2.2 are ignored (reasonable for small bubbles) and only a temperature difference between the gas and the surface is assumed.

Using simple thermodynamics, the internal energy change, dU, of the gas is:[7]

$$dU = \delta Q - pdV + \mu dN, \tag{7.3.3}$$

with δQ the heat added to the gas system and μ the chemical potential. (the work due to surface tension, σdA, is not included in eq.7.3.3, as it determines the work on the gas via $pdV=\sigma dA$. Note that for a spherical bubble this gives exactly the condition $p=2\sigma/R$.) The heat δQ in a time Δt is determined by the heat production due to recombination and the heat flow through the surface:

$$\delta Q = -(T-T_s)\, R_k\, \Delta t \; - E\, \dot{N}\, \Delta t, \tag{7.3.4}$$

where $E\equiv(D/2)>0$ the recombination energy per atom released in the hydrogen gas and R_k the thermal boundary resistance as discussed in section 7.2.3:

$$R_k = 2k\, a(T)\, (1/4)\; \bar{v}\, (N/V)\, A \equiv G_k\, (N/V)\, A. \tag{7.3.5}$$

As long as the classical ideal gas behavior is valid the internal energy, chemical potential and equation of state are given by:[7] $U=(3/2)NkT$, $\mu=kT\ln((N/V)\Lambda^3)$ and $pV=NkT$. Using this in eq.7.3.3 yields:

(7.3.6a)

$$(3/2)Nk\dot{T} = -(T-T_s)\,R_k - (E-\mu+3/2kT).\dot{N} - p\dot{V}.$$

Additional relations are the decay rate equation:

(7.3.6b)

$$\dot{N} = -f(N,V,A,T)\,N,$$

the spherical bubble condition:

(7.3.6c)

$$p=\hat{\alpha}\,V^{-(1/3)} \text{ and } A = \alpha\,V^{(2/3)},$$

with $\hat{\alpha} = ((4\pi)/3)^{(1/3)}\,2\sigma$ ($\simeq 1.19\times10^{-3}$ Nm^{-1} for ^{4}He) and $\alpha=(36\pi)^{(1/3)}$, and the equation of state:

(7.3.6d)

$$pV = NkT.$$

Eqs.7.3.6 describe the evolution of a self-compressing bubble including heating due to recombination and cooling due to thermal contact with the wall for a classical ideal gas. To simplify eq.7.3.6a we use $E - \mu + 3/2kT \simeq E$.

Elimination of p and V from this equation leads to a set of autonomous equations in N and T that can be solved numerically. The particular choice eq.7.3.2 for f results in a differential equation between the temperature T and the number of particles N:

(7.3.7)

$$dT/dN = (T-T_s)\,g\,T^2\,(T/N)^{1/2} - (E/(3k))\,(1/N),$$

with

$$g = (1/6)\,((\bar{v}\,a(T)\,\alpha)/L_3)\,(k/\hat{\alpha})^{5/2}.$$

For example, $L_3=7\times10^{-39}$cm^{6}s^{-1} and $a(T)=0.2$ at 300mK: $g\simeq26.5K^{-5/2}$ and $E/(3k)\simeq8667K$.

The first term in eq.7.3.7, describing the heat conduction through the boundary has a dependence on N different from that of the second term which describes the recombination heat production. For small enough N, the second term will dominate and the system tends to heat up. The temperature is more or less independent of the number of particles if $dT/dN\approx0$; i.e. the temperature does not change while the decay continues. For a small temperature deviation $\delta=(T-T_s)/T_s$ the number of particles should than at least be:

(7.3.8)

$$N > [\,(E/(3k))\,/\,(g\,T_s^{7/2}\,\delta)\,]^2.$$

For example, at T_s=0.3K and δ=1.e-2: $N > 5.x10^{12}$. This corresponds to a volume $V > 2.3x10^{-3}mm^3$ and $n<2.2x10^{18}cm^{-3}$.

Although derived under restrictive conditions (surface recombination not included in eq.7.3.2 and eq.7.3.6d for the equation of state), this result indicates that the thermal conditions in a self compressing hydrogen bubble become unstable for small enough bubbles. It depends on the precise values of the parameters under which conditions this occurs. For example, if the effective recombination energy per atom E reduces for small bubbles (see section 7.2.1), the limits become less stringent. For a gas under BEC conditions eq.7.3.8 is not valid, since the equation of state for the ideal Bose gas differs from eq.7.3.6d. Furthermore, to be realistic, also surface recombination should be included. In principle the method for analysis remains the same, but is more complicated and will not be pursued here.

References

1 W.R. Abel, R.T. Johnson, J.C. Wheatley, W. Zimmermann, Phys.Rev.Lett. 18 737 (1967).
W.R. Abel, J.C. Wheatley, Phys.Rev.Lett. 21 1231 (1968).
R.L. Rosenbaum, J. Landau, Y. Eckstein, J. of Low Temperature Physics, 16 131 (1974).

2 I.F. Silvera, Phys.Rev.B 29, 3899 (1984).

3 J.M. Greben, A.W. Thomas and A.J. Berlinsky, Can.J.Phys. 59, 945 (1981).

4 Yu. Kagan, I.A. Vartanyantz and G.V. Shlyapnikov, Sov.Phys.JETP 54, 590 (1981).
Yu. Kagan and G.V. Shlyapnikov, Phys.Lett. 88A 356 (1982).

5 L.P.H. de Goeij, J.P.J. Driessen, B.J. Verhaar, J.T.M. Walraven, Phys.Rev.Lett. 53 1919 (1984).

6 A.J.C. Varandas, M.C.A. Gomes, Mol.Phys. 45 317 (1982) and references in this article.

7 see e.g. L.E. Reichl, 'A Modern Course in Statistical Physics', Edward Arnold Ltd. (1980).
J.O. Hirschfelder, C.F. Curtiss, R.B. Bird, John Wiley & Sons (1964)

8 Yu. Kagan, G.V. Shlyapnikov and N.A. Glukhov, Preprint , (1985).

9 R.E. Roberts, R.B. Bernstein and C.F. Curtiss, J.Chem.Phys. 50, 5163 (1969).

10 P.A. Whitlock, J.T. Muckerman, R.E. Roberts, J.Chem.Phys. 60 3659 (1974).

11 R.T. Pack, R.L. Snow, W.D. Smith, J.Chem.Phys. 56 926 (1972).

12 D.G. Truhlar, C.J. Horowitz, J.Chem.Phys. 68, 2466 (1978). P. Siegbahn, B. Liu, J.Chem.Phys. 68, 2457 (1978); B. Liu, ibid. 58 1925 (1973).

13 W. Meyer, P.C. Hariharan, W. Kutzelnigg, J.Chem.Phys. 73 1880 (1980).

14 H.R. Mayne, J.Chem.Phys. 81, 2684 (1984).
P.L. Thompson, N.C. Blais, D.G. Truhlar, J.Chem.Phys. 78, 1335 (1983).
D.C. Clary, J.N.L. Connor, J.Chem.Phys. 74, 6991 (1981).

J.M. Bowman, K.T. Lee, J.Chem.Phys. 72, 5071 (1980).
15 J. Schaefer, W.E. Köhler, Physica 129A 469 (1985).
16 J.F. Clarke, M. McChesney, 'Dynamics of Relaxing Gases', Butterworth & Co. (1976).
17 R. Gayet, R. McCarroll, P. Valiron, Chem.Phys.Lett. 58 501 (1978).
J.P. Toennies, W. Welz, G. Wolf, Chem.Phys.Lett. 44 5 (1976).
18 Yu. Kagan, G.V. Shlyapnikov and I.A. Vartanyantz, Phys.Lett. 101A, 27 (1984).
19 T. Tommila, S. Jaakkola, M. Krusius, I. Krylov, E. Tjukanov, Phys.Rev.Lett. 56, 941 (1986).
T. Tommila, S. Jaakkola, M. Krusius, K. Salonen and E. Tjukanov, Proceedings LT-17 (Karlsruhe) Elsevier Science Publishers, 453 (1984).
20 L.D. Landau, E.M. Lifshitz, Course of Theoretical Physics volume 6, 'Fluid Mechanics', Pergamon Press (1959) .
21 E.H. Kennard, 'Kinetic Theory of Gases', McGraw-Hill (1938).
22 C. Lhuillier, J.de phys. 44, 1 (1983).
23 D.A. Bell, H.F. Hess, G.P. Kochanski, S. Buchman, L. Pollack, Y.M. Xiao, D. Kleppner and T.J. Greytak, preprint, (1985).
24 V.V. Goldman, Phys.Rev.Lett. 56, 612 (1986).
25 K.T. Salonen, I.F. Silvera, J.T.M. Walraven and G.H. van Yperen, Phys.Rev.B 25, 6002 (1982).
26 K. Salonen, S. Jaakkola, M. Karhunen, E. Tjukanov and T. Tommila, LT-17, 543 (1984).
27 M. Morrow, R. Jochemsen, W.N. Hardy, Phys.Rev.Lett. 46, 1985 (1980); 47, E455 (1981).
28 Yu. Kagan, G.V. Shlapnikov and N.A. Glukhov, Pis'ma Zh.Eksp.Teor.Fiz. 40, 287 (1984).
29 B.W. Statt, Phys.Rev.B 32 7160 (1985).
30 B. Castaing and M. Papoular, J.Physique Lett. 44, L-537 (1983).
31 D.S. Zimmerman and A.J. Berlinsky, Can. J. Phys. 61, 508 (1983).

Chapter 8 Prospects and afterthoughts

Since the first attempts to stabilize atomic hydrogen at low temperature, good progress has been made towards the conditions where BEC should be observable. The current (compression) experiments get us approximately a factor 20 below the region where the transition should occur. The limitation is caused by three-body recombination in the bulk and on the surface and the associated thermal conditions in the gas. In this final chapter of the thesis some of the proposed ways to reach BEC conditions, making use of the experience obtained in previous experiments and calculations, are considered. It is outside the scope of this thesis to treat them in detail; where relevant, reference will be made to material in this thesis. Some of these schemes form the basis of current experiment at Amsterdam and other places.

As already indicated in the previous chapter, the stability is dramatically enhanced if one is able to reduce the amount of recombination energy that is released in the H gas. One way is to reduce the recombination rate constants (i.e. L_3). The observed decrease of the three-body recombination rate as function of the magnetic field leaves hope that the rate can be decreased by applying very high fields (B>12T). The theoretical models up to now do not describe the field-dependence satisfactorily thus the predictions for the very high field region are of limited value. Furthermore, it is not clear how the energy transfer between the 'hot' molecules and the hydrogen gas proceeds. It seems likely that for very small samples, when the mean-free-path for relaxation of these molecules becomes comparable with the sample size, a considerable fraction of the energy is dumped into the helium. (e.g. Tommila et al.[1] observe an enhanced stability for the very small bubbles $V<0.001mm^3$ in their compression experiment, see section 7.2.2). A combination of very high field with a compression technique using very small bubbles, therefore seems to be an approach worth considering.

A completely new approach is the use of an open system. Currently three different techniques are proposed for this approach. Kagan et al.[2] proposed a half-open system. Hydrogen gas is confined close to the helium surface with the use of a strongly inhomogeneous magnetic field (see e.g. chapter 2). In principle the confinement region could be made smaller than the mean-free-path of the 'hot' molecules (see section 7.2.1 of this thesis) and molecules moving outwards from the wall will escape and dump the main part of their recombination energy outside the H system. Also the H atoms with relatively high kinetic energy that are produced during three-body hydrogen recombinations, are able to escape from the half-trap. The presence of the wall still provides a thermal coupling by which the H system is kept cold. The confining magnetic field needs gradients in the order of 10^4-10^6T/cm to fulfill the conditions.[2] Such magnetic fields are hard to create. For example, taking a single superconducting wire with a current I=10A, the

field strength and the gradient at a distance r=100μm yields B=0.02T and dB/dr=200T/m. Condat[3] discusses a half-trap using an annulus of superconducting wires, although he does not optimize for the escape conditions in the gas.

Two other methods apply a completely-open system by confining the hydrogen magnetically. Such an open system introduces a few new aspects. First of all the same arguments apply as for the half-open system, the 'hot' molecules escape from the sample and release only part of their energy. Secondly, the thermal contact of the H system with the wall is absent and the system has to be cooled in some other way.

Complete magnetic confinement of neutral particles in space has its pecularities. The Maxwell equations do not allow a static local field maximum (see e.g. ref. 4) and thus the construction of a static magnetic bottle for H atoms in the electron spin ↓ state (hyperfine states a and b) is impossible. With the application of time dependent fields, one can construct a system that works effectively as a magnetic bottle for the a and b state. The action principle of such a trap can be interpreted as a saddle point that is constantly changing its sign. Before the atoms are able to 'descend' the hill, the direction of the sadlle-point is reversed and the atoms will have to 'climb' the hill. Lovelace et al.[5] analyzed such a system and found that in principle a trap can be constructed with a well depth ≃3mK in a coil with radius 0.5cm operated with a total A.C. current of ≃7.7 kA at a frequency 6.6kHz. The experimental realization of such a system is very difficult to say the least. At these low temperatures the required densities to obtain BEC are also very low (N_c=1.5x$10^{16}$$cm^{-3}$ at 1mK) and the three-body recombination is not important, only the two-body bulk processes remain. An additional problem for this type of trap is viscous heating due to collisions in the gas.

The second approach to magnetic confinement as suggested by Hess[6] is to use the electron-spin up states (hyperfine states c,d) which are attracted by field minima. Local field minima can be constructed by adding an appropriate combination of static fields (see e.g.[7]). Local field minima ≃0.2K can be designed.

In principle also a sample of c and d states displays a BEC transition. The stability of the sample is determined in particular by the electron spin transitions from the c→a and d→b. After the relaxation the atoms are repelled from the trap. Also spin-exchange is possible in such systems. Lagendijk et al.[8] examined all the possible relaxation processes, which can be used to examine the stability of a c,d trap in more detail.

Both the a,b- and the c,d-trap require some cooling to lower the temperature of the gas. In principle the system may be cooled by adiabatic expansion. To examine if the BEC conditions are approached by the expansion, the fugacity z of the gas has to be considered. The BEC transition occurs at a fugacity z=1 and 0<z<1 below the transition.[9] When any additional heating of the gas due to some other process (e.g. viscous heating in the

a,b-trap) is ignored, adiabatic expansion is done at fixed entropy. The entropy of an ideal (quantum) gas depends only on the number of particles and on the fugacity.[9] As long as the number of particles is constant during the expansion, the fugacity is also fixed and the BEC condition z=1 is never reached. The entropy per atom has to change to realize this.

The finite height of the trap allows fast atoms to escape from the trap and in such a way decrease the temperature in the trap. To illustrate the effect of evaporative cooling, consider a trap where the potential energy is given by V=0 inside and $V=V_e$ outside the trap. Assume further that the velocities of the atoms in the trap are always distributed consistent with a temperature T ($kT \ll V_e$), although constantly high velocity atoms are escaping. A small fraction of the atoms has the appropriate velocity to escape from the trap. The energy flux due to the escaping atoms is at least: $dE/dt \simeq (kT + V_e)\, dN/dt$. Using the internal energy of a classical ideal gas $E=(3/2)NkT$, the temperature of the gas becomes:

$$T(N) = (2V_e/k) + (T_0-(2V_e/k))\,(N_0/N)^{(1/3)} \qquad (8.1)$$

with T_0 and N_0 the starting conditions. The temperature is monotonically decreasing and within the model for a value $N/N_0 \equiv C_{max} \equiv (1-kT_0/(2V_e))^3$ even reaches T=0. The fugacity first decreases, but near C_{max} z diverges to infinity (for an ideal classical gas the fugacity is given by: $z=(N/V)\Lambda^3$) and in principle the gas reaches BEC conditions. For a more realistic model other heating mechanisms and particle loss mechanisms also should be considered and a more detailed analysis of the particle escape should be done.

Both the mentioned traps have to be filled with relatively low energy atoms. The method to realize this is not clear yet. If one relies on cooling by collisions with the helium surface before entering the trap, the predicted accommodation and sticking coefficients (see section 7.2.3) are not very favorable.

Further experiments and theoretical studies are needed to work out the concepts discussed in the preceding section. The traps certainly add many new aspects to the problem of reaching BEC conditions in atomic hydrogen.

References

1 T. Tommila, S. Jaakkola, M. Krusius, I. Krylov, E. Tjukanov, Phys.Rev.Lett. 56 941 (1986).
T. Tommila, S. Jaakkola, M. Krusius, K. Salonen, E. Tjukanov, Proceedings LT-17 (Karlsruhe) Elsevier Science Publishers, 453 (1984).

2 Yu. Kagan, G.V. Shlyapnikov, N.A. Glukhov, JETP Lett 41 238 (1985).

3 C.A. Condat, Phys. Rev. B 25 1550 (1982).

4 W.H. Wing, Natl. Bur. Stand. (U.S.) Spec. Publ. 653, 74 (1983).

5 R.V.E. Lovelace, C. Mehanian, T.J. Tommila, D.M. Lee, preprint 1985.

6 H.F. Hess, Bull. Am. Phys. Soc. 30, 854 (1985).

7 Proceedings of the work-shop on 'Laser-cooled and Trapped Atoms' Progr. Quant. Electr. 8 3/4 (1984).
8 A. Lagendijk, I.F. Silvera, B.J. Verhaar, Phys. Rev. B 33, 626 (1986).
9 L.E. Reichl , 'A Modern Course in Statistical Physics', Edward Arnold Ltd (1980).

Summary

After the stabilization of electron-spin polarised atomic hydrogen (H↓) to densities of $\simeq 10^{15}cm^{-3}$ by Silvera and Walraven (1980), a number of experiments have been done to study this new material. One of the main objectives is to reach densities where the many-particle quantum-properties become important. In particular, for spin polarized atomic hydrogen, a Bose system, one predicts a phase transition to the Bose Einstein condensed phase at $n_c=1.6x10^{19}cm^{-3}$ for a temperature of $T_c=100mK$.

This thesis describes two experiments which increased the attainable density of H-gas. In the first experiment (chapter 2 and 3) doubly-polarized atomic hydrogen was produced in Amsterdam. The stability is dramatically increased when the mixed a-state is removed from the sample. (The lowest hyperfine state, a, has a small admixture of the opposite electron-spin due to the hyperfine coupling between the electron- and proton-spins. Usually the hyperfine states are labeled a,b,c,d in order of increasing hyperfine eigenstate energies). The elimination occurs spontaneously by preferential recombination of the a-state and a sample of purely b-state is obtained (H↓↧). The stability of the b-state is determined by magnetic relaxation to the other hyperfine states (in particular a- and c-state) and by recombination between b-state atoms. Our first attempt to see H↓↧ was jeoperdized by magnetic impurities in the copper walls of the cell, which destroyed the double-polarization due to rapid relaxation. In the construction of a new cell, such magnetic impurities were carefully avoided and H↓↧ was observed at densities up to $2x10^{17}cm^{-3}$. Initially, also the decay at low temperatures, when the atoms adsorbed on the wall determine the stability of the sample, was attributed to (second order) relaxation. More recent experiments showed that it is more likely due to third order recombination between three adsorbed H atoms.

The second experiment (chapter 4-6) used the knowledge obtained in experiments with H↓↧ to design a new experiment where even higher densities could be obtained. This experiment is the second experiment described in this thesis. It is based on volume compression of a sample of low density H↓↧ to very high densities with the use of a 'piston' of liquid helium. Eventually the hydrogen is compressed into a small bubble-like volume ($<1mm^3$) under a column of liquid helium which applies a constant hydrostatic pressure on the gas-bubble. Since the applied pressure is nearly constant, the recombination of atomic hydrogen will result in a decrease of the volume as a function of time (the molecules formed in the recombination will not contribute to the pressure in the bubble, but will most likely penetrate the helium and freeze out on the walls of the cell). With such a 'isobaric' technique we produced atomic hydrogen at densities up to $3x10^{18}cm^{-3}$ at $\simeq 700mK$. The limiting process is third order recombination between three H atoms and, when the temperature is high enough, electron spin relaxation between the b and c-state. The first process was observed for particles on

the surface by other experimental groups and in retrospect this knowledge was used to reanalyze the decays of our first experiment (chapter 2). The latter process, since it is thermally activated, becomes important for conditions where B/T<10T/K (B is the magnetic field). It may ultimately lead to a explosive recombination of the gas. Due to cryogenic problems in our compression cell, we could not perform compressions of H↓↑ at T<600mK.

Using the knowledge gathered with the compression and other experiments, one can try to design a next generation of experiments with which hopefully even higher densities can be obtained (chapter 7-8). An interesting new development is to seek this improvement at low temperatures (≈1mK) where the required densities to obtain BEC conditions are much less. A major improvement could be the construction of a electromagnetic trap without walls to confine the H atoms at these low temperatures, thus eliminating the wall recombination. It certainly will add many new aspects to the research of spin polarized atomic hydrogen.

Samenvatting

Na de stabilisatie van electron-spin gepolariseerde atomaire waterstof (H↓) tot dichtheden van $\simeq 10^{15} cm^{-3}$ door Silvera en Walraven (1980), zijn een aantal experimenten uitgevoerd om dit nieuwe materiaal te bestuderen. Eén van de uiteindelijke doelen hierbij is het bereiken van dichtheden waar de veel-deeltjes kwantum eigenschappen belangrijk worden. Voor spin gepolariseerde waterstof, een boson systeem, verwacht men een faseovergang naar de Bose Einstein gecondenseerde fase voor een dichtheid $n_c = 1.6 \times 10^{19} cm^{-3}$ bij een temperatuur van $T_c = 100 mK$.

Dit proefschrift beschrijft twee experimenten welke de realiseerbare dichtheid van atomaire waterstof hebben verhoogd. In het eerste experiment (hoofdstukken 2 en 3) is dubbel-gepolariseerde (kern- en electron spin) waterstof (H↓↑) geproduceerd in Amsterdam. De stabiliteit van het gas is aanzienlijk groter wanneer de gemengde hyperfijntoestand, a, uit het gas is verdwenen en alleen de b toestand overblijft. (De hyperfijn toestand a heeft een kleine bijmenging van de tegengestelde electron-spin toestand tengevolge van de hyperfijn koppeling tussen de electron en de proton spin van het atoom. De hyperfijn niveaus worden meestal benoemd met a,b,c,d naar oplopende grootte van de hyperfijn energie). Deze zuivering gebeurt spontaan door preferentiele recombinatie van de a toestand en uiteindelijk ontstaat een gas met alleen b toestand atomen (H↓↑). De stabiliteit van H↓↑ wordt bepaald door de magnetische relaxatie naar de andere hyperfijn niveaus (in het bijzonder de a- en c-toestand). of door recombinatie tussen twee b toestand atomen. Onze eerste pogingen om H↓↑ te zien werden verstoord door magnetische verontreinigingen in het koper van de cel wand. Bij de constructie van een nieuwe cel werden dergelijke verontreinigingen zorgvuldig vermeden en werd inderdaad H↓↑ waargenomen tot dichtheden van $2 \times 10^{17} cm^{-3}$. Aanvankelijk werden ook de vervallen bij lage temperatuur, wanneer de aan de wand geadsorbeerde atomen de stabiliteit van het gas bepalen, toegeschreven aan (tweede orde) relaxatie. Meer recente experimenten hebben aangetoond dat waarschijnlijk drie deeltjes recombinatie processen op het oppervlak tussen geadsorbeerde waterstof atomen bij lage temperatuur domineren.

In het tweede experiment (hoofdstuk 4-6) is gebruik gemaakt van de over H↓↑ verworven kennis om een nieuw experiment te ontwerpen waarmee nog hogere dichtheden kunnen worden bereikt. Het experiment is gebaseerd op volume compressie van een H↓↑ gas van lage dichtheid tot zeer hoge dichtheid door middel van een 'zuiger' van supervloeibaar helium. Uiteindelijk wordt het waterstof gas gecomprimeerd in een klein belvormig volume ($<1 mm^3$) onder een kolom van vloeibaar helium. Deze kolom oefent een hydrostatische druk uit op het gas belletje. De gasdruk in de bel is zodoende bijna constant en de recombinatie van waterstof atomen zal leiden tot een afname van het volume van de bel als functie van de tijd (de moleculen die worden gevormd tijdens recombinatie zullen niet bijdragen tot de gas druk, maar verdwijnen door het helium oppervlak en vriezen uit op de koper wand van de cel). Met behulp van

een dergelijk 'isobare' vervals techniek hebben wij dichtheden tot $3x10^{18}cm^{-3}$ bij 700mK gerealiseerd. Het beperkende proces blijkt drie deeltjes recombinatie tussen waterstof atomen in de b toestand te zijn. Bij voldoend hoge temperatuur is bovendien electron-spin relaxatie tussen het b- en c-niveau van belang. Het drie deeltjes proces tussen aan het oppervlak geadsorbeerde waterstof atomen is waargenomen door andere experimentele groepen en deze informatie hebben wij achteraf gebruikt om een her-analyse te doen van de resultaten van het eerste experiment in dit proefschrift (hoofdstuk 2). Het electron-spin relaxatie proces is thermisch geactiveerd en wordt belangrijk voor condities waar B/T<10T/K (B de magnetische veldsterkte). Dit kan uiteindelijk leiden tot een explosief recombineren van het waterstof gas. Tengevolge van cryogene problemen met de experimenteer cel kunnen wij geen zinnige experimenten verrichten bij T<600mK.

Door gebruik te maken van de informatie verkregen uit de compressie experimenten en uit andere experimenten kan men proberen een volgende generatie van experimenten ontwerpen waarmee hopelijk nog hogere dichtheden kunnen worden bereikt (hoofdstuk 7-8). Een interessante nieuwe ontwikkeling zoekt meer in de richting van zeer lage temperaturen (≈1mK), waardoor de vereiste dichtheden voor het bereiken van de BEC condities veel lager zijn. Een belangrijke verbetering zou het realiseren van een wandloze put door middel van electromagnetische velden zijn. Op die manier wordt de recombinatie van waterstof atomen op de wand geelimineerd. Het zal zeker een aantal nieuwe aspecten toevoegen aan het onderzoek van spin-gepolariseerde waterstof.

Nawoord

Ter afsluiting van dit proefschrift past het om allen die direct (of indirect) bij het tot een (geslaagd) einde brengen van dit werk een bijdrage hebben geleverd te bedanken. In de eerste plaats mijn promotor Ike Silvera en mijn co-promotor Jook Walraven, die beiden een voortdurende bron van inspiratie en steun zijn geweest bij het opzetten, uitvoeren en begrijpen van de in dit proefschrift beschreven experimenten. Ik heb het geluk gehad om als student betrokken te zijn geraakt bij de experimenten aan spin gepolariseerde waterstof toen deze nog in een pril stadium verkeerde en heb de eerste successen van nabij meegemaakt. De daarmee gepaard gaande opwinding en de bijna voelbare hete adem van concurrenten in de nek hebben zeker hun invloed gehad op mijn opvattingen over experimentele fysica. Hoewel de experimenten zeer bewerkelijk van aard zijn, wat waarschijnlijk kan worden beaamd door een ieder die experimenten bij lage temperatuur doet, stimuleren de telkens weer verrassende uitkomsten van de experimenten om onverdroten door te gaan. Het einddoel BEC wordt daarbij voorgehouden, als ware het de graal waarvoor men immer strijden moet.

Experimenten aan spin gepolariseerde waterstof hebben het karakter van een raket lancering. In de eerste fase wordt het experiment op papier voorbereid, gebruik makend van de informatie zoals die op dat moment voor handen is en door allerlei (wilde) ideeen te genereren en te verwerken. De tweede fase bestaat uit het daadwerkelijk omzetten van dit idee in een technisch realiseerbaar ontwerp, wat vervolgens in de derde fase wordt gebouwd. De verschillende onderdelen worden samengebouwd en voortdurend getest. Onderwijl wordt de cryostaat klaar gemaakt, bedrading van thermometers etc. onderhanden genomen, computerprogrammas voor de analyse van de data geschreven (mits men van te voren weet wat er eventueel te zien zal zijn) etc.... Uiteindelijk zit alles in de cryostaat en zijn de verschillende meetinstrumenten via een dikke bos kabels met het inwendige van de cryostaat verbonden. Het aftellen voor de 'lancering' is dan al in feite begonnen en de controle kamer kan 'lift off' melden als de cryostaat inderdaad met succes lage temperatuur heeft gehaald. Dan begint een uitvoerig programma voor het testen en ijken van thermometers, inlaten van helium tbv. de wandbedekking van de cel, uittesten van de dissociator voor het produceren van de atomen etc. Tenslotte, als de cryostaat al zo'n 1 à 2 weken koud is, worden de eerste serieuze experimenten gestart. Meestal zijn de eerste resultaten zeer verwarrend en onbegrijpelijk en is er geruime tijd nodig om te 'weten wat men meet' om inderdaad te kunnen voldoen aan 'meten is weten'. Al bij al duurt een dergelijke run, als alles zonder al te veel problemen verloopt, al gauw 1 à 2 maanden. In die tijd geven meestal een aantal instrumenten het op en moet er het een en ander worden geimproviseerd om toch de zo begeerde resultaten binnen te halen. De laatste fase is het verwerken van de resultaten voorzover dit niet tijdens de meting is geschied en dan, wanneer de resultaten inderdaad wat voorstellen, als de donder een publicatie de deur uit zenden. Ik geef toe dat het een en ander in de

bovenstaande beschrijving wat gechargeerd is, maar geheel beneven de waarheid is het zeker niet.

In de loop der jaren heb ik in de verschillende fasen van die lanceringen zeer prettig samen gewerkt, althans wat mij betreft, met een aantal collega promovendi: Gert van Yperen, Stijn Mattheij, Jaap Berkhout en doctoraal studenten: Erik Salomons, Hans van Zwol en Erik Wolters, die allen hun waardevolle bijdrage hebben geleverd aan de in dit proefschrift beschreven experimenten. Verder zouden de experimenten zonder de technische steun van Otto Höpfner onmogelijk zijn geweest. Cryogene experimenten zijn nu eenmaal onmogelijk zonder de daarbij benodigde cryogene vloeistoffen, die ten tijde van de soms maanden lange runs zonder problemen werden verzorgd door de bemanning van de koud gas afdeling: Nico Jonker en Herman Pothoven. Ook de steun van de afdeling metallurgie (Ton Riemersma en Hugo Schlatter) en de vacuumafdeling (Bert Zwart) voor het oplossen van allerhande problemen was onontbeerlijk.

Voorts wil ik, naast Ike en Jook, Ad Lagendijk en Victor Goldman en alle anderen bedanken voor de immer boeiende discussies over atomaire waterstof en alle andere onderwerpen die toevalliger wijze ter sprake kwamen tijdens de 'lunch pauzes in de koffieshop om de hoek' of tijdens de meestal wat tumultueuze groepsbesprekingen op vrijdagmiddag.

Amsterdam, april 1986.